To the Graduate Council:

We are submitting herewith a dissertation written by Paul Scott Holder entitled "Photochemical Transformation of Polycyclic Aromatic Compounds Sorbed on Coal Stack Ash in the Absence and Presence of Coadsorbates." We have examined the final copy of this dissertation for form and content and recommend that it be accepted in partial fulfillment of the requirements for the degree of Doctor of Philosophy, with a major in Chemistry.

Gleb Mamantov, Co-major Professor

E.L. Wehry, Co-major Professor

We have read this dissertation
and recommend its acceptance:

James Q. Chambers

Richard Pagni

Wayne T. Davis

Accepted for the Council:

Associate Vice Chancellor
and Dean of the Graduate School

PHOTOCHEMICAL TRANSFORMATION OF POLYCYCLIC AROMATIC COMPOUNDS SORBED ON COAL STACK ASH IN THE ABSENCE AND PRESENCE OF COADSORBATES

A Dissertation

Presented for the

Doctor of Philosophy

Degree

The University of Tennessee, Knoxville

Paul Scott Holder

December, 1993

DEDICATION

to *Shannon*

ACKNOWLEDGEMENTS

The names of all of those who have had a positive impact on the work described herein are too numerous to mention here. There are those, however, whose contributions are worthy of special notice.

The author thanks Dr. Gleb Mamantov and Dr. Earl Wehry for the opportunity to be involved in this project, for the sound guidance that they have provided as the work progressed, and for their invaluable assistance in preparing this dissertation.

The Department of Energy, Pittsburgh Energy Technology Center, is thanked for its financial support of the dissertation research. Dr. Mamantov and Dr. Bill Bull are thanked for their support in the form of a Teaching Assistanship for the duration of the author's enrolment. A special thanks goes to Dr. Fred Grimm for the opportunity to be Technical Director of General Chemistry Laboratories in partial fulfillment of departmental teaching responsibilities, and for his friendship and guidance.

Dr. Don Dunstan is thanked for the training that he provided in group methods and procedures. Dr. Rob Mauldin and Dr. John Sanders, former graduate students, are likewise thanked for their tutelage and for the use of instrumentation which they designed and constructed. Thanks also go to David Jenkins and Gary Woody, current graduate students, for their advice, for their assistance, and for use of instrumentation and materials that they built and provided. Bobby Stanton, another graduate student, is thanked for his assistance with several of the figures contained herein.

A host of support staff have provided much assistance during the author's graduate school tenure. Worthy of special thanks are Bill Gurley, Clax Hallman, Roy Hodge, Bobby Lay, Darrell Lay, Pat Martin, Elder Mellon, Carol Moulton, John Nelson, and Arthur Pratt.

The author's family, and that of his wife, are thanked for their encouragement and love. Finally, a very special thanks goes to the author's wife, Shannon, who has been his near constant companion from the onset of graduate studies. She has endured much time alone and has sacrificed many things, but her support and commitment have never wavered. Words cannot begin to adequately express the nature and scope of her contribution to the work described herein.

ABSTRACT

The combustion of coal and other fossil fuels releases into the atmosphere particles and potentially toxic organic compounds. A particular class of these compounds, polycyclic aromatic hydrocarbons and their derivatives, is known to be associated with combustion-generated particles in the environment. This association may prolong the atmospheric lifetimes of these compounds, may facilitate their transport to remote environments, and provides an avenue by which humans may be exposed to them. The work described herein attempts to better understand the nature and the consequences of the interactions of PAH and related compounds with atmospheric particles.

A typical coal stack ash was fractionated according to particle size, and then according to chemical composition, specifically into fractions enriched in ferromagnetic, carbonaceous, and mineral content. 1-Nitropyrene, a representative polycyclic aromatic compound, was deposited from the vapor phase onto these adsorbents and onto a model adsorbent, then exposed to UV/visible light. Its photochemical behavior was compared to that of its parent, pyrene. It was found that 1-nitropyrene is more strongly associated with the carbonaceous component of coal stack ash and is quite resistant to photodegradation on that fraction and on the unfractionated stack ash. It was concluded that nitro-substituted polycyclic aromatic compounds are unlikely to be photolyzed on atmospheric fly ash.

The photochemical behavior of pyrene in the presence of coadsorbates was then compared to the photochemical behavior of sorbed pyrene in the absence of coadsorbates. Pyrene was deposited from the vapor phase onto model and coal stack ash adsorbents containing a coadsorbate, succinic acid. In other studies, *n*-decane was deposited onto adsorbents containing pyrene. It was found that the photolysis of pyrene was enhanced when the coadsorbate was deposited first, and inhibited when pyrene was deposited first. Observed behaviors were tentatively attributed to the ability of a coadsorbate to shield from, or to facilitate the exposure of sorbed pyrene to, incident light.

TABLE OF CONTENTS

CHAPTER 1 BACKGROUND TO THE RESEARCH

1.1 Introduction 1

1.2 Some Basic Aspects of Atmospheric Chemistry 6
1.2-A General Characteristics of the Atmosphere 6
1.2-B Major Sources of Air Pollutants 6
1.2-C Characteristics of Airborne Particles 9
1.2-D Fates of Atmospheric Constituents 11

1.3 PAH Emission Sources and Formation Mechanisms 14

1.4 Origin, Morphology, and Composition of Coal Fly Ash Particles 16

1.5 The Interaction of PAH with Coal Fly Ash Particles 24

1.6 Transformations of Atmospheric PAH 32

1.7 The Importance of Nitro-Substituted PAH 41

1.8 The Importance of Other Atmospheric Organic Compounds 43

1.9 The Focus of the Dissertation Research 45

CHAPTER 2 EXPERIMENTAL MATERIALS AND METHODS

2.1 Introduction 47

2.2 Fractionation and Characterization of Coal Stack Ash 48
2.2-A Coal Stack Ash Material 48
2.2-B Fractionation of Coal Stack Ash According to Particle Size 48
2.2-C Fractionation of Coal Stack Ash According to Chemical Composition 48
2.2-C1 Removal of Ferromagnetic Particles 48
2.2-C2 Separation of Mineral and Carbonaceous Particles 49
2.2-D Characterization of Coal Stack Ash and Its Subfractions 51
2.2-D1 Determination of % Carbon 51
2.2-D2 Determination of % Iron 51

2.3 Deposition of PAH and Related Compounds Onto Coal Fly Ash and Silica Gel 53
2.3-A Adsorbents 53
2.3-B Adsorbates 54
2.3-C Depositions 54
2.3-C1 Solution Depositions 54
2.3-C2 Vapor Depositions 55

2.4 Irradiations of Sorbed PAH and Related Compounds 62
2.4-A Samples 62
2.4-B Control Exposures 63
2.4-C Irradiations 64

2.5 Extraction and Quantification of Sorbed Organic Compounds 68
2.5-A Supercritical Fluid Extractions 68
2.5-A1 Apparatus 68
2.5-A2 Procedure 70
2.5-B Ultrasonic Extractions 72

CHAPTER 3 FRACTIONATION AND CHARACTERIZATION OF KANEB COAL STACK ASH

3.1 Introduction 73
3.1-A Background 73
3.1-B Objectives 79

3.2 Results and Discussion 80
3.2-A Kaneb coal stack ash fractionation 80
3.2-B Kaneb coal stack ash characterization 82

3.3 Conclusions 83

CHAPTER 4 PHOTOCHEMISTRY OF 1-NITROPYRENE SORBED ON COAL STACK ASH

4.1 Introduction 84
4.1-A Background 84
4.1-B Objectives 91

4.2 Results and Discussion 92
4.2-A Background experiments: 1-nitropyrene photochemistry 92
4.2-B Background experiments: supercritical fluid extractions 95
4.2-C Vapor depositions of 1-nitropyrene and pyrene 99
4.2-D Sorptivity of 1-nitropyrene and pyrene 105
4.2-E Non-photochemical degradation of 1-nitropyrene 107
4.2-F Photochemical degradation of 1-nitropyrene and pyrene 109

4.3 Conclusions 113

CHAPTER 5 PHOTOCHEMISTRY OF ADSORBED PYRENE IN THE PRESENCE OF COADSORBATES

5.1 Introduction 114
5.1-A Background 114
5.1-B Objectives 116

5.2 Results and Discussion 117
5.2-A Retention of Sorbed Succinic Acid 117
5.2-B Retention of Sorbed Pyrene 119
5.2-C Non-photochemical and photochemical stability of succinic acid 120
5.2-D Non-photochemical and photochemical stability of *n*-decane 127
5.2-E Vapor depositions of pyrene and coadsorbates 130
5.2-F Sorptivity of pyrene in the presence of coadsorbates 133
5.2-G Photochemistry of pyrene in the presence of coadsorbates 136

5.3 Conclusions 140

CHAPTER 6 SUMMARY

6.1 Conclusions 143

6.2 Suggestions for Future Work 144

LIST OF REFERENCES 147

VITA 155

LIST OF TABLES

TABLE 1.1 NATURAL SOURCES OF AIR POLLUTANTS 8

TABLE 1.2 ANTHROPOGENIC SOURCES OF AIR POLLUTANTS 8

TABLE 1.3 STATIONARY AND MOBILE PAH SOURCES 15

TABLE 1.4 ELEMENTAL DISTRIBUTIONS FOR MINERAL PHASES OF COAL STACK ASH 21

TABLE 1.5 CARBON CONTENT FOR THREE SIZE-FRACTIONATED COAL STACK ASHES 23

TABLE 1.6 MOLECULAR STRUCTURE, VAPOR PRESSURE OF REPRESENTATIVE PAH 25

TABLE 1.7 SPECIFIC SURFACE AREAS FOR SIZE FRACTIONS OF A COAL STACK ASH 27

TABLE 1.8 SORPTIVITIES OF CARBONACEOUS FRACTIONS, COAL STACK ASH 27

TABLE 1.9 SURFACE AREAS, SORPTIVITIES OF COAL ASH, CARBONACEOUS FRACTIONS 28

TABLE 1.10 SORPTIVITIES OF SIZE FRACTIONATED COAL STACK ASH 29

TABLE 1.11 SORPTIVITIES OF REPRESENTATIVE COAL STACK ASHES 30

TABLE 1.12 SORPTIVITIES OF COAL STACK ASH, FRACTIONS, MODEL ADSORBENTS 30

TABLE 1.13 PHOTOLYTIC HALF LIVES (IN HR) OF PAH ON MODEL ADSORBENTS 35

TABLE 1.14 PHOTODEGRADTION (% LOSS) OF PAH ON MODEL ADSORBENTS 35

TABLE 1.15 PHOTODEGRADATION OF BENZO[A]PYRENE ON COAL STACK ASH 37

TABLE 1.16 PHOTOLYTIC HALF LIVES (IN HR) OF PAH ON COAL STACK ASH 38

TABLE 1.17 PHOTODEGRADATION (% LOSS) OF PAH ON COAL STACK ASH 39

TABLE 1.18 PHOTODEGRADATION OF PYRENE ON COAL ASH, MODEL ADSORBENTS 40

TABLE 1.19 CARBOXYLIC ACIDS, *n*-ALKANES DETECTED ON ATMOSPHERIC PARTICULATE MATTER 45

TABLE 2.1 CONDITIONS EMPLOYED FOR VAPOR DEPOSITIONS 63

TABLE 3.1 PROPERTIES OF KANEB COAL STACK ASH FRACTIONS 80

TABLE 3.2 KANEB COAL STACK ASH FRACTIONS: % CARBON, IRON 83

TABLE 4.1 ATMOSPHERIC ABUNDANCES AND MUTAGENICITIES OF NITRO-PAH 86

TABLE 4.2 EXTRACTION OF 1-NITROPYRENE FROM SILICA GEL 97

TABLE 4.3 RETENTION OF MASS FLOW OF PYRENE BY SILICA GEL AND KANEB COAL STACK ASH FRACTIONS 101

TABLE 4.4 ESTIMATED SATURATION COVERAGES OF ADSORBENTS FOR 1-NITROPYRENE 102

TABLE 4.5 COMPARISON OF FID RESPONSE FOR 1-NITROPYRENE AND PYRENE 103

TABLE 4.6 DEPOSITION PARAMETERS AND PREDICTED COVERAGE LEVELS FOR 1-NITROPYRENE 103

TABLE 4.7 DEPOSITION PARAMETERS AND PREDICTED COVERAGE LEVELS FOR PYRENE 104

TABLE 4.8 1-NITROPYRENE EXTRACTION RECOVERIES 106

TABLE 4.9 PYRENE EXTRACTION RECOVERIES 106

TABLE 4.10 COMPARISON: 1-NITROPYRENE AND PYRENE EXTRACTION RECOVERIES 108

TABLE 4.11 1-NITROPYRENE: NON-PHOTOCHEMICAL EXPERIMENTS 108

TABLE 4.12 1-NITROPYRENE: PHOTOCHEMICAL EXPERIMENTS 110

TABLE 4.13 PYRENE: PHOTOCHEMICAL EXPERIMENTS 111

TABLE 4.14 COMPARISON OF PHOTOCHEMICAL RESULTS FOR 1-NITROPYRENE AND PYRENE 112

TABLE 5.1 MELTING AND BOILING POINTS OF PYRENE AND POTENTIAL COADSORBATES 116

TABLE 5.2 RETENTION OF SORBED SUCCINIC ACID AS A FUNCTION OF OVEN TEMPERATURES 119

TABLE 5.3 RETENTION OF SORBED SUCCINIC ACID DURING DEPOSITIONS OF PYRENE 120

TABLE 5.4 RETENTION OF PYRENE UNDER CONDITIONS USED FOR *n*-DECANE EXPERIMENTS 121

TABLE 5.5 STABILITY OF SUCCINIC ACID TO NON-PHOTOCHEMICAL DEGRADATION 124

TABLE 5.6 STABILITY OF SUCCINIC ACID TO PHOTOCHEMICAL DEGRADATION 124

TABLE 5.7 STABILITY OF *n*-DECANE TO NON-PHOTOCHEMICAL DEGRADATION ... 128

TABLE 5.8 STABILITY OF *n*-DECANE TO PHOTOCHEMICAL DEGRADATION 128

TABLE 5.9 DEPOSITION PARAMETERS AND PREDICTED COVERAGE LEVELS FOR SUCCINIC ACID 131

TABLE 5.10 DEPOSITION PARAMETERS AND PREDICTED COVERAGE LEVELS FOR PYRENE WITH SUCCINIC ACID AS COADSORBATE 131

TABLE 5.11 SUMMARY OF COVERAGE LEVELS FOR PYRENE AND SUCCINIC ACID AS COADSORBATES 132

TABLE 5.12 DEPOSITION PARAMETERS AND PREDICTED COVERAGE LEVELS FOR *n*-DECANE 132

TABLE 5.13 SUMMARY OF COVERAGE LEVELS FOR PYRENE AND *n*-DECANE AS COADSORBATES 134

TABLE 5.14 EXTRACTION RECOVERY OF PYRENE IN THE PRESENCE OF SUCCINIC ACID 134

TABLE 5.15 EXTRACTION RECOVERY OF PYRENE IN THE PRESENCE OF *n*-DECANE 135

TABLE 5.16 PYRENE EXTRACTION RECOVERIES IN THE ABSENCE AND PRESENCE OF COADSORBATES 135

TABLE 5.17 PYRENE: PHOTOCHEMICAL EXPERIMENTS WITH FILTERED LAMP OUTPUT 137

TABLE 5.18 PYRENE: PHOTOCHEMICAL EXPERIMENTS WITH SUCCINIC ACID AS COADSORBATE 137

TABLE 5.19 PYRENE: COMPARISON OF PHOTOCHEMICAL LOSS IN THE ABSENCE AND PRESENCE OF SUCCINIC ACID 138

TABLE 5.20 PYRENE: PHOTOCHEMICAL EXPERIMENTS WITH *n*-DECANE AS COADSORBATE 139

TABLE 5.21 PYRENE: COMPARISON OF PHOTOCHEMICAL LOSS IN THE ABSENCE AND PRESENCE OF *n*-DECANE 139

TABLE 5.22 PYRENE: COMPARISON OF PHOTOCHEMISTRY WITH SUCCINIC ACID AND *n*-DECANE AS COADSORBATES 141

LIST OF FIGURES

Figure 1.1 Generation, interactions, and fates of PAH and airborne particles. 5

Figure 1.2 Atmospheric divisions based on variation of temperature with altitude. 7

Figure 1.3 Classification and abundances of atmospheric particles. 10

Figure 1.4 Tropospheric life cycle of airborne particles and pollutants. 12

Figure 1.5 Schematic diagram of a pulverized coal fired boiler. 17

Figure 1.6 Fly ash morphology: particle shape, opacity as a function of composition, combustion time. 19

Figure 1.7 Solar intensity as a function of wavelength. 34

Figure 2.1 Schematic diagram of *elutriator*. 50

Figure 2.2 Fractionation scheme for Kaneb coal ash: size fraction 2 to subfractions. 52

Figure 2.3 Schematic diagram of vapor deposition apparatus. 56

Figure 2.4 Schematic diagram of primary vapor deposition cell. 57

Figure 2.5 Schematic diagram of alternate vapor deposition cell. 58

Figure 2.6 Flame ionization detector profile of a typical vapor deposition. 61

Figure 2.7 Schematic diagram of irradiation apparatus. 65

Figure 2.8 Xenon lamp output. 66

Figure 2.9 Quartz irradiation cell. 67

Figure 2.10 Schematic diagram of supercritical fluid extraction apparatus. 69

Figure 3.1 Fractionation scheme for Kaneb coal ash: size fraction 2 (45-74 μm) to subfractions. Mass % of each subfraction is listed. 81

Figure 4.1 UV/visible absorption spectrum: **1-nitropyrene**, 10 ppm in methanol. 93

Figure 4.2 UV/visible absorption spectrum: **pyrene**, 10 ppm in methanol. 94

Figure 4.3 SFE/GC chromatograms for *blank* (CO_2-only) runs.
(a) range = 11; attenuation = 2.
(b) range = 8; attenuation = 2. 96

Figure 4.4 SFE/GC chromatograms as a function of 1-nitropyrene coverage level (deposited from solution on silica gel).
(a) blank silica gel; 81.6 mg.
(b) 1-nitropyrene on silica gel; 10 μg/g, 87.4 mg of sample.
(c) 1-nitropyrene on silica gel; 90 μg/g, 83.8 mg of sample. 98

Figure 5.1 UV/visible absorption spectrum: **succinic acid**, 10 ppm in methanol. 122

Figure 5.2 UV/visible absorption spectrum: **Pyrex** test tube. 125

Figure 5.3 UV/visible absorption spectrum: **quartz** cuvette. 126

Figure 5.4 UV/visible absorption spectrum: ***n*-decane**, 10 ppm in hexane. 129

CHAPTER 1

BACKGROUND TO THE RESEARCH

1.1 Introduction

The atmosphere that surrounds our planet is essential for the survival of its plant and animal kingdom inhabitants. Any phenomenon which tends to disturb the quality of that portion of the environment may, therefore, disturb the quality of planetary life. Beginning with the treatise of John Evelyn in 1661 [1], there has been a well-documented connection between domestic and industrial emissions associated with fuel consumption and/or manufacturing processes, and potentially dire atmospheric consequences.

In this century there have been several acute industrial pollution episodes that have been detrimental to human life (e.g., 4000 fatalities from 1952 London sulfurous smog) and plant life (e.g., crop damage due to photochemical smogs of Los Angeles and other urban areas, first recognized in 1944) [2]. In the last decade or so societal concern has shifted somewhat to more chronic pollution problems such as acidic rain due to nitrogen and sulfur oxide emissions [3], halocarbon-induced depletion of stratospheric ozone [4], and the threat of global warming due to a buildup of greenhouse gases [5].

Another contemporary issue that merits significant attention is the anthropogenic emission of toxic organic compounds. That such a phenomenon exists was recognized in the late 19th century, when unusually high incidences of skin cancer were discovered among paraffin refinery, shale oil, and coal tar industrial workers [6].

A fraction of the carcinogenic culpability traceable to raw materials used in such industries was later attributed to one member of a class of compounds known as polycyclic aromatic hydrocarbons (PAH). Molecules of these compounds consist of two or more aromatic subunits fused in some geometric (i.e., linear, angular, cluster) arrangement. They, by definition, contain only carbon and hydrogen. One of the simplest of these compounds is naphthalene,

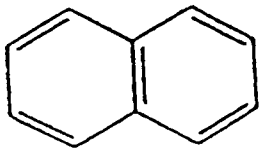

which contains two benzene rings. The first PAH identified as a carcinogen was benzo[a]pyrene,

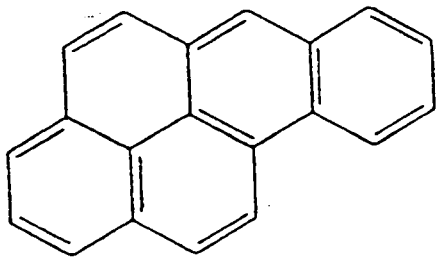

a higher analogue of naphthalene.

It is now known that examples of this compound class, as well as a wide variety of analogues and derivatives, are ubiquitous in the environment. Total atmospheric emissions of PAH were believed to exceed 10 metric tons in the United States alone in 1981 [7]. Since the initial identification of the coal tar carcinogen in 1931 [6], other PAH have been shown to be carcinogenic in laboratory animal testing. The development of the Ames *Salmonella*/Mammalian-Microsome test in the mid-1970s [8] provided a quick method to screen the mutagenic potential of a given compound. Subsequently, many more PAH have been shown to induce bacterial DNA mutations and are, therefore, potential carcinogens.

PAH may originate from any process, natural (e.g., volcanic eruptions, forest fires) or anthropogenic (e.g., fossil fuel consumption) involving the combustion of carbon- and hydrogen-containing materials [6,7]. They may, during their atmospheric lifetimes, be subject to any of several transformation processes such as dark or photo-induced degradation, or reaction with atmospheric species [9-11]. The products generated through such processes may be less harmful, or may be potentially more harmful, than the parents from which they are derived. PAH have been identified in plant tissues [12], and in water supplies [13], so indirect human exposure to them is possible.

The concomitant existence of airborne particles further complicates this scenario. Atmospheric particulate matter may emanate directly or indirectly from natural processes (e.g., scatter of dust, sea spray) or from human activities (e.g., pesticide, fertilizer use) [14,15]. In the late 1970s it was discovered that some types of airborne particles were mutagenic [16], that at least a portion of the mutagenicity was attributable to PAH and related compounds not native to, but nonetheless associated with, these particles [16,17], and that these associations occurred preferentially with particles in the respirable size range [16,18]. Direct human exposure via inhalation, then, is yet another potential fate for these compounds.

One of the more important types of airborne particles is coal fly ash, the fraction of the residue resulting from the combustion of coal that escapes into the atmosphere. Power plants burning fossil fuels are responsible for as much as 25 % of the anthropogenic particulate matter emitted into the

atmosphere in the United States, with coal combustion believed to be the leading fossil fuel contributor [19]. In 1978 it was estimated that 2.6 million tons of fly ash were released from U.S. coal-burning facilities [16]. Total U.S. emissions of coal fly ash were projected to exceed 5 million tons by 1985 [20]. Because coal is our most abundant domestic fuel, its usage is expected to continue to increase [21]. It follows, then, that emissions of coal fly ash will continue to be of environmental significance.

The complex atmospheric life cycle of PAH and related compounds and of atmospheric particulate matter such as coal fly ash is summarized in **Figure 1.1**. Shown are two of the primary sources of PAH and airborne particles, industrial power plants and internal combustion engines. Already alluded to (p. 3) were possible avenues toward human exposure to PAH. It has been shown that the interaction of PAH with airborne particles can facilitate their transport to remote areas [22,23], so the inherent threat from these substances is not limited to industrial and/or urban areas.

What is not fully understood is the nature of the interaction between PAH and coal fly ash (and other airborne particles) and the effect of that interaction on possible PAH transformation processes. Our research group attempts to address these questions. Specifically, we attempt to elucidate chemical and physical factors influencing the interactions of PAH (and related compounds) with coal fly ash, and we attempt to simulate atmospheric exposures of ash-bound PAH and related compounds to sunlight and reactive species.

In the remainder of this chapter, background material further elaborating on the origins, interactions, and fates of PAH and related compounds and coal fly ash is presented. This discussion culminates in a specific statement of focus for the dissertation research. To lay a foundation for such a discussion, the next section reviews salient characteristics of the atmosphere and discusses general origins and interactions of airborne pollutants and particles.

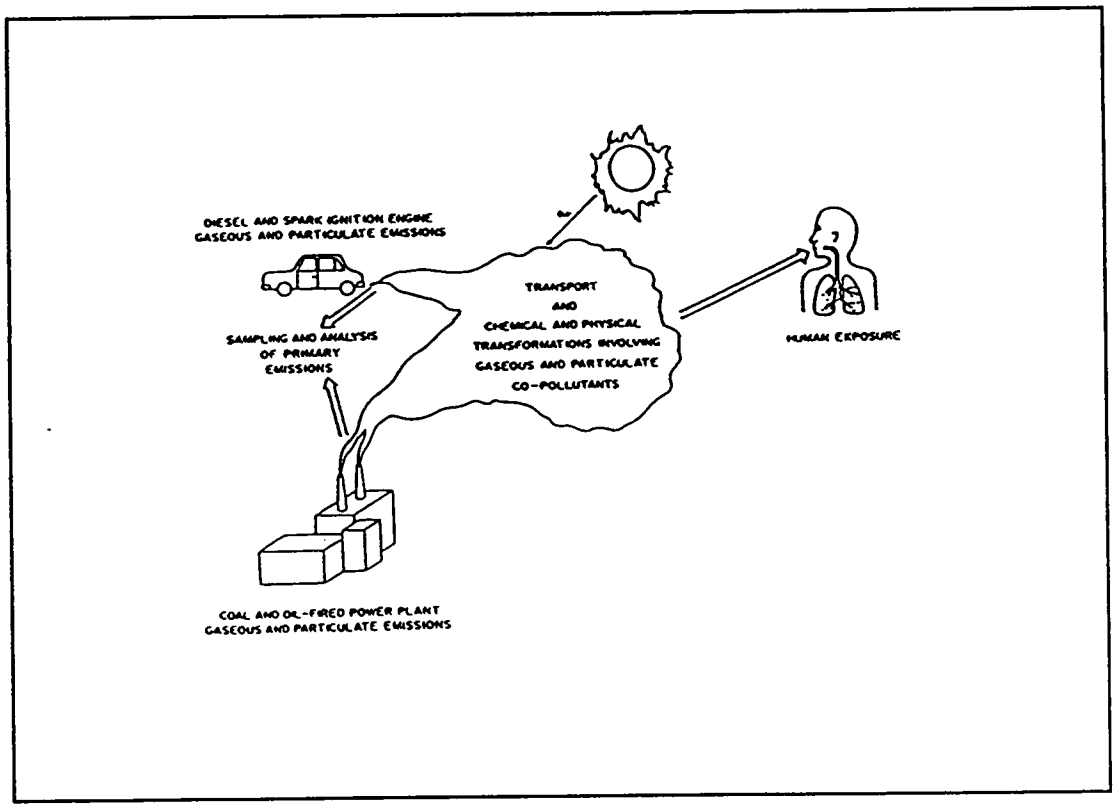

Figure 1.1 Generation, interactions, and fates of PAH and airborne particles.
Source: Pitts, J.N., Jr. *Environ. Health Perspect.*, 1983, *47*, 117.

1.2 Some Basic Aspects of Atmospheric Chemistry

1.2-A General Characteristics of the Atmosphere

Essential to an understanding of the physical and chemical behavior of coal fly ash-associated PAH is an understanding of some basic characteristics of the atmosphere and the general influence of these characteristics on the transport and transformation of a given airborne particle and/or pollutant. The earth's atmosphere can be divided into a number of distinct regions as a function of its altitude and temperature profile. **Figure 1.2** lists these divisions for average atmospheric temperatures at mid-latitudes.

In the *troposphere* temperature generally decreases with increasing altitude, or, put another way, with increasing distance from solar-induced surface heating [2]. At about 15 km the influence of surface heating becomes negligible and, from that point to an altitude of approximately 50 km (region defined as the *stratosphere*), temperature increases with altitude. The altitude/temperature profile changes twice more in the lower atmosphere, giving rise to the *mesosphere* (50-85 km) and the *thermosphere* (85-110 km). Note that, throughout the lower atmosphere, pressure decreases linearly with altitude.

1.2-B Major Sources of Air Pollutants

In the strictest sense an air pollutant is *any substance changing the natural composition of the atmosphere* [24]. For the sake of the present discussion, a distinction will be made between airborne *particle* and airborne *pollutant*. The former will refer to any *minute piece of solid or liquid* [14] having a finite airborne residence time, and the latter to any toxic chemical species released into the atmosphere, existing in either the gaseous state or associated with a particle [25].

Schroeder and Lane [25] have reviewed the major natural and anthropogenic sources of airborne pollutants, and these are listed in **Table 1.1** and **Table 1.2**. These substances may be directly

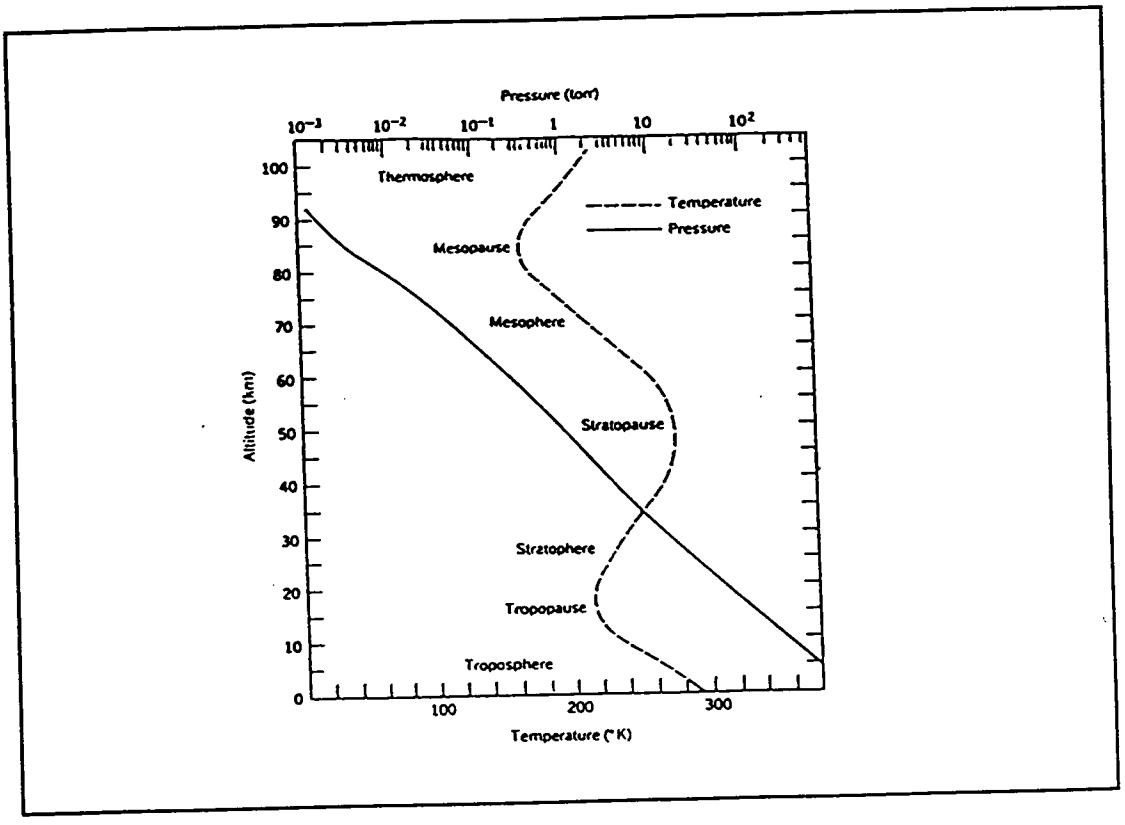

Figure 1.2 Atmospheric divisions based on variation of temperature with altitude.
Source: Finlayson-Pitts, B.J.; Pitts, J.N., Jr. *Atmospheric Chemistry: Fundamentals and Experimental Techniques*, Wiley: New York, 1986, p. 9.

TABLE 1.1 NATURAL SOURCES OF AIR POLLUTANTS

Sources	Examples of Pollutants
Crustal rock and soils	Heavy metals: cadmium, manganese, mercury
Vegetation	Selenium, zinc
Swamps	Hydrogen sulfide, volatile organics
Volcanoes	Heavy metals
Fires (forest, brush, grass)	PAH, heavy metals

Source: Schroeder, W.H.; Lane, D.A. *Environ. Sci. Technol.*, 1988, *22*, 240.

TABLE 1.2 ANTHROPOGENIC SOURCES OF AIR POLLUTANTS

Sources	Examples of Pollutants
Industrial processes, manufacturing, and commercial operations	Various organic, inorganic, and organometallic substances
Transportation (land, sea, air)	Hydrocarbons and other organic compounds, sulfur and nitrogen compounds, and PAH
Waste treatment and disposal	Various organic, inorganic, and organometallic substances
Combustion processes (waste, fossil fuel, biomass)	Heavy metals, trace elemnts, PAH polychlorinated dibenzodioxins, and polychlorinated dibenzofurans
Pesticide manufacture, use	Chlorinated hydrocarbons

Source: Schroeder, W.H.; Lane, D.A. *Environ. Sci. Technol.*, 1988, *22*, 240.

emitted into the atmosphere or they may be introduced there after an initial discharge and residence in some other medium (e.g., water, soil).

All such direct and indirect emissions can be thought of as *primary* pollutants (i.e., those that are generated directly from emission sources). *Secondary* pollutants are those which originate from atmospheric chemical transformations of primary emissions. The nature and extent of the toxic potential of a given pollutant, whether primary or secondary, is a function of the chemical nature and availability of that pollutant. The full range of PAH, analogues, and derivatives with which this research group is concerned encompasses both primary and secondary pollutants and encompasses a wide range of toxic potential.

1.2-C Characteristics of Airborne Particles

Airborne particles can also be classified as *primary* or *secondary*, depending on whether they are directly emitted or result from atmospheric transformations of primary particles and/or chemical species [14]. These transformations include nucleation of gaseous species, and the combination of gases and pre-existing particles. The nature and extent of the interaction between a given particle and pollutant are a function of the availability and nature of the pollutant and the availability and composition of the particle. The chemical composition and physical properties of a particle depend primarily on its source. One of the most important factors in determining the availability of a particle type, in addition to its concentration, is its atmospheric residence time. This, in turn, is largely a function of particle size. **Figure 1.3** illustrates the classification of atmospheric particles based on size. Shown are abundances (implied vertical axis) of *coarse* particles ($>2.5\ \mu m$), and of the two particle size distributions, *nuclei range* ($<0.1\ \mu m$) and *accumulation range* ($0.1\ \mu m < (size) < 2.5\ \mu m$), of *fine* particles ($<2.5\ \mu m$).

Coarse particles originate primarily from mechanical processes (e.g., grinding, wind, erosion). This size class, on average, is responsible for 1/2 to 2/3 of the total mass of atmospheric particulate

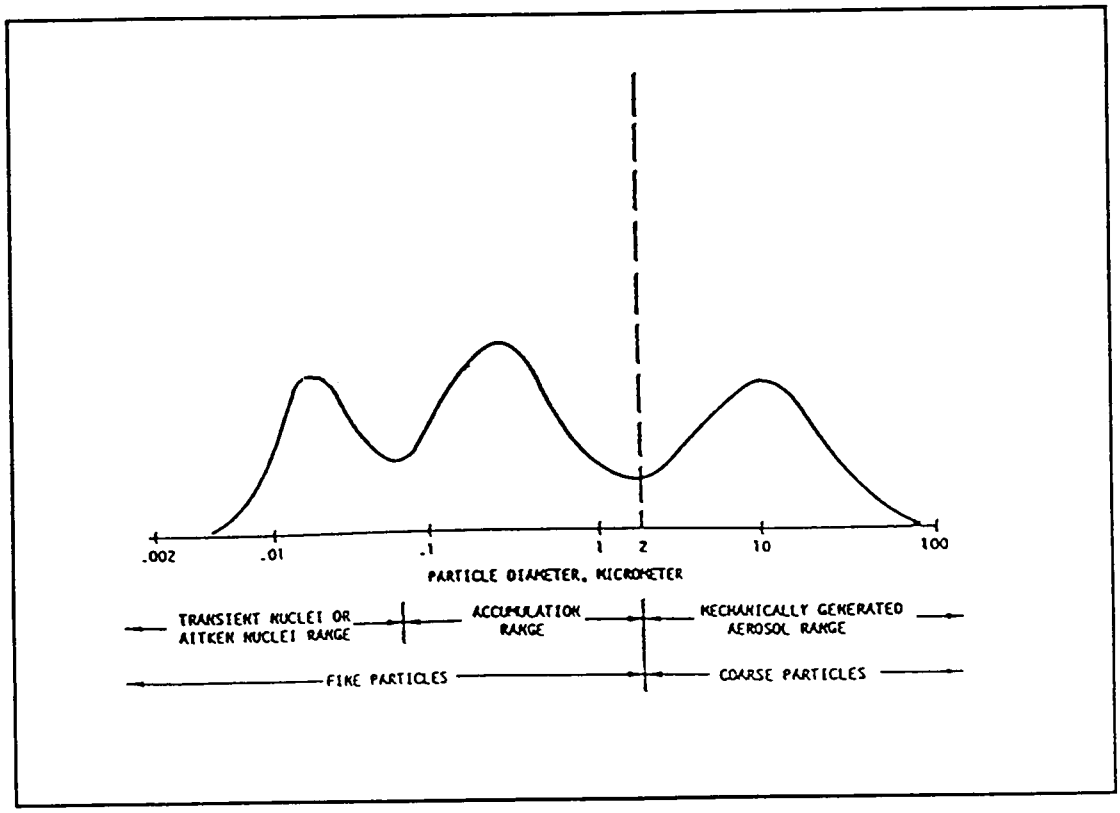

Figure 1.3 Classification and abundances of atmospheric particles.
Source: National Research Council. Subcommittee on Airborne Particles *Airborne Particles*, University Park Press: Baltimore, MD, 1979, p. 11.

matter [15]. Though more prone to atmospheric fallout than fine particles, coarse particles have been shown to have atmospheric lifetimes sufficient to interact with, and transport to the surface of the earth, a number of pollutant species, such as SO_4^{2-}, Pb, and polychlorinated biphenyls [26]. The coarse particle atmospheric distribution exhibits a maximum at the 10 μm particle size. This particle size also represents the upper size cutoff for particles that may be inhaled by the average adult [15].

Accumulation range particles result from gaseous condensation of vapor (e.g., vapors due to fuel combustion) and from the growth of particles in the *nuclei* size range. Particles in this size range comprise about 50 % of the total number of particles in the atmosphere, but only contribute 5 % of the overall mass of atmospheric particulate matter [15]. Because of their size, the atmospheric lifetimes of these particles can be significant. In fact, particles with diameters of approximately 0.5 μm may reside for years in the atmosphere [14]. They are also, like the smaller coarse particles, respirable.

Particles in the *nuclei* size range arise primarily from the condensation of hot (e.g., associated with combustion) vapors. This size class contains most of the total number of particles but only a small fraction of the overall mass of atmospheric particulate matter [15]. Because they are prone to coagulation, *nuclei range* particles possess relatively short (typically a few minutes) atmospheric lifetimes.

1.2-D Fates of Atmospheric Constituents

The existence of pressure and temperature gradients in the various atmospheric divisions (as pointed out on p. 6) influences the behavior of a particle or pollutant in that region. Of primary concern for the present discussion is the influence of these factors on species residing in the troposphere or stratosphere. Also of importance are prevailing conditions relative to wind velocity and direction, sunlight levels, and precipitation events.

Figure 1.4 summarizes the range of interactions and fates available to particles and pollutants emitted into the troposphere. The temperature and pressure gradient just alluded to allows for a cyclical rising and falling of hot and cool air and provides the opportunity for vertical mixing of airborne

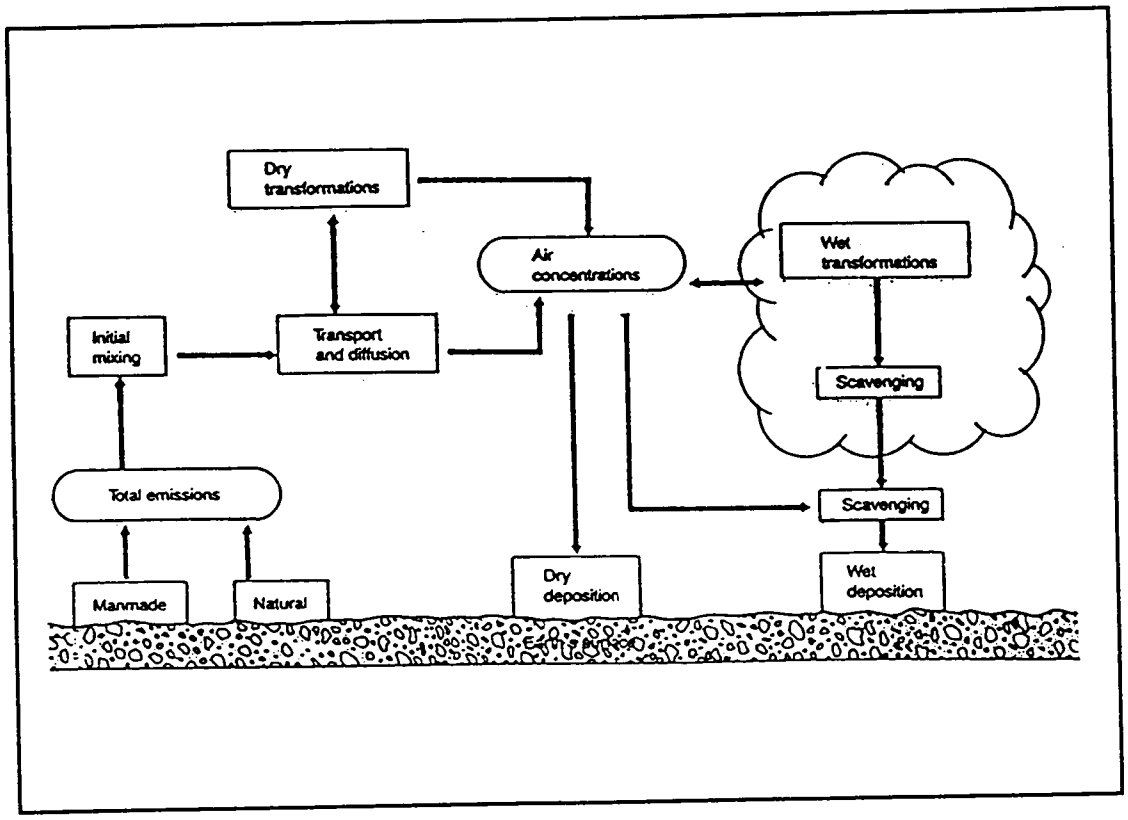

Figure 1.4 Tropospheric life cycle of airborne particles and pollutants.
Source: Schroeder, W.H.; Lane, D.A. *Environ. Sci. Technol.*, 1988, *22*, 241.

particles and pollutants. Through this mechanism species may be transported from the earth's surface to the upper level of the troposphere or into the stratosphere in a matter of days [2]. Counteracting this phenomenon are periodic occasions of hot/cool/hot air mass sequences. These events, called *inversions*, inhibit vertical mixing and may result in the dangerous surface buildup of toxic pollutants [25].

Particles and pollutants residing in the troposphere are also subject to horizontal movements (as a function of climatic conditions), during which time there is additional opportunity for interaction. Also possible is a wide range of transformations of gaseous PAH and of PAH associated with particles. Ultimately, pollutants, particles, and/or their transformation products are subject to direct removal from the atmosphere or may be removed indirectly during precipitation episodes. Particle-associated pollutants are particularly susceptible to removal via the latter mechanism [25]. Wet and dry depositions together enable a range of potential sources for human exposure to toxic pollutants.

Stratospheric particles and pollutants are also subject to the same potential transformation mechanisms as those of particles and pollutants residing in the troposphere. Absent in this region, though, are opportunities for precipitation-aided scavenging and removal [25]. This fact, coupled with the absence of an altitude/temperature profile conducive to vertical mixing, allows stratospheric particle-associated pollutants to have significant airborne residence times (as pointed out on p. 11), and to be transported over long distances (as pointed on p. 4).

In summary, primary and secondary gaseous pollutants that are emitted into the troposphere are subject to a wide variety of fates. As has been shown, these fates are influenced in large part by atmospheric and climatic phenomena, and by the coexistence of atmospheric particles. With this background in mind this presentation can now turn to a more specific discussion of origins and characteristics of PAH and related compounds, of coal fly ash, and of the nature and consequences of the interactions between PAH and coal fly ash.

1.3 PAH Emission Sources and Formation Mechanisms

More than 70 different PAH with from four to seven aromatic rings have been identified in ambient air [27,28]. Their atmospheric concentration, whether they be gaseous or associated with particles, ranges from sub-ppt to low ppb levels [6]. Airborne pollutant concentrations are typically expressed in mass/volume units for uniformity in particle-associated and gaseous PAH levels. All values in this text will be expressed in a mass/mass basis since the work described will deal only with particle-associated PAH.

Though PAH may be formed during slow, low temperature decomposition of biological material [29], their primary point of origin is the incomplete high temperature combustion of organic fuel [6,7,29,30]. At temperatures of approximately 1000° C in oxygen-deficient flames, reactive C_1 and higher radical species and C_n fragments are produced and combine ultimately to yield PAH. Precursors and/or intermediates postulated to be important in PAH synthesis are acetylene, phenylacetylene, and styrene [6,29,30].

Even though a large number and variety of PAH may be formed through the primary reactions involved in this mechanism, only those which are thermodynamically stable survive the combustion process [6,29]. The chemical profile of the range of emitted PAH, then, depends more on the combustion conditions than on the original fuel composition. The amount of PAH produced, however, is influenced by the make-up of the fuel [29].

Emission sources of PAH can be classified as *stationary* or *mobile*. Examples of each these source types are summarized in **Table 1.3**. Of these, vehicular traffic (25-35 %) and industrial emissions (26-41 %), are the chief PAH sources in the United States [7,29]. Leading contributors to the industrial total are coke and aluminum manufacturing [7,29]. Residential combustion, especially of wood and coal, also contributes significantly to the overall U.S. total, being responsible for 12-16 % of total PAH emissions [7,29].

TABLE 1.3 STATIONARY AND MOBILE PAH SOURCES

Stationary Sources	Mobile Sources
1. Residential Heating	1. Motor vehicle
Furnaces, fireplaces, and stoves (wood and coal)	Gasoline engines
Gas Burners	Diesel engines
	Airplanes
2. Industry	Sea traffic
Coke production	Rubber tire wear
Carbon black production	
Petroleum catalytic cracking	
Asphalt production	
Aluminum smelting	
Iron and steel sintering	
Ferroalloy industry	
3. Power and heat generation	
Coal-, oil-, wood-, and peat-fired power plants	
Industrial and commercial boilers	
4. Incineration and open fires	
Municipal and industrial burning	
Refuse burning	
Forest fires	
Structural fires	
Agricultural burning	

Source: Bjorseth, A.; Ramdahl, T. *Handbook of Polycyclic Aromatic Hydrocarbons*; volume 2, Marcel Dekker: New York, 1985, p. 5.

Coal fired power stations are responsible for less than 5 % of United States PAH emission [7,30]. It is assumed, then, that the bulk of coal fly ash-associated PAH does not originate with combustion of that fuel material, but, instead, results from interactions at some point after generation of fly ash and PAH. These interactions are further explored in a later section.

1.4 Origin, Morphology, and Composition of Coal Fly Ash Particles

The physical and chemical nature of fly ash particles emanating from the stacks of coal-fired power plants is dependent on several factors. These include the physical and chemical characteristics of the original fuel, the type of combustion process employed, the specific conditions under which that process was carried out, and the choice and effectiveness of downstream particle abatement devices. These parameters may vary from power plant to power plant, and they may differ for a given power plant as a function of time and of distance downstream of the combustion zone. Nonetheless, some general principles are worth noting.

Coal derives from the decomposition of plant material. It is a heterogeneous substance, consisting of both organic and inorganic species. The specific composition of a coal is a function of several parameters, including the nature of the plant material from which it has been derived [31], the extent of decomposition of that material [32], and the sediment in which decomposition takes place [33]. Its elemental makeup consists primarily of C, H, O, N, and S, but scores of other elements may be present at trace levels [32].

Figure 1.5 is a diagram of a typical coal fired boiler. In such a device, pulverized coal is burned and mixed in a suspension in which thermal radiation and turbulence are provided by flames, by secondary heat from combustion components, and by the introduction of heated air. Important parameters influencing the efficiency of combustion of organic content, the degree of volatilization of inorganic species, and the ultimate chemical composition and physical properties of ash particles generated are the temperature of the combustion zone, the time spent at that temperature, and the magnitude and rate of heat loss to the walls of the furnace [34].

The volume and size distribution of coal fly ash particles ultimately released into the atmosphere is strongly influenced by the choice and the effectiveness of downstream particle abatement technology. The most popular of such technologies is the electrostatic precipitator. In such a device,

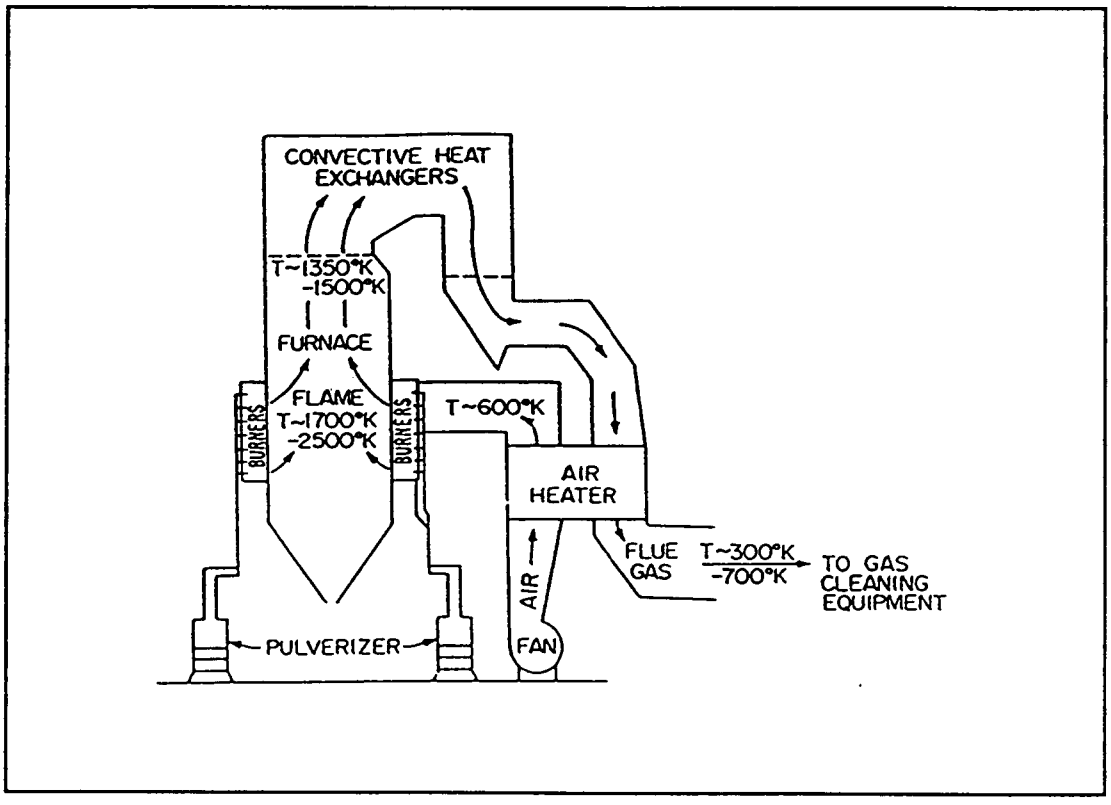

Figure 1.5 Schematic diagram of a pulverized coal fired boiler.
Source: Flagan, R.C.; Friedlander, S.K In *Recent Developments in Aerosol Science*, Shaw, D.T. (Ed.), John Wiley and Sons: New York, 1978, p. 29.

particles are ionized as they pass through a cylindrical chamber across which a potential difference has been generated. They are then attracted and captured by the oppositely charged outer walls. Electrostatic precipitators have high collection efficiencies (95-100 %) for a wide range of particle sizes (0.005-5 μm), but they do exhibit a minimum in collection efficiency for atmospherically important particles in the 0.1-1.0 μm size range [34].

Coal fly ash particles exhibit, as do other atmospheric particles, a trimodal size distribution [34,35]. As with other atmospheric particles, the most abundant are those in the 0.1-1 μm size range, while the less abundant coarse particles (> 2.5 μm in diameter) comprise the bulk of the mass of emitted particles. In terms of chemical composition, coal fly ash can be described as an inhomogeneous mixture of three distinct particle types. These include a *mineral non-magnetic* fraction [36,37], a *magnetic mineral* fraction [38,39], and a *carbonaceous* fraction [40,41]. Coal fly ash may also be classified according to particle morphology. Eleven different morphological coal fly ash particle types have been identified [28,42]. The relationship between the chemical composition and morphology of fly ash particles is summarized in **Figure 1.6**. Morpholgical classes depicted were identified for coarse coal fly ash particles with diameters between 2 and 20 μm [42].

The mineral non-magnetic fraction is the most abundant component of coal fly ash, accounting for up to 95 % of the mass of a typical sample [42]. It consists largely of an aluminosilicate *glassy* phase, as well as a mullite-quartz *crystalline* phase. Both phases are of general composition $(SiO_2)_x{\cdot}(Al_2O_3)_y$. The mineral non-magnetic fraction of coal fly ash is manifested primarily as the nonopaque solid spherical particles depicted in **Figure 1.6** [42]. This fraction is also the primary component of other particle types which are nonopaque, and a primary component of those particles of mixed opacity. The relative abundances of various particle morphologies is a function of particle size, time of exposure in the combustion chamber, and particle composition [42]. In general, the spherical particles are favored as time of exposure increases and as particle size decreases [20,42]. It is worth noting that the spherical particles may be solid, hollow (*cenospheres*), or solid particles encapsulated in larger spheres (*plenospheres*).

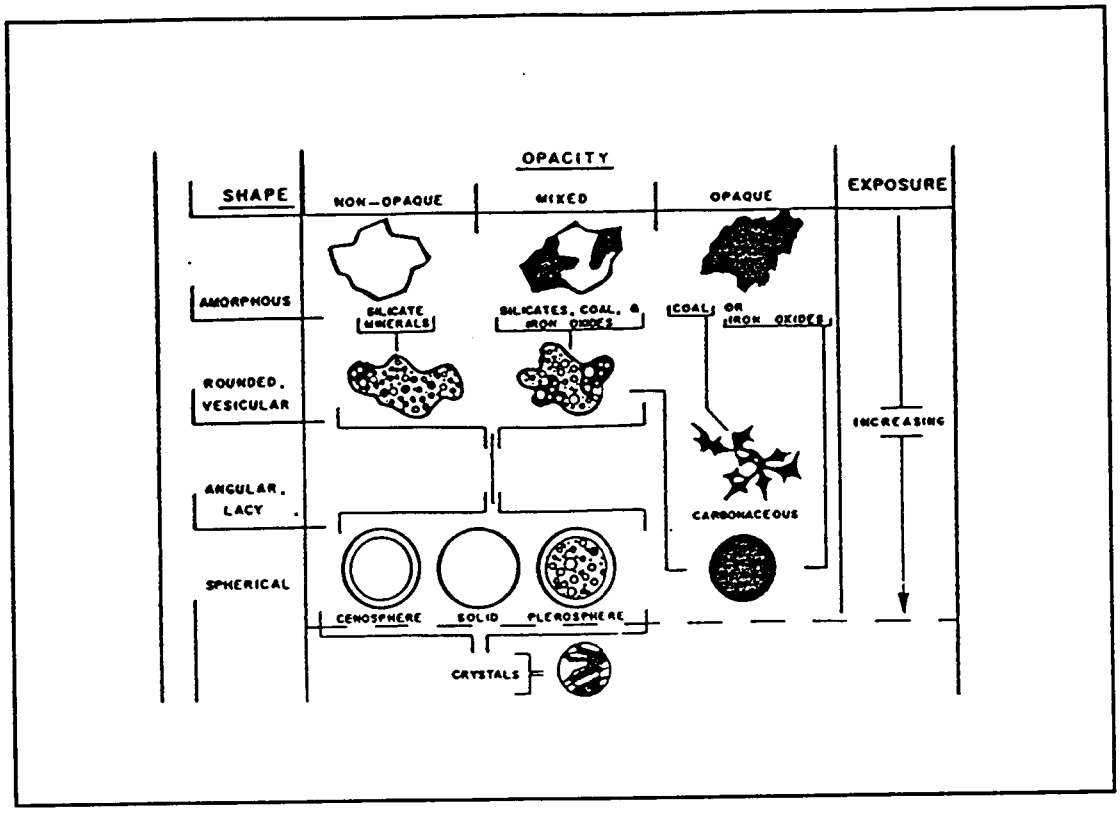

Figure 1.6 Fly ash morphology: particle shape, opacity as a function of composition, combustion time. Source: Fisher, G.L. *et al. Environ. Sci. Technol.*, 1978, *12*, 450.

In addition to Al and Si, mineral non-magnetic particles contain many other elemental species, primarily metals, as major, minor or trace constituents. These may exist as isomorphic substitutions in the aluminosilicate crystal lattice [36], or as oxide impurities [20] or in solid solutions in the aluminosilicate matrix [37]. Natusch *et al.* [35] have determined the elemental distributions for mullite-quartz and glassy mineral fractions of a typical coal *stack* ash (i.e., ash sampled at the electrostatic precipitator). Analyzed particles were in the 100-200 μm size range. The most abundant metals and metalloids for these fractions are listed in **Table 1.4.**

Smith *et al.* [35] and Keyser *et al.* [43] have shown that concentrations of trace elemental species tend to be greater near fly ash particle surfaces than in the interior of those particles. This tends to be especially true for fine particles. This is of environmental significance because several of the elements listed in **Table 1.4** (e.g., Co, Cr, Cu, Ni) are toxic if ingested (e.g., via inhalation of respirable particles) in excessive amounts. The tendency of these elements to concentrate at particle surfaces may, furthermore, facilitate their biological uptake.

The mineral magnetic fraction of coal fly ash typically accounts for between 2 and 20 % of the mass of a typical coal fly ash [35,39,44]. It exists in the form of a ferrite *spinel* ($FeAl_xO_y$) or as a mixture of iron oxides, particularly Fe_2O_3 and Fe_3O_4, dissolved in the glassy aluminosilicate matrix. Levels of magnetic iron oxides have been shown to increase with decreasing particle size [45]. Like their non-magnetic counterparts, these mineral particles contain several elemental species as major, minor, and trace constituents. Among the most abundant, after Fe and Al, are K, Ni, Na, Cr, and Mn [37]. Iron oxides are dark in color and are therefore responsible for some of the opacity of coal fly ash particles. Referring to **Figure 1.6** (p. 19) particles with significant mineral magnetic content may be opaque spheres or, to a lesser extent, opaque but of amorphous shape. They may be of mixed opacity and of rounded vesicular or amorphous shape [42].

Carbonaceous particles are likewise dark in color. Referring again to **Figure 1.6** (p. 19), they exist primarily as either amorphous or angular, lacy opaque particles, or as amorphous and rounded, vesicular particles of mixed opacity [37]. The surfaces of carbonaceous particles may be contaminated

TABLE 1.4 ELEMENTAL DISTRIBUTIONS FOR MINERAL PHASES OF COAL STACK ASH

Element	*Glassy* phase, ppm	Mullite-quartz phase, ppm
Al	87,000	204,000
Si	393,000	287,000
Fe	19,600	3,400
Na	1,710	256
K	25,000	5,270
Rb	532	12
Mg	10,400	10,500
Sr	798	174
Ba	319	69
Sc	31	7
Ti	10,900	4,630
V	176	127
Cr	169	311
Mn	87	9
Co	25	2
Ni	174	78
Cu	144	17
Zn	209	17

Source: Hulett, J.D., Jr.; Weinberger, A.J.; Northcutt, K.J. *Science*, 1980, 1357.

contaminated with mineral inclusions which contain metallic/mettaloid species as impurities [40]. Chief among these impurities are Al, Si, Fe, Ti, and K. The carbon of carbonaceous particles exists primarily in *elemental* form [40]. Carbonaceous particles may contain, to a much lesser degree, elemental carbon that has been oxidized [41], or *organic* carbon deriving from uncombusted fuel material [40]. The carbon content of coal fly ash varies from much less than 1 % of the total mass to as much as 12 % of that mass [35,41,44].

Griest and Harris [40] have measured total carbon content (by combustion of sample followed by gravimetric determination of C as CO_2) of three representative bulk and size-fractionated (via the use of mechnical sieves) coal stack ashes. These results are summarized in **Table 1.5**. The percentage by mass of each size fraction (relative to the bulk unfractionated ash) of each ash fraction is also listed in parentheses following each carbon content.

Carbonaceous content was found to increase with increasing particle size. This would follow logically from the fact that incomplete combustion of coal favors the release of larger particles (i.e., less thermally induced *breakup* of particles), and favors the retention of combustible carbon. To illustrate, ashes designated as *1* and *2* were obtained during normal furnace operating conditions. Ash *3*, which contains a higher carbon content than ashes 1 and 2, was obtained while the furnace was operating at a lower temperature. Furthermore, the largest size fractions (14-21 μm and 21-150 μm) of ash 3 constituted 32.5 % of the mass of the bulk ash, while for ashes 1 and 2, derived from operation at higher temperatures, those fractions accounted for only 9.1 and 22.7 % of the overall bulk masses, respectively.

Note also that there is a second maximum in % carbon values, particularly for ashes 1 and 2, for particles less than 2.3 μm in diameter. Smith and co-workers have observed a similar phenomenon in fine ash particles, specifically those fine particles in the 0.1-1.0 μm size range [35]. The reason for this second *mode* of carbon distribution is not understood at this time. Also note that, as pointed out on page 18, the coarse (> 2.5 μm diameter) particles are responsible for most of the overall mass of each unfractionated bulk ash.

TABLE 1.5 CARBON CONTENT FOR THREE SIZE-FRACTIONATED COAL STACK ASHES

Size fraction, μm	Ash # 1	Ash # 2	Ash # 3
< 2.3	0.66 % (9.0 %)	1.12 % (2.8 %)	4.7 % (2.1 %)
2.3 - 3.3	0.57 % (33.1 %)	0.71 % (24.3 %)	3.6 % (17.2 %)
3.3 - 6.3	0.67 % (28.7 %)	0.90 % (31.0 %)	3.4 % (25.3 %)
6.3 - 14	1.0 % (11.4 %)	1.34 % (17.0 %)	9.8 % (16.3 %)
14 - 21	4.3 % (4.0 %)	3.78 % (9.7 %)	28.5 % (12.4 %)
21 - 150	4.0 % (5.1 %)	6.52 % (13.0 %)	21.8 % (20.1 %)
bulk ash	0.93 %	1.95 %	12.5 %

Source: Griest, W.H.; Harris, L.A. *Fuel*, **1985**, *64*, 822.

It should be clear from the preceding discussion that coal fly ash is a complex and inhomogeneous mixture of widely varying particle sizes, shapes, colors, and compositions. It was pointed out in the last paragraph that Griest and Harris used mechanical sieves to separate coal stack ash according to particle size. Implicit in the previous discussion has been the ability to further fractionate coal ash according to chemical composition. *Complete* separation of particles according to composition is difficult, but one may obtain fractions *enriched* in a particular composition through simple experimental procedures. For instance, a magnet may be used to isolate magnetic mineral particles from non-magnetic particles [39,40,44]. The density of carbonaceous particles is less than that of other non-magnetic particles. This property may be exploited to physically separate these ash components [40,44]. Such separations are important for experiments, like those described in this section, designed to characterize coal fly ash components. In the next two sections, the influence of the various chemical constituents and particle sizes of coal fly ash on the behavior of sorbed PAH and related compounds is discussed. Separations according to particle size and chemical composition are also important, then, to ascertain *cause-and-effect* relationships among particles, sorbed compounds and observed behaviors.

1.5 The Interaction of PAH with Coal Fly Ash Particles

The interactions between PAH and particulate matter (including coal fly ash) may be governed by either physical or chemical factors or a combination thereof. Specific parameters influencing the nature of these interactions are the concentration and vapor pressure of the PAH, the ambient temperature and climatic conditions, and the availability, physical properties, and chemical compositions of the particles [6,7,18,30,46].

At relatively high atmospheric levels of PAH (i.e., > 30 ppb), adsorption of PAH on coal fly ash is controlled largely by the vapor pressure of the PAH [30,46]. **Table 1.6** lists the vapor pressures of several representative PAH. Note that vapor pressure generally decreases as the number of benzene rings in the molecular structure of the PAH increases. Under ordinary atmospheric conditions, PAH with fewer than four rings are encountered predominately in the gas phase, four ring PAH may be in either the gaseous or particulate phase, and five ring and larger PAH are primarily associated with particles [6,7].

Since particles may be scavenged by precipitation more efficiently than are gaseous species, gas/particle ratios exhibit climatic fluctuations [47]. Gas/particle ratios also exhibit seasonal fluctuations, with lower ratios in winter when temperatures are lower and combustion emissions associated with residential heating are more abundant [48,49].

Not only is the concentration of available particles an important factor in determining the degree of PAH/particle association, but their size also has a significant influence. As much as 90-95% of atmospheric particle-associated PAH is found on particles with a diameters less than 3 μm, while as much as 70-80% is associated with particles smaller than 1 μm [7,49]. The preferential association of PAH with smaller particles may be due in part to the increased specific surface areas (i.e., surface area per unit mass) of those particles relative to those of coarse particles.

TABLE 1.6 MOLECULAR STRUCTURE, VAPOR PRESSURE OF REPRESENTATIVE PAH

PAH	Molecular structure	Vapor pressure at 150° C, torr
Naphthalene	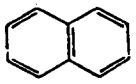	7.8×10^{-2}
Pyrene	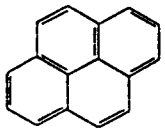	6.2×10^{-6}
Benz[a]anthracene	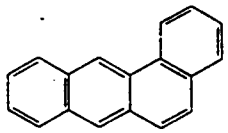	4.5×10^{-6}
Chrysene	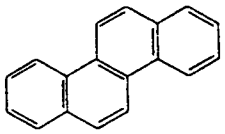	6.4×10^{-9}
Benzo[a]pyrene	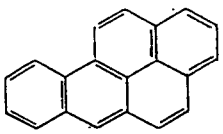	5.6×10^{-9}

Source: Finlayson-Pitts, B.J.; Pitts, J.N., Jr. *Atmospheric Chemistry: Fundamentals and Experimental Techniques*, Wiley: New York, 1986, p. 881.

This phenomenon is illustrated in **Table 1.7**, which lists specific surface areas for coal stack ash particles of various size fractions. Specific surface areas were measured by the *Brunauer, Emmett, and Teller* (BET) method [50], which quantifies the amount of an inert gas adsorbate required to generate a *monolayer* of coverage for a given adsorbent.

The adsorption of PAH on coal fly ash is also greatly influenced by the chemical composition of the particles. At this point, distinguishing between behaviors driven by *physical* or *chemical* factors becomes, somewhat, a semantic matter. In other words, both the physical and chemical nature of a particular *type* of particle (i.e., one separated from the bulk according to chemical composition) influences the affinity of that particle for a given PAH. A few examples will illustrate this point.

Soltys *et al.* [41] separated a representative coal stack ash into carbonaceous and mineral fractions by placing the bulk ash in an appropriate solvent and exploiting the difference in densities of the fractions (the *float-sink* method). They determined the affinity (or *sorptivity*) of each fraction for PAH by monitoring the amount of benzo[a]pyrene adsorbed and desorbed from and into a combination of solvents. Specific surface areas of the two fractions were also measured. The carbonaceous fraction was found to be more than 100 times more retentive for benzo[a]pyrene than was the mineral fraction. Furthermore, the specific surface area of the carbonaceous fraction was 50 times greater than that of the mineral fraction.

Three bulk coal stack ashes were then analyzed for specific surface area and elemental (total inorganic) carbon content. Specific surface areas and sorptivities were determined for carbonaceous fractions of these bulk ashes. These results are summarized in **Table 1.8** and **Table 1.9**. Values listed for *sorptivity* are a measure of the tendency of PAH to be associated with particle surfaces and to resist desorption by a given solvent. Larger values denote greater affinity for PAH. It can be seen (**Table 1.8**) that the affinity of a particular ash fraction for benzo[a]pyrene is directly related to the carbon content of the bulk ash. Note further (**Table 1.9**) that, for these ashes, as the specific surface area of the carbonaceous particles increased, the sorptivity actually decreased. This would imply that carbon content influences sorptivity more than specific surface area. It is interesting to note, however, that, in all cases,

TABLE 1.7 SPECIFIC SURFACE AREAS FOR SIZE FRACTIONS OF A COAL STACK ASH

Particle size fraction, μm	Specific surface area, m^2/g
< 2.3	1.71
2.3 - 3.3	1.19
3.3 - 6.3	0.99
6.3 - 14	0.60
14 - 21	0.57
21 - 150	0.42

Source: Griest, W.H.; Tomkins, B.A. *Environ. Sci. Technol.*, 1986, *20*, 293.

TABLE 1.8 SORPTIVITIES OF CARBONACEOUS FRACTIONS, COAL STACK ASH

Ash	% C, bulk ash	Sorptivity[a], carbonaceous subfraction
1	0.32	0.17
2	1.29	0.63
3	8.50	1.23

[a]units = [ng benzo[a]pyrene/mg ash]/[ng benzo[a]pyrene/mL solvent].
Source: Soltys, P.A,; Mauney, T.; Natusch, D.F.S.; Schure, M.R. *Environ. Sci. Technol.*, 1986, *20*, 177.

TABLE 1.9 SURFACE AREAS, SORPTIVITIES OF COAL ASH, CARBONACEOUS FRACTIONS

Ash	Surface area, bulk ash, m^2/g	Surface area, carbonaceous fraction, m^2/g	Sorptivity[a]
1	1.19	92.94	0.17
2	4.39	63.03	0.63
3	3.43	12.30	1.23

[a]units = [ng benzo[a]pyrene/mg ash]/[ng benzo[a]pyrene/mL solvent].
Source: Soltys, P.A,; Mauney, T.; Natusch, D.F.S.; Schure, M.R. *Environ. Sci. Technol.*, **1986**, *20*, 177.

specific surface areas of the carbonaceous fractions were significantly higher than those of the bulk ashes from which they were derived. The sorptivity of carbonaceous particles, in general, may be in some way influenced by the relatively large specific surface areas of those particles.

Specific surface area, in addition to being a function of particle size (as pointed out on p. 24), is also related to the porosity, or irregularity, of a surface, and to the size of the surface pores (i.e., are they large enough to entrap a given molecule?) [51]. It was pointed out earlier (pp. 18,20) that carbonaceous particles are manifested primarily in irregular shapes, while mineral and magnetic particles are primarily of spherical shape. This may explain some of the difference between the surface areas of carbonaceous particles and those of bulk ashes, which are comprised primarily of mineral, and to a lesser extent, magnetic particles.

Griest and Tomkins [52] also noted a direct correlation between the ability of a coal ash or fraction thereof to retain a representative PAH (benzo[a]pyrene) and the carbon content of that ash/fraction. Using techniques similar to those employed by Soltys and co-workers, they measured specific surface area, total % carbon, and sorptivity of a stack ash that had been fractionated according to particle size. Those results are listed in **Table 1.10**. Note that sorptivity increases with carbon content, but decreases with specific surface area. Again, any possible contribution to sorptivity by specific surface area may be masked by differences in sorptivity due to carbon content.

TABLE 1.10 SORPTIVITIES OF SIZE FRACTIONATED COAL STACK ASH

Size fraction, μm	Surface area, m^2/g	% Carbon	Sorptivity[a]
< 2.3	1.71	1.1	4.7
2.3 - 3.3	1.19	0.71	0.8
3.3 - 6.3	0.99	0.90	ND[b]
6.3 - 14	0.60	1.3	8.5
14 - 21	0.57	3.8	2.5
21- 150	0.46	6.5	190
bulk ash	0.82	2.0	2.7

[a]units = [ng benzo[a]pyrene/mg ash]/[ng benzo[a]pyrene/mL solvent].
[b]sorptivity not detected.
Source: Griest, W.H.; Tomkins, B.A.; *Environ. Sci. Technol.*, **1986**, *20*, 292.

Griest and Tomkins also determined sorptivities of benzo[a]pyrene on three separate bulk coal stack ashes of varying carbon content. These results are presented in **Table 1.11**. Again, sorptivity was directly proportional to the carbon content of the ash.

They also separated two coal stack ashes according to particle size, then further separated one of the fractions (21-150 μm) into magnetic and non-magnetic subfractions. The nonmagnetic subfraction was separated into mineral and carbonaceous subfractions by further size fractionation (i.e., exploiting the fact that carbon content increases with particle size). They then measured specific surface area, total carbon content, and sorptivity for each ash sample and specific surface area and sorptivity for each of several *model* adsorbents. These results are listed in **Table 1.12**. Again, the most highly retentive surfaces (for benzo[a]pyrene) were those fractions highest in carbon content. Of surfaces derived from ash 1, the mineral subfraction was found to be the weakest adsorbent. The magnetic subfraction was the weakest adsorbent of fractions originating from ash 2. Note that the porous glass beads, with 100 times the specific surface area of any of the ash fractions and with a specific surface area significantly

TABLE 1.11 SORPTIVITIES OF REPRESENTATIVE COAL STACK ASHES

Ash	% Carbon	Sorptivity[a]
1	0.93	7.9
2	2.0	27
3	12.5	1300

[a]units = [ng benzo[a]pyrene/mg adsorbent]/[ng benzo[a]pyrene/mL solvent].
Source: Griest, W.H.; Tomkins, B.A. *Environ. Sci. Technol.*, **1986**, *20*, 293.greater than either of the two

TABLE 1.12 SORPTIVITIES OF COAL STACK ASH, FRACTIONS, MODEL ADSORBENTS

Adsorbent	% Carbon	Surface area, m^2/g	Sorptivity[a]
Ash # 1, bulk (21-150 μm)	21.08	1.42	1100
mineral fraction	5.24	1.14	110
magnetic fraction	13.0	0.69	340
carbonaceous fraction	35.1	2.40	1200
Ash # 2, bulk (21-150 μm)	6.52	0.42	190
mineral fraction	7.22	0.26	65
magnetic fraction	0.33	0.41	2.1
carbonaceous fraction	48.1	1.20	6000
Porous glass beads	- - -	169	11
Amorphous carbon black	- - -	8.21	9200
Graphite	- - -	13.2	2700

[a]units = [ng benzo[a]pyrene/mg ash]/[ng benzo[a]pyrene/mL solvent].
Source: Griest, W.H.; Tomkins, B.A. *Environ. Sci. Technol.*, **1986**, *20*, 293.

greater than either of the two carbonaceous model adsorbents, had, with the exeption of the magnetic subfraction of ash 2, the least affinity for PAH. There was no direct correlation between specific surface area and sorptivity among the ash samples.

Finally, Dunstan and co-workers [44] have used a gas-solid chromatographic technique to approximate heats of adsorption for fractions of a representative coal stack ash. The ash was first fractionated according to particle size, then further fractionated according to chemical composition. Heats of adsorption measurements were carried out by injecting known amounts of PAH (pyrene) onto columns packed with the various fractions, and then monitoring the amount of PAH that eluted as a function of temperature. They found that the relative retention of pyrene was greatest for the carbonaceous fraction, followed by the mineral fraction. The magnetic fraction was the weakest adsorbent. Expressed as a ratio, the weight of pyrene sorbed on these subfractions, under equilibrium (reversible adsorption/desorption) conditions, followed the relation: 100: 2.5: 1, carbonaceous: mineral: magnetic.

Two primary mechanisms have been postulated to explain the affinity of carbonaceous surfaces for PAH. It has already been pointed out (p. 20) that carbonaceous particles have highly porous, irregular shapes and, in general, have higher specific surface areas than particles low in carbon content (see, for example, results in **Tables 1.8**, p. 27, and **1.9**, p. 28). Results presented in this section, however, do not establish a direct link between specific surface area and sorptivity. In all cases, though, there was a direct link between sorptivity and carbon content. Fisher *et al.* [18], and Masclet and co-workers [30] suggest that PAH adsorption on coal fly ash is partially a *chemisorption*, i.e., an adsorption influenced by the *chemical* properties of adsorbate and adsorbent. Soltys and co-workers [41] carried out solid-phase NMR analyses of carbonaceous particles and determined that the carbon of such surfaces was found to be partially *graphitic*. The fused planar ring structure of graphite is aromatic in nature [53]. Fitch and Smith [54] have pointed out that dispersion forces between large aromatic molecules and surfaces which are aromatic in nature may result in strong adsorption. This may explain at least part of the affinity of PAH for coal fly ash, particularly for carbonaceous components thereof.

It should be pointed out, however, that, based on results presented in **Table 1.12**, p. 30, some other type of PAH/carbonaceous particle interaction is also likely. The measured sorptivity of pure graphite was no greater than that of the carbonaceous subfraction of ash 1, and was significantly less than that of the carbonaceous fraction of ash 2, and of the carbon black sample. The latter adsorbent was described as a petroleum-derived substance of amorphous, polyhedral morphology. It was pointed out on p. 22 that the elemental carbon content of carbonaceous coal fly ash particles may be partially oxidized. Soltys and co-workers [41] speculate that undefined interactions between PAH and surface oxygen species may be partly responsible for the affinity of carbonaceous particles for PAH. It is possible that the carbonaceous fractions of ashes 1 and 2 and the amorphous carbon black of **Table 1.12** (p. 30) contain a greater degree of oxidized carbon than the graphite sample used in the cited work.

1.6 Transformations of Atmospheric PAH

According to Atkinson *et al.* [55], gaseous organic compounds such as PAH may be degraded in the atmoshere primarily by three reaction pathways: photolysis, reaction with ozone, and reaction with hydroxyl radical. Investigations with PAH containing four or fewer rings, which exist in the ambient environment primarily in the gas phase, indicate that the primary loss process is reaction with hydroxyl radical to form oxygenated or, in the presence of NO_x, nitrated products [56-58].

Potential atmospheric decay routes for particle-associated PAH have, likewise, been extensively investigated. The effect of humidity, temperature, and sunlight on PAH decay [59] and the likelihood of reactions with atmospheric chemical species such as SO_2 [60], ozone [60,61], and potential nitrating species such as NO_2, N_2O_5 and HNO_3 [60-65] has been evaluated for PAH associated with model adsorbents such as glass fiber and Teflon filters and with atmospheric soot particles. Attention has also been devoted to the photochemical transformations of PAH associated with particles [61].

Figure 1.7 shows a portion of the electromagnetic spectrum of sunlight. Included is solar radiation in the 290-700 nm region. This range includes near-UV and visible photons that can be absorbed by organic molecules such as PAH and have sufficient energy to initiate photochemical reactions. Of particular importance is radiation in the 290-400 nm region, where PAH are prone to absorb [66]. Solar intensity is expressed in units of photons per unit area per unit time. Atmospheric solar intensities are typically 10^{15} to 10^{17} photons/cm^{2}s [67,68]. The solar intensity may be attenuated by atmospheric species which scatter or absorb light, or may be diminished as a function of season, time of day, climatic conditions, or height above the earth's surface [68]. The range of potential photochemical processes for PAH includes photodissociation, intermolecular rearrangement, photoisomerization, hydrogen atom abstraction, and photosensitized reactions (e.g, with O_2) [69].

The photochemical behavior of particle-associated PAH has been studied for a number of model adsorbents. Korfmacher and co-workers [70,71] evaporated solutions containing benzo[a]pyrene and anthracene onto alumina-based thin layer chromatography plates (the general procedure hereafter referred to as *solution* deposition). They irradiated prepared plates under a xenon lamp. A 40-50 % loss of benzo[a]pyrene was observed after an 80 minute exposure, while 95 % of anthracene disappeared after 3 hours of irradiation.

Behymer and Hites [72,73] measured photolytic half lives of several PAH on silica gel and alumina. They prepared samples by solution deposition, then subjected each to irradiation under a mercury vapor lamp. Results are presented in **Table 1.13**. PAH showed a wide range of half lives, indicating that the extent of photolysis was compound-dependent.

Yokley *et al.* [74] and Dunstan *et al.* [44] deposited pyrene and benzo[a]pyrene from the vapor phase (by passing gas phase PAH in N_2 through an expanded bed of adsorbent) onto silica gel, alumina, and controlled pore glass. Samples were then subjected to irradiation with a xenon lamp for 24 hours. Baseline and post-irradiation coverages were quantified. Results are summarized in **Table 1.14**. Significant photodegradation was evident on each of the substrates. It should be pointed out that the

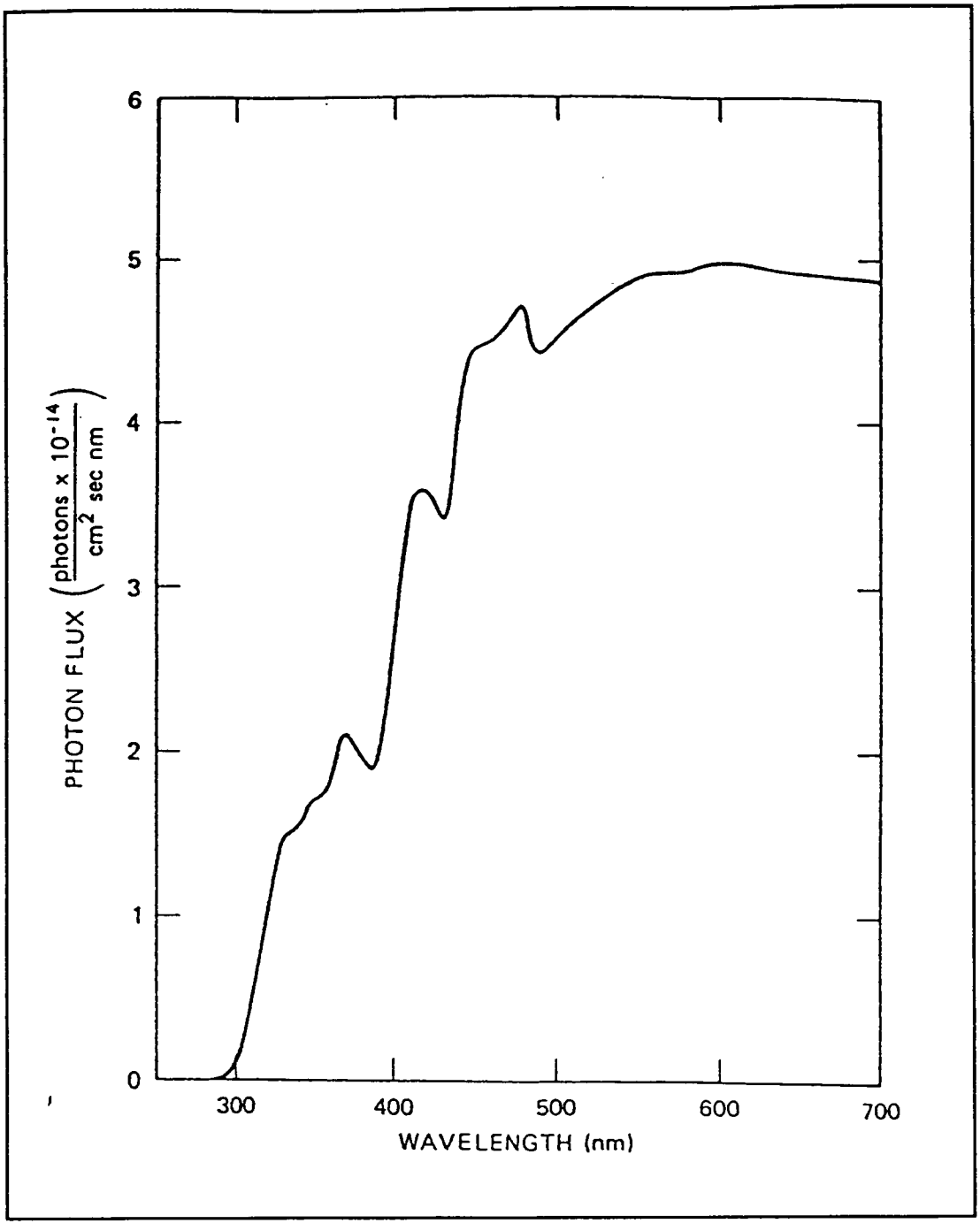

Figure 1.7 Solar intensity as a function of wavelength.
Source: Dublin, D.; Mill, T. *Environ. Sci. Technol.*, **1982**, *16,* 815.

TABLE 1.13 PHOTOLYTIC HALF LIVES (IN HR) OF PAH ON MODEL ADSORBENTS

PAH	Silica gel	Alumina
acenaphthylene	0.7	2.2
fluorene	1.0	62
dibenzothiophene	18	45
phenanthrene	150	45
anthracene	2.9	0.5
fluoranthene	74	23
pyrene	21	31
benz[a]anthracene	4.0	2.0
chrysene	100	78
benzo[e]pyrene	70	110
benzo[a]pyrene	4.7	1.4
perylene	3.9	1.2

Source: Behymer, T.D.; Hites, R.A. *Environ. Sci. Technol.*, **1985**, *19*, 1005.

TABLE 1.14 PHOTODEGRADATION (% LOSS) OF PAH ON MODEL ADSORBENTS[a]

PAH	Silica gel	Alumina	Controlled pore glass
Pyrene	79 %	99 %	86 %
Benzo[a]pyrene	93 %	60 %	96%

[a]24 hr illumination.

Source: Dunstan, T.D.J.; Mauldin, R.F.; Zhong, J.; Hipps, A.D.; Wehry, E.L.; Mamantov, G. *Environ. Sci. Technol.*, **1989**, *23*, 305.

primary expected photoproducts of sorbed PAH are oxygenated species, such as quinones, epoxides, and lactones [10,70,72,75].

Korfmacher *et al.* [70,71] were the first to observe that photochemical degradation of PAH was inhibited when PAH are associated with coal stack ash. They deposited five representative PAH from the vapor phase onto samples of size fractionated (particle size = 45-74 μm) coal stack ash. Samples were irradiated with light from a variety of sources. These sources, and results for benzo[a]pyrene, one of the representative PAH studied, are listed in **Table 1.15**. Results are also listed for samples that were not subjected to irradiation (source listed as *none*). Note that there was no apparent photodegradation of this compound when sorbed on coal stack ash, relative to experiments in which samples were not subjected to irradiation. Contrast these results with those for model adsorbents in **Table 1.14**. Anthracene, 95 % of which disappeared after irradiation on an alumina plate, was likewise found to exhibit little or no photoreactivity when adsorbed on this coal stack ash.

Several possible explanations for the tendency of coal ash to suppress the photolysis of PAH were listed by Korfmacher *et al.* [71]. It has been pointed out previously (pp. 20,22) that coal stack ash surfaces contain appreciable concentrations of metallic species. Metal ions are known to be efficient *quenchers* of photochemically excited states of organic molecules [76]. Their presence on coal stack surfaces, then, may be partially responsible for this tendency. However, no further evidence to support this hypothesis has been reported. The ability of coal ash to suppress photolysis of PAH may be due to an *inner filter* effect [77], which can be described as a decrease in absorption of incident light by a given analyte due to the coexistence of a second species which absorbs some fraction of the light. It was pointed out previously that coal stack ash surfaces are highly porous (p. 27), and dark in color (p. 20). PAH may, therefore, be entrapped in pores and *shielded* from incident light.

Behymer and Hites [72] carried out solution depositions of several PAH onto coal stack ash (150-250 μm particle size). Photolytic half lives were determined, as described previously for model adsorbents (p. 35), for PAH on this adsorbent and for those found on carbon black. These results are

TABLE 1.15 PHOTODEGRADATION OF BENZO[A]PYRENE ON COAL STACK ASH

Light source	Illumination period, hr	% Loss
sunlight	3.8	17 %
sunlamp	23	10 %
xenon lamp	5	14 %
mercury lamp	6	9 %
quartzline	11.3	16 %
none	190	11 %
none	1335	18 %

Source: Korfmacher, W.A.; Wehry, E.L.; Mamantov, G.; Natusch, D.F.S. *Environ. Sci. Technol.*, **1980**, *14*, 1096.

summarized in **Table 1.16**. Contrast half lives for these adsorbents with those for model adsorbents listed in **Table 1.13** (p. 35). Half lives for coal stack ash and for carbon black are larger, often significantly so, than those for model adsorbents. Note also that, in contrast to those for model adsorbents, half lives for coal stack ash are quite similar, indicating that photolysis is substrate-dependent.

These authors noted that silica gel and alumina are light in color and that coal stack ash and carbon black are quite dark. They measured specific surface areas of all adsorbents. They postulated that the greater surface areas of silica gel (637 m^2/g) and alumina (224 m^2/g) relative to those of their coal stack ash material (5.10 m^2/g) and carbon black (11.6 m^2/g) may allow a greater dispersion of PAH on the adsorbent surface, and, hence, greater *access* to incident light. In view of the larger photolytic half lives for PAH on carbon black, which was no darker than the coal stack ash but which undoubtedly contained a higher percentage of carbon, they speculated that the suppression of photolysis of PAH on coal ash could also be influenced by the chemical composition of the ash, particularly its carbon content.

TABLE 1.16 PHOTOLYTIC HALF LIVES (IN HR) OF PAH ON COAL STACK ASH

PAH	Coal stack ash	Carbon black
acenaphthylene	44	170
fluorene	37	> 1000
dibenzothiophene	49	> 1000
phenanthrene	49	> 1000
anthracene	48	310
fluoranthene	44	> 1000
pyrene	46	> 1000
benz[a]anthracene	38	650
chrysene	38	690
benzo[e]pyrene	25	> 1000
benzo[a]pyrene	31	570
perylene	33	570

Source: Behymer, T.D.; Hites, R.A. *Environ. Sci. Technol.*, **1985**, *19*, 1005.

Yokley and co-workers [74] evaluated photoreactivities of vapor-deposited pyrene and benzo[a]pyrene on several coal stack ashes (45-75 μm particle size). Specific surface area, total carbon content and % iron (by ion microprobe analyses) values of ashes were also determined. These results are summarized in **Table 1.17**. Ash designations denote the source (i.e., power plant) from which obtained. Note that ashes high in carbon (KA), iron (WK, IL) or carbon and iron (EA) were more effective at suppressing photolysis of PAH than those ashes low in carbon and iron (TX, AR). The one exception to this trend was behavior on ET ash, which was low in carbon and iron, but which did effectively suppress photolysis of PAH. This ash, however, did have a relatively large specific surface area. No photochemical degradation was evident for PAH on graphite.

TABLE 1.17 PHOTODEGRADATION (% LOSS) OF PAH ON COAL STACK ASH[a]

Adsorbent	% C	% Fe	Surface area, m^2/g	% loss of Pyrene	% loss of Benzo[a]pyrene
KA	2.8	- - -	3.15	7 %	17 %
ET	0.5	1.7	4.01	5 %	4 %
EA	1.8	10.9	- - -	0 %	8 %
UK	0.3	16.9	- - -	3 %	12 %
IL	0.3	16.5	- - -	6 %	13 %
TX	0.5	3.4	2.61	35 %	53 %
AR	0.3	4.0	0.84	66 %	18 %
graphite	- -	- - -	4.43	< 1 %	0 %

[a]24 hr illumination.

Source: Yokley, R.A.; Garrison, A.A.; Wehry, E.L.; Mamantov, G. *Environ. Sci. Technol.*, **1986**, *20*, 86.

These authors also determined pore sizes (extension of BET method) for graphite and for several of the coal stack ashes studied. They concluded that the surfaces of these adsorbents were sufficiently porous to entrap PAH. Given the dark color of the adsorbents used, the suppression of PAH photolysis may, in fact, be due to the *inner filter* phenomenon described previously (p. 36).

Behmeyer and Hites [73] studied the photochemical behavior (laboratory irradiations) of 18 representative PAH on 15 typical coal stack ashes. They likewise found that coal stack ashes which had high (> 5 %) carbon and were dark in color were more effective at suppressing photolysis of PAH than those low in carbon content and light in color.

Dunstan *et al.* [44] fractionated two coal stack ashes according to particle size and chemical composition. The < 45 μm size fraction of the bulk ashes and the 75-124 μm fractions of carbonaceous, magnetic, and mineral subfractions were analyzed for % carbon. The subfractions were also analyzed for iron content (atomic absorption, results expressed as % Fe_2O_3). Pyrene was deposited from the

vapor phase onto these adsorbents and samples were irradiated for 24 hours with a xenon lamp. Photochemical losses of pyrene were also evaluated for three iron- and carbon-containing *model* adsorbents. These results are summarized in **Table 1.18.** Note that, of the two bulk ashes, the one with the higher carbon content (KA) was more effective at suppressing pyrene photolysis. For the subfractions, the carbonaceous particles were quite effective at suppressing photolysis. The magnetic subfractions were somewhat less effective, and the mineral subfractions permitted the most loss. Note also that practically no photodegradation was observed for graphite and the two iron oxides. These results reinforce the notion that carbon and/or iron content significantly influence the photochemical behavior of PAH on coal ash.

TABLE 1.18 PHOTODEGRADATION OF PYRENE ON COAL ASH, MODEL ADSORBENTS[a]

Adsorbent	% C	% Fe_2O_3	% Loss of pyrene
KA, bulk	2.8	- - -	7 %
mineral fraction	0.25	4.5	32 %
magnetic fraction	0.64	50	8 %
carbonaceous fraction	36	2.9	3 %
TX, bulk	0.5	- - -	21 %
mineral fraction	0.65	3.5	26 %
magnetic fraction	0.15	52	15 %
carbonaceous fraction	23	2.4	3 %
graphite	- -	- - -	1 %
Fe_2O_3	- -	- - -	2 %
Fe_3O_4	- -	- - -	2 %

[a]24 hr illumination.

Source: Dunstan, T.D.J.; Mauldin, R.F.; Zhong, J.; Hipps, A.D.; Wehry, E.L.; Mamantov, G. *Environ. Sci. Technol.*, **1989**, *23*, 305.

Finally, Miller *et al.* [78] studied the photoreactivity of pyrene on fractions of a high carbon stack ash as a function of the carbon and iron content and specific surface areas of the fractions. Significant photolysis of pyrene occurred only for those fractions low in carbon content (0.4-0.7 %) and with low specific surface areas (0.50-0.60 m^2/g). Fractions with a carbon content of 4 % or greater and surface areas of 2.85 m^2/g and higher allowed no detectable photodegradation. No definite correlation was observed between iron content and photochemical reactivity.

The photochemical behavior of a particle-associated PAH can thus be thought of as a function of several parameters. The physical and chemical properties of the substrate are of chief importance. Of these properties, carbon content and surface area seem to be the most important in governing the ability of a given ash to suppress photolysis of sorbed PAH. Other surface properties of fly ashes (such as the presence of metal ions that act as effective excited-state quenchers) may also play important roles in specific situations, but do not appear to be of broad general significance.

1.7 The Importance of Nitro-Substituted PAH

It has become apparent in recent years that all of the mutagenic activity of the organic compounds associated with coal fly ash and other atmospheric particles cannot be attributed solely to PAH [6]. Indeed, only a small fraction of that mutagenicity can justifiably be attributed to PAH content.

Evidence now exists that polar derivatives of PAH are responsible for some of the unaccounted-for mutagenicity. For instance, Wang *et al.* [79] and Talcott and Harger [80] showed in the early 1980s that nitro-substituted compounds were present on airborne particulate matter and contributed to the mutagenicity of those particles. Since that time nitro-substituted PAH have been detected on coal fly

ash [81], on diesel particulate matter [82-84], and on atmospheric particles sampled in urban [85-87] and rural [88] environments. In fact, Paputa-Peck and co-workers [83] isolated and identified over seventy-five examples of this compound class on diesel particulate matter. Parallel evaluations have revealed that many nitro-PAH are strong, direct-acting mutagens [89-92], often exhibiting significantly more mutagenic activity than the parent from which they derive [6]. Nitro-PAH have also been shown to be phototoxic [93].

A particular class of these compounds, the nitropyrenes, are believed to be particularly ominous [90-92]. Especially worthy of note are the dinitropyrenes, which are among the most potent mutagenic compounds reported to date [90,91]. Siak and co-workers assert that mono- and di-substituted nitropyrenes are responsible for as much as 3 % of the overall mutagenicity of atmospheric particles [91]. Rosenkranz [92] has estimated that annual worldwide emissions of nitropyrenes may soon exceed 30,000 kg.

Pitts and co-workers have suggested that 2-nitrofluoranthene and 2-nitropyrene are the most abundant nitro-PAH found on atmospheric particles sampled at locations far removed from combustion sources [94]. These two compounds, however, have never been identified on particulate matter sampled at or near combustion sites, suggesting that they are the result of atmospheric transformations of parent molecules. It is believed that one of the primary routes to formation of atmospheric nitro-PAH is an OH radical-activated addition of NO_2 (OH in the presence of NO_x) to gaseous parent followed by condensation of the less volatile product [57,58,95].

For gas-phase pyrene, the reaction is believed to be

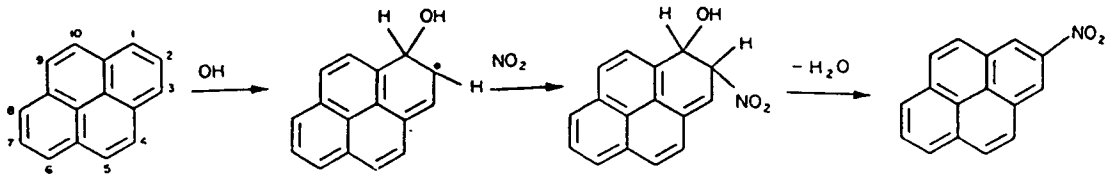

and this reaction scheme does yield 2-nitropyrene. Similarly, 2-nitrofluoranthene is the primary product of the reaction of fluoranthene with OH/NO_x [95]. Indeed, in laboratory simulations, this is the only reaction scheme that leads to these nitro-substituted compounds [95]. Other reaction schemes which utilize other possible atmospheric nitrating species (e.g., NO, NO_2, NO_3, N_2O_5, and HNO_3) do not yield these products, but one or more of these are doubtless responsible for formation of other atmospheric nitro-PAH.

Particle-associated nitro-PAH are presumably susceptible to the same type of atmospheric transformations as their unsubstituted counterparts. Little work, however, has been done to investigate these processes. Grosjean and co-workers found 1-nitropyrene to be resistant to attack by O_3, SO_2, and NO_2 when adsorbed onto Teflon and glass filters [96]. Atkinson *et al.* evaluated the gas phase chemistry of nitro-PAH in the presence of simulated sunlight, N_2O_5, OH, and NO_3 [97]. They concluded that, under atmospheric conditions, the primary route to nitro-PAH decay is through photolysis.

The validity of this assertion has not been evaluated for particle-bound nitro-PAH. Also not understood is the nature of nitro-PAH/coal fly ash interactions. Again, nitro-PAH are an important class of PAH derivatives. Not only are they quite prevalent in the environment and potentially more dangerous than unsubstituted PAH, but they are also more likely, as a compound class, to be associated with particles because they are more polar and, therefore, less volatile than the parent PAH from which they derive. This adds further weight to the importance of their atmospheric chemistry.

1.8 The Importance of Other Atmospheric Organic Compounds

In addition to PAH and atmospherically derived analogues, there are many aliphatic compounds prevalent in the environment that are likewise associated with anthropogenic emissions. These include

n-alkanes and alkenes [48,49,98-100], aldehydes and ketones [98], and carboxylic acids [98-102]. Depending on their availability and chemical nature, these compounds may be less volatile than PAH and be preferentially adsorbed on atmospheric particles such as coal fly ash. They may, in so doing, change the chemistry of the surface that a PAH encounters on first contact and/or provide a medium in which PAH may *dissolve*. Those aliphatic hydrocarbons with volatilities similar to those of PAH may compete with PAH for active surface sites. Those which are more volatile may be, in effect, layered on top of sorbed PAH.

In addition to the potential effect on the nature and extent of the interaction of PAH with coal fly ash, these phenomena may also impact on the efficiency of particle-associated PAH transformation processes such as photolysis. Such behaviors have not been widely investigated. Masclet and co-workers assert that any correlation between PAH adsorption and the specific surface area of a particle is complicated by the presence of other organic compounds with a strong affinity for the particle [30].

In another study, Koester and Hites noted a decrease in the extent of photodegradation of polychlorinated dibenzo-p-dioxins and polychlorinated dibenzofurans sorbed on silica gel when they were co-deposited on the silica gel with organic compounds extracted from incinerator fly ash samples [103]. They concluded that the organic compounds present in the extracts from the incinerator fly ash could be shielding the chlorinated compounds from incident light (i.e., an *inner filter* effect).

Many of these aliphatic compounds are at levels in the environment comparable to those at which PAH and related compounds are found [98-101]. **Table 1.19** lists levels of *n*-alkanes and carboxylic acids found on atmospheric particulate matter sampled at rural locations. It has already been pointed out (p.14) that atmospheric concentrations of PAH range from sub-ppt to low ppb levels. Values for *n*-alkanes and carboxylic acids on atmospheric particulate matter sampled near industrial and/or urban areas would be expected to be significantly higher than those found in **Table 1.19**. The effect of the presence of these compounds as coadsorbates on the atmospheric behavior of particulate PAH and their derivatives might be quite profound.

TABLE 1.19 CARBOXYLIC ACIDS, *n*-ALKANES DETECTED ON ATMOSPHERIC PARTICULATE MATTER

Compound name	Molecular formula	Average concentration at 3 rural sites, ppt
succinic acid	$C_4H_6O_4$	3.3
glutaric acid	$C_5H_8O_4$	6.1
palmitic acid	$C_{16}H_{32}O_2$	1.5
stearic acid	$C_{18}H_{36}O_2$	0.05
heneicosane	$C_{21}H_{44}$	0.1
tricosane	$C_{23}H_{48}$	0.1
tetracosane	$C_{24}H_{50}$	0.07
pentacosane	$C_{25}H_{52}$	0.12

Source: Barkenbus, B.D.; MacDougall, C.S.; Griest, W.H.; Caton, J.E. *Atmos. Environ.*, **1983**, *17*, 1542.

1.9 Focus of the Dissertation Research

Chemical and physical factors possibly influencing the nature and extent of the interaction of coal fly ash particles with toxic organic compounds have been extensively evaluated in this and other laboratories. Also investigated was the effect of coal fly ash surfaces on the photoreactivity of these compounds. These studies have, for the most part, dealt with unsubstituted PAH in the absence of other potential adsorbates.

Among the range of logical next steps for the direction of this research are extensions into the realm of atmospherically relevant substituted PAH and into an investigation of particle-associated PAH photochemistry in the presence of coadsorbates. Toward those ends, the focus of the dissertation research has centered on three main areas:

1. Fractionation and characterization of a coal stack ash with respect to parameters most likely to influence PAH and nitro-PAH association and photoreactivity; these parameters include particle size and chemical composition, with particular emphasis on carbonaceous, mineral magnetic, and mineral non-magnetic content.
2. Investigation of the behavior of 1-nitropyrene, a representative nitro-PAH, when sorbed onto particles. The behavior of this compound is compared with that of its unsubstituted precursor, pyrene. This study includes a comparison of compound/coal fly ash retention as a function of the chemical composition (carbonaceous, mineral magnetic, mineral non-magnetic) of the ash. Also to be compared is the extent of photochemical degradation of 1-nitropyrene and pyrene as a function of the chemical composition of the ash.
3. Investigation of the behavior of pyrene sorbed onto coal stack ash whose surface has been largely covered by succinic acid, an environmentally important dicarboxylic acid. A similar investigation is reported for coal stack ash-associated pyrene over which *n*-decane, a representative *n*-alkane, has been deposited. Again, behavior (pyrene/ash retention and photochemistry) is evaluated as a function of the chemical composition of the ash.

Following a description of the methods and materials used in these experiments, subsequent chapters will deal, in order, with each of these topics.

CHAPTER 2

EXPERIMENTAL MATERIALS AND METHODS

2.1 Introduction

The research areas outlined at the end of the preceding chapter (p. 46) mandate the implementation of a variety of experimental techniques. These include:

1. methods designed to separate a bulk coal stack ash into fractions according to particle size and chemical components and to quantify important chemical constituents of these fractions.
2. methods designed to mimic the atmospheric adsorption of PAH and related compounds onto coal stack ash surfaces.
3. methods designed to mimic the atmospheric exposure of sorbed PAH/related compounds to sunlight.
4. methods used to extract PAH and related compounds from the surfaces of adsorbents and to quantify surface coverage levels following deposition and/or irradiation experiments.

Subsequent sections of this chapter describe materials and methods used in these experiments. Rationales for the choices of specific materials and experimental approaches will be provided when necessary in the chapter which discusses experiments in which they were used.

2.2 Fractionation and Characterization of Coal Stack Ash

2.2-A Coal Stack Ash Material

The coal stack ash used in these studies, designated as *Kaneb* (KA) ash, was obtained from the electrostatic precipitator of the McIntosh coal-fired power plant in Lakeland, Florida. This facility was operating inefficiently at the time of collection, and this coal stack ash, therefore, has an unusually high percentage of carbon. It has been determined [44] that the bulk ash contains 5.5 % carbon.

2.2-B Fractionation of Coal Stack Ash According to Particle Size

Bulk samples of Kaneb coal stack ash were fractionated according to particle size by David Jenkins and Gary Woody, graduate students in this research group. They employed the procedure outlined by Mauldin in his dissertation [104]. Ash was passed successively through mechanical sieves of mesh size 150, 125, 75, and 45 μm. The five fractions so generated were given the general designation *U* for *unfractionated*. Each of the five fractions was further designated according to specific particle diameter. This procedure led to fractions designated as *U1* (< 45 μm particle diameter), *U2* (45-74 μm), *U3* (75-124 μm), *U4* (125-149 μm), and *U5* (> 150 μm). Of these, the Kaneb stack ash fraction U2 was chosen for further study.

2.2-C Fractionation of Coal Stack Ash According to Chemical Composition

2.2-C1 Removal of Ferromagnetic Particles

The Kaneb coal stack ash fraction U2 (45-74 μm) was separated into magnetic and non-magnetic subfractions using a procedure similar to that described by Mauldin [104]. A bar magnet in

a 50 mL beaker was passed 3-5 times over 25 g portions of the bulk ash. After each pass the magnet was removed from the beaker and the ferromagnetic particles adhering to the outside of the container were separated from the nonmagnetic particles left behind.

The bar magnet/beaker apparatus was then placed inside a 250 mL beaker. This device was then passed 3-5 times, as before, over the ferromagnetic-enriched subfraction previously generated. This second treatment favored the retention of the more strongly magnetic particles, and, therefore, resulted in further enrichment of the ferromagnetic subfraction, designated as *F2* (ferro-magnetic, size fraction 2). That portion of the ash which remained was designated *N2* (non-magnetic, size fraction 2).

2.2-C2 Separation of Mineral and Carbonaceous Particles

Kaneb coal stack fraction N2 (non-magnetic, 45-74 μm) was separated into mineral and carbonaceous enriched subfractions by exploiting the difference in density of the mineral and carbonaceous components. **Figure 2.1** is a schematic diagram of the device, termed the *elutriator*, used to effect such separations. This device was designed and its use described by Sanders [105]. The originally described procedure was closely followed in carrying out these separations.

Four-gram portions of the Kaneb N2 subfraction were placed on the frit shown at the base of the elutriator. The device was secured with a clamp at the O-ring. A water saturated stream of prepurified nitrogen (supplied by National Welders) was allowed to pass through the frit with a velocity (controlled by an upstream rotameter) sufficient to generate a fluidized bed of adsorbent. The downstream funnel created a high velocity region above the fluidized bed, and, with appropriate manipulation of N_2 volume flow, the lighter carbonaceous particles passed through the orifice and were deposited at the base of the outside of the funnel. The mineral particles remained suspended below the funnel orifice. Nitrogen eventually passed to a hood, or to the atmosphere, as shown. After the accumulation of carbonaceous particles ceased, the N_2 flow was stopped and the mineral and carbonaceous subfractions were removed. To further enrich the mineral subfraction and the yield of

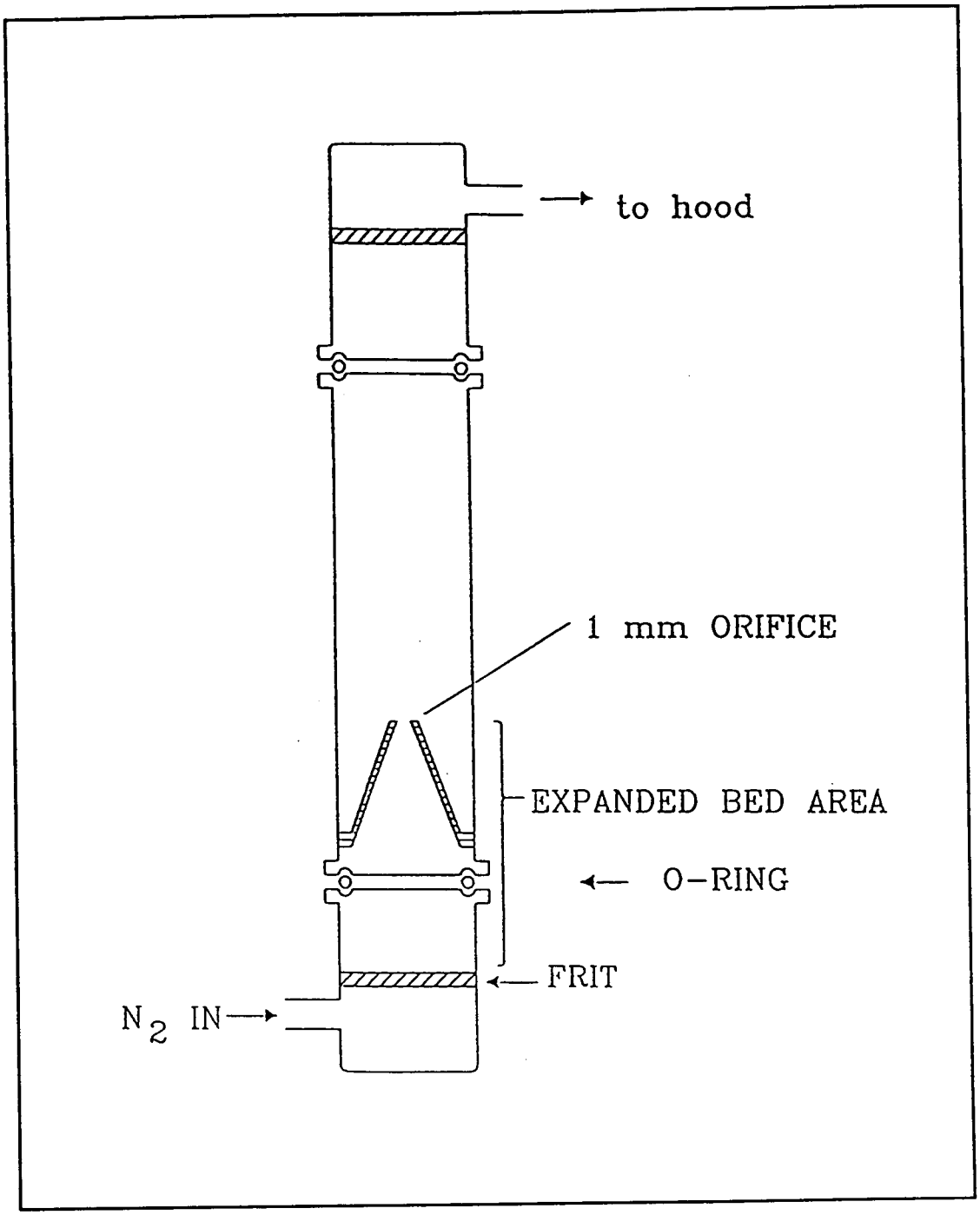

Figure 2.1 Schematic diagram of *elutriator*.
Source: Sanders, J.K. *Chromatographic and Spectroscopic Studies of the Interaction of Pyrene with Coal Stack Ash*, Ph.D. Dissertation, The University of Tennessee, Knoxville, 1991, 17.

the carbonaceous subfraction, small portions (1-2 g) of the mineral subfraction were subjected to a second elutriation. The subfractions so generated were designated as *M2* (mineral-enriched, size fraction 2) and *C2* (carbonaceous-enriched, size fraction 2). The entire fractionation procedure beginning with bulk Kaneb ash is summarized in **Figure 2.2.**

2.2-D Characterization of Coal Stack Ash and Its Subfractions

2.2-D1 Determination of % Carbon

Total carbon content of the unfractionated Kaneb stack ash, size fraction 2 (U2), as well as that of ferromagnetic (F2), carbonaceous (C2), and mineral (M2) enriched subfractions was determined by Galbraith Laboratories in Knoxville, TN. The analysis of each involved combustion of sample, followed by gravimetric determination of carbon as CO_2. Values are reported as % carbon by mass.

2.2-D2 Determination of % Iron

The iron content of the unfractionated Kaneb stack ash, size fraction 2 (U2), and of subfractions enriched in ferromagnetic (F2), carbonaceous (C2), and mineral (M2) content were carried out according to the procedure originally described by Nardkarni [106], and later modified by Miller *et al.* [78]. The method involves the dissolution/extraction of iron in a hydrochloric/nitric/hydrofluoric acid mixture with subsequent determination by atomic absorption spectrophotometry.

The basic procedure is as follows: a portion of each adsorbent was placed in a 50 mL Teflon beaker. In order to minimize the effects of static electricity, which tends to cause these samples to accumulate on container walls, samples were added through a glass funnel and thereby introduced into the bottom of the beaker. The exact amount of each adsorbent used was governed by the expected iron content. Sample masses ranged from 10 to 200 mg.

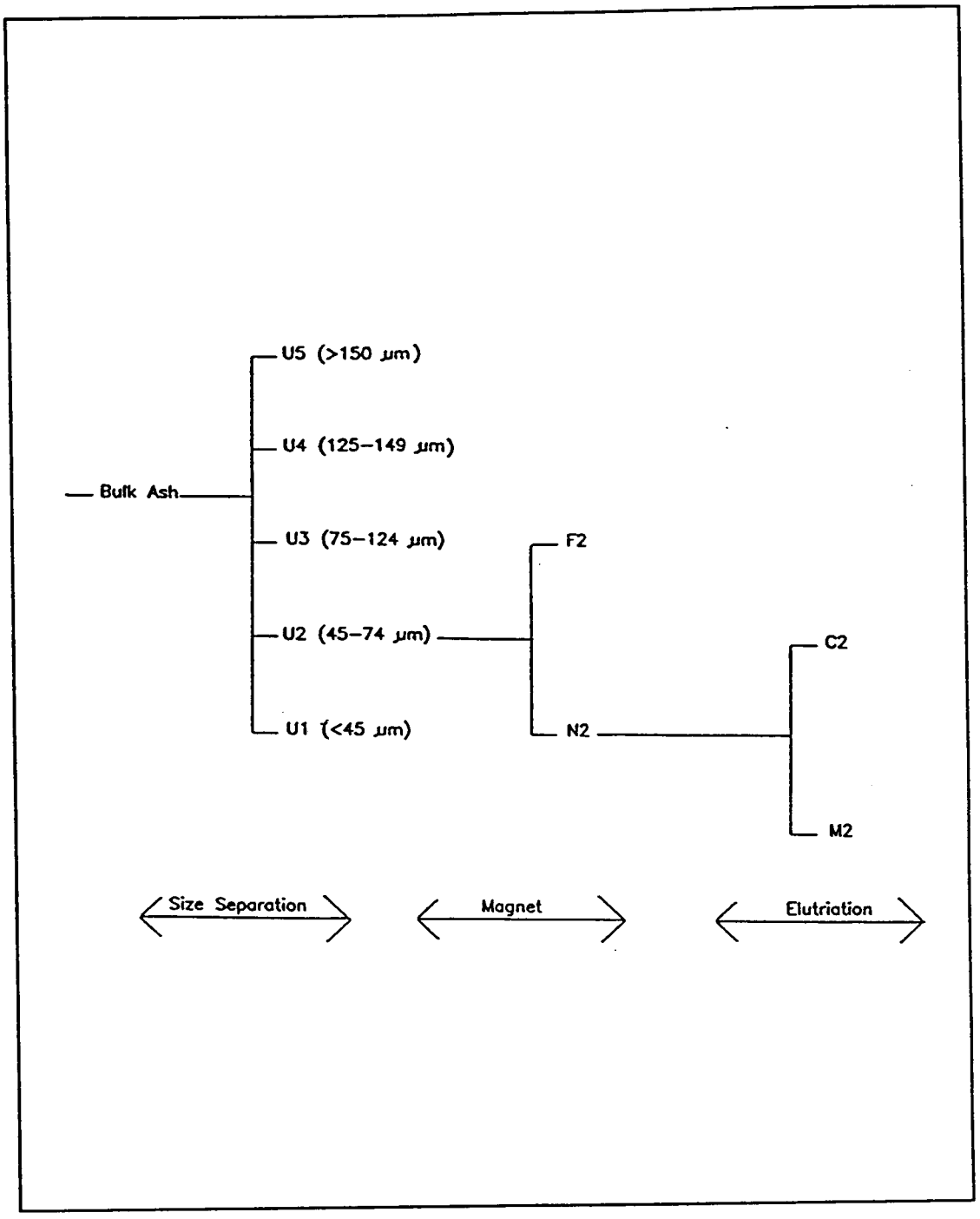

Figure 2.2 Fractionation scheme for Kaneb coal ash: size fraction 2 to subfractions.

To initiate dissolution and extraction of iron, 3 mL of hydrochloric acid (12 M), 1 mL of nitric acid (16 M) and 2 mL of hydrofluoric acid (29 M) were added to each sample. All acids were supplied by Mallinckrodt. Beakers were then covered with a small Pyrex watch glass, placed in a vacuum desiccator, and evacuated (two at a time) for 20 sec using a water aspirator (final pressure = 250-300 torr). The desiccator was then placed in a household 650 W microwave oven (Sharp Carousel), and its contents were heated for 3 minutes on a *high* setting. The desiccator was then removed, and vented and allowed to cool in a hood.

After samples had cooled, they were removed from the desiccator and the watch glasses and sides of the beakers were rinsed with distilled water. To each was then added 1.0 g of boric acid (Mallinckrodt) in a little hot water to complex the hydrofluoric acid. Samples were heated on a steam bath for 15-30 min, and then cooled. Solutions were then filtered (Whatman #5) into 100 mL glass volumetric flasks which contained 100 mg of La^{3+} (lanthanum chloride heptahydrate, Aldrich Chemical Company). This reagent was added to suppress interference by silicon. Samples were diluted to the mark and then assayed using a Varian atomic absorption spectrophotometer (model #1475) equipped with a hollow cathode lamp. Determinations were carried at 372.2 nm with an oxidizing air-acetylene flame (gases supplied by National Welders) and a lamp current of 5 mA. Analyses were calibrated against standard solutions of aqueous iron (III) oxide (Fe_2O_3 99.998%; Aldrich). The iron content of each adsorbent are reported as % Fe_2O_3 by mass.

2.3 Deposition of PAH and Related Compounds Onto Coal Fly Ash and Silica Gel

2.3-A Adsorbents

Kaneb ash fractions U2 (particle size 45-74 μm) and its subfractions F2 (ferromagnetic enriched), C2 (carbonaceous enriched) and M2 (mineral enriched) were used as adsorbents. Silica gel

(EM 60, particle size 0.063-0.200 mm, 70-230 mesh), obtained from Brinkman Instruments, Inc., was used as a *model* adsorbent. To remove adsorbed gases all adsorbents were subjected to a stream of prepurified nitrogen (National Welders) at 200° C for 24 hrs.

2.3-B Adsorbates

Adsorbates used in these studies included *n*-decane (Aldrich), pyrene (Aldrich), 1-nitropyrene (Aldrich), and succinic acid (Fisher Scientific Company). Adsorbates also evaluated but not used were 9-nitroanthracene, adipic acid, stearic acid, and tricosane. Each of these was supplied by Aldrich. All compounds were of 99 % or greater purity (except for 9-nitroanthracene, which was at 97 % purity) and were used as received. Because 1-nitropyrene is a suspected carcinogen (see p. 86), a dust/mist respirator was worn when working with the pure compound. Latex gloves were also worn on those occasions and when solutions and adsorbents containing 1-nitropyrene were handled.

2.3-C Depositions

2.3-C1 Solution Depositions

Solution depositions were carried out according to the procedure outlined by Mauldin [104]. One-mL aliquots of 500 ppm solutions of pyrene and 1-nitropyrene and of a 5000 ppm solution of succinic acid (all in UV grade methanol; American Burdick and Jackson) were pipetted onto 5 g samples of silica gel, contained in a 50 mL beaker. Samples were left, uncovered, overnight, to allow evaporation of solvent. Samples (100 μg/g silica gel in pyrene and 1-nitropyrene, and 10,000 μg/g in succinic acid) were then transferred to small glass vials for subsequent analysis. When not in use sample vials were stored in the dark in a desiccator.

2.3-C2 Vapor Depositions

Depositions of adsorbates from the vapor phase were carried out using an apparatus based on that originally described by Korfmacher [107]. The specific design employed included modifications outlined by Mauldin [104]. **Figure 2.3** is a schematic diagram of this apparatus. To mimimize exposure to potentially toxic adsorbate vapors, the entire system was contained in a fume hood.

The basic procedure used in carrying out vapor depositions is as follows: a small amount (1-2 g for solid adsorbates, 4-5 mL for liquid) of the adsorbate under study was placed in a glass diffusion cell and placed in an oven (Precision Mechanical Convection Oven, Model STM 40) maintained at a temperature about 5° C below the melting point of the adsorbate (or for liquids, about 100° C below the boiling point). The *oven 1* (see **Figure 2.3**) temperature controls, to a large extent, the mass flow rate of the adsorbate.

Sublimed adsorbate was delivered through the system by a stream (30-40 mL/min) of prepurified N_2 (National Welders) in 1/16" o.d. stainless steel tubing. Volume flow of carrier was controlled and maintained by a rotameter. A second oven (same design as oven 1) was maintained at a temperature of about 5° greater than that of oven 1 to prevent condensation of adsorbate on system plumbing. The oven 2 temperature controls, to a large extent, the quantity of adsorbate retained by the adsorbent.

A second diffusion cell (oven 2) contained an expanded bed of adsorbent (0.5-2 g) through which the adsorbate/carrier stream flowed. A detailed representation of the diffusion cell is contained in **Figure 2.4**. The main body of the cell contains a glass frit (25-50 μm pore diameter) on which the adsorbate or adsorbent resides. The main body is connected via clamps at the O-ring (Viton, Ace Glass, Inc.) joints at either end to Pyrex inlet and exit tubing. Both inlet and exit tubing are connected to upstream/downstream stainless steel tubing via Swagelok connectors. The exit section also contains a glass frit (25-50 μm pore diameter) to prevent adsorbate or adsorbent from entering downstream plumbing. **Figure 2.5** shows the diffusion cell used when *n*-decane, which is a liquid at room temperature, was used as the adsorbate. In this design the adsorbate is placed on a glass surface (in

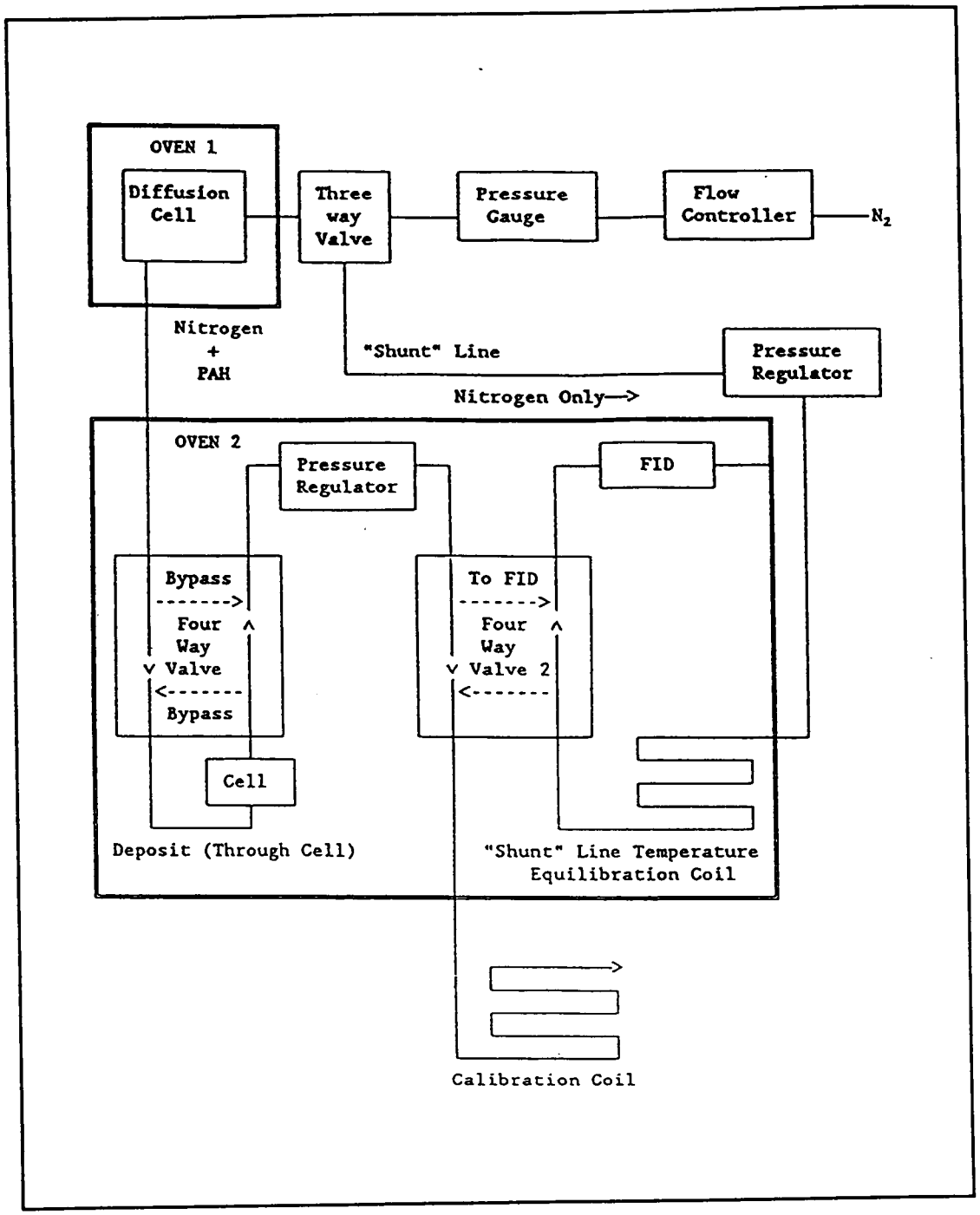

Figure 2.3 Schematic diagram of vapor deposition apparatus.
Source: Mauldin, R.F. *Photochemical and Supercritical Fluid Extraction Studies of Polycyclic Aromatic Hydrocarbons Adsorbed on Coal Stack Ash Particles*, Ph.D. Dissertation, University of Tennessee, Knoxville, 1990, p. 41.

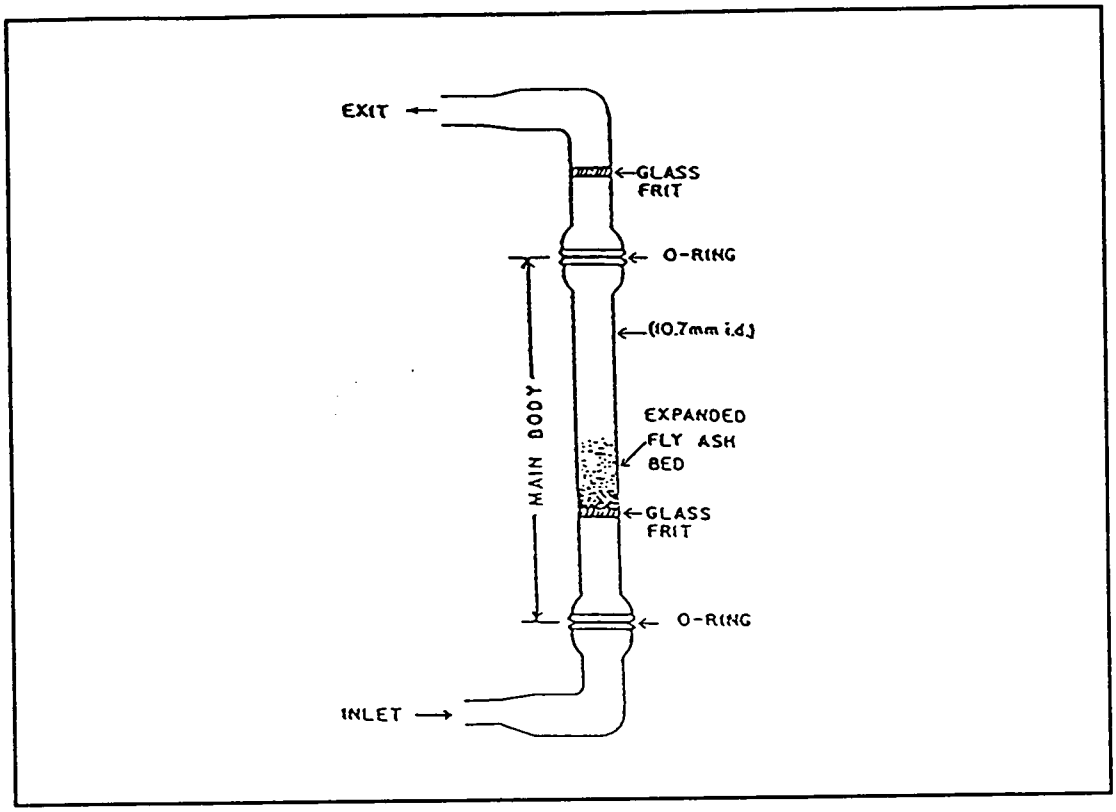

Figure 2.4 Schematic diagram of primary vapor deposition cell.
Source: Korfmacher, W.A. *The Decomposition of Organic Matter Adsorbed on Coal Fly Ash*, Ph.D. Dissertation, University of Illinois, Urbana-Champaign, 1978, p. 46.

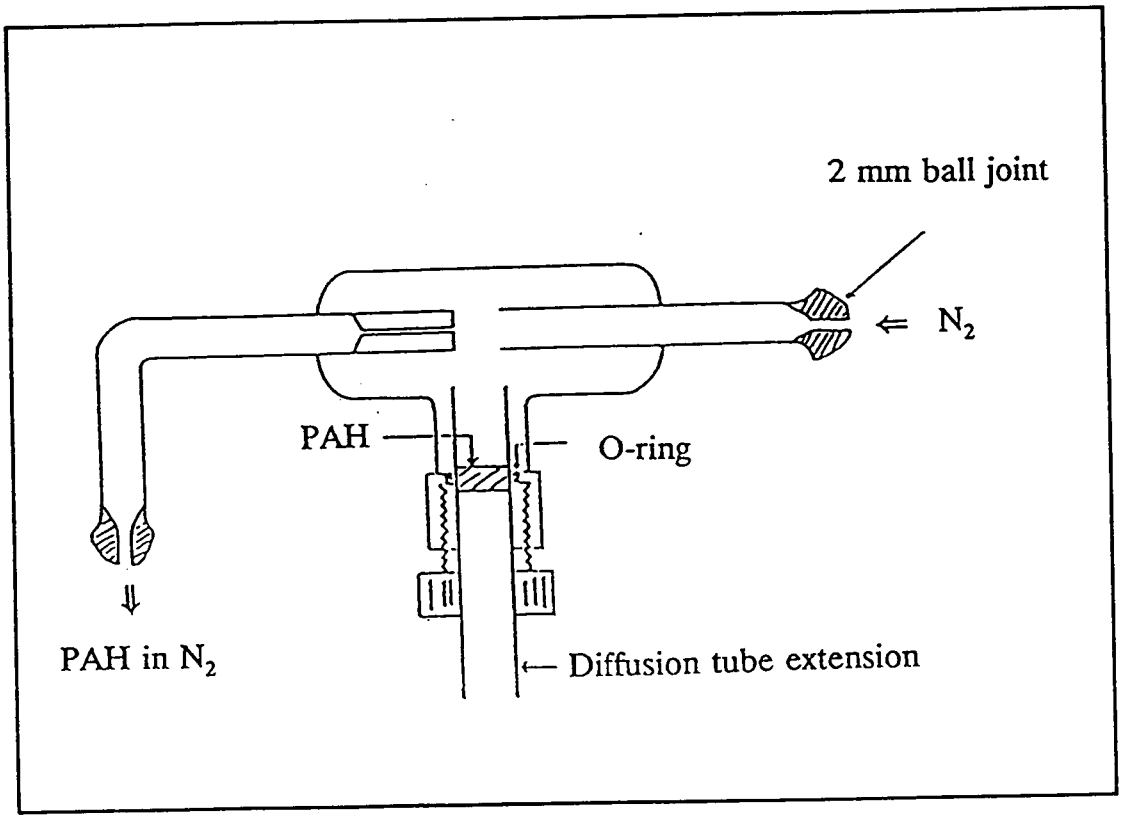

Figure 2.5 Schematic diagram of alternate vapor deposition cell.
Source: Korfmacher, W.A. *The Decomposition of Organic Matter Adsorbed on Coal Fly Ash*, Ph.D. Dissertation, University of Illinois, Urbana-Champaign, 1978, p. 44.

a diffusion cell of 10.7 mm inside diameter) rather than on a frit. The difference in size of the carrier entry and the exit openings allows for a greater mixing of carrier and adsorbate vapor (in the 20 mm i.d. region above the diffusion cell) and a larger mass flow of adsorbate relative to that which would be achieved with equivalent diameters for entry and exit openings.

A downstream pressure regulator controlled the backpressure generated by the various flow impediments that the adsorbate/carrier stream encountered (e.g., glass frits, adsorbent). The mass flow of adsorbate through the system was monitored by a flame ionization detector (FID). Compressed air (at volume flow ≈ 250 mL/min) and hydrogen (at volume flow ≈ 25 mL/min) gases used to fuel this device were supplied by National Welders. Adsorbate signal was monitored by a GowMac FID (Model # 40-900) electrometer, set for a 1 mV input and a range of 10^{-10} amperes. This was connected to a Kipp and Zonen BD40 chart recorder, which operated at a chart speed of 1 mm/min.

The system contained several switching valves which diverted carrier and/or adsorbent flow as a function of the application desired. The three-way valve (see **Figure 2.3**, p. 56) provided the capacity to deliver adsorbate-free carrier through a heated *shunt* line for the purposes of *zeroing* the detector signal. The first of two four-way valves (see **Figure 2.3**, p. 56) permits adsorbate/carrier flow to be diverted directly to the FID to monitor the maximum mass flow of adsorbate (*bypass* mode). Maximum adsorbate flow may also be monitored when flow is in *deposit* mode (flow through the cell) through an empty adsorbent cell. The second four-way valve (see **Figure 2.3**, p. 56) allowed carrier and/or adsorbate flow to be expelled into a water-filled flask or diverted to a *calibration coil*. The calibration coil, immersed in an ice bath, can be used to trap exiting adsorbate. Following a timed collection, adsorbate is washed (typically in methanol) into a volumetric flask (10 or 25 mL). Contents are diluted to volume and the concentration of adsorbate can be quantified (typically by UV/visible spectrophotometry). In so doing, the mass flow rate of adsorbate can be determined. Mass flow rates of adsorbates for the current work were measured by quantifying the amount of adsorbate deposited on a known amount (0.5-1.0 g) of silica gel as a function of deposition time. The rationale for this

approach is described in **Chapter 4** (pp. 99-100). The method used to quantify adsorbate/adsorbent coverages is described in Section **2.5-A** (pp. 68-72).

Figure 2.6 illustrates a typical FID signed profile obtained before, during, and after a deposition. The maximum mass flow rate of adsorbate, maintained as the carrier gas and adsorbate travel through an empty diffusion cell, is designated as M_d. The point on the vertical axis designated as *zero* represents the signal obtained when the carrier gas is diverted directly to the flame ionization detector. This signal is adjusted to correspond to the electrometer/chart *zero*.

Two types of depositions may be carried out: those in which the adsorbent retains the maximum amount of adsorbate possible for a given set of experimental conditions (termed *saturation* deposition), or those stopped at some point short of *saturation* (*sub-saturation* deposition). Both commence with a switch from *bypass* (carrier/adsorbate diverted from cell) to *deposit* (carrier/adsorbate through cell, adsorbent) at some time t_0. Once the deposition has started, the FID signal decreases because of retention of adsorbate by the adsorbent. The FID signal during the deposition is designated as M_e. The profile of M_e relative to *zero* (i.e., how closely is *zero* approached? for what period of time is M_e at a minimum?) is a function of the adsorbent and the oven 2 temperature.

Sub-saturation depositions are stopped at some time t_f, and the FID signal returns to M_d. *Saturation* depositions are allowed to proceed until M_e approaches M_d (at some point t_m), signifying no further retention of adsorbate. Adsorbent coverages are predicted by multiplying the mass flow rate of adsorbate, the deposition time, and the fraction of the total flow of adsorbate retained by the adsorbent. For *sub-saturation* depositions, the latter quantity is the ratio of the area, A, (see **Figure 2.6**) to the area of the rectangle defined by M_d, *zero*, and lines connecting t_0 and t_f with M_d. This ratio is determined in a similar manner for *saturation* depositions, with slightly different *rectangle* and *area* boundaries.

Predicted coverage levels of adsorbate for *sub-saturation* depositions may alternatively be approximated by computing the product of mass flow rate of adsorbate and deposition time, and assuming the fraction of the total flow of adsorbate retained by the adsorbent to be unity. The validity of this assumption is discussed in **Chapter 4** (p. 100). This approach is not apllicable for *saturation*

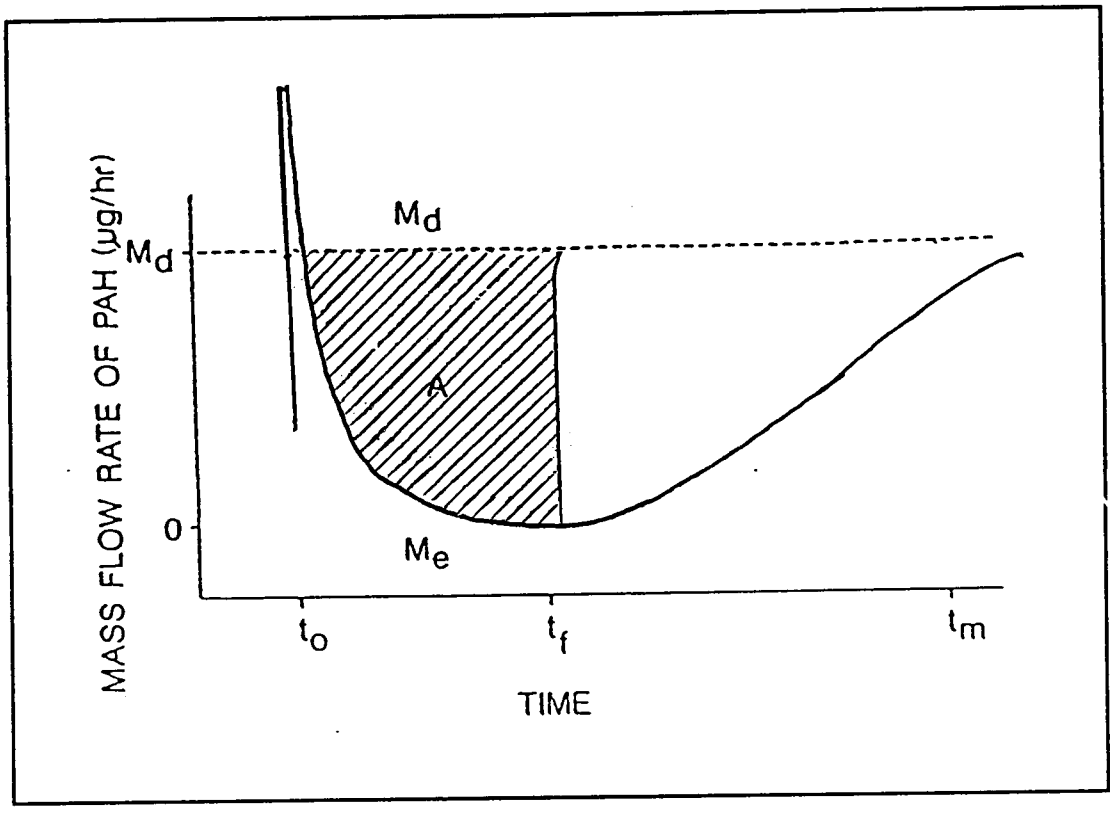

Figure 2.6 Flame ionization detector profile of a typical vapor deposition.
Source: Engelbach, R.J.; Garrison, A.A.; Wehry, E.L.; Mamantov, G. *Anal. Chem.*, **1987**, *59*, 2542.

depositions where the fraction of the total flow of adsorbate retained by the adsorbent may be significantly less than 1. The areas of the flame ionization detector profiles corresponding to total mass flows of adsorbates, and fractions thereof retained by the adsorbents used, were determined via a *cut-and-weigh* approach.

This approach was used to effect *sub-saturation* depositions of pyrene and 1-nitropyrene, and *saturation* depositions of the coadsorbates succinic acid and *n*-decane, onto adsorbents listed on p. 53. **Table 2.1** summarizes conditions employed for depositions involving these adsorbents. The first two lines list parameters for an experiment designed to compare the photochemical behavior of pyrene and 1-nitropyrene. Pyrene depositions were effected at oven temperatures considerably less than the melting point of pyrene so that adsorbate coverages in this experiment would be comparable to those of subsequent coadsorbate experiments. The temperature chosen was mandated by the pyrene/succinic coadsorbate experiments, wherein succinic acid was first loaded onto adsorbents at the oven temperature listed. Coverages were at *saturation* levels to maximize the possibility that the first *contact* of pyrene, which was later deposited onto succinic-laden adsorbents, was with succinic acid and not the surface of the adsorbent. In a similar manner, *saturation* depositions of *n*-decane were carried out on adsorbents which contained pyrene at *sub-saturation* levels. The motivation here was to maximize the possibility that all pyrene was *covered* with *n*-decane.

2.4 Irradiations of Sorbed PAH/Related Compounds

2.4-A Samples

The surfaces used in experiments designed to mimic atmospheric exposure of PAH and related compounds were silica gel, Kaneb coal stack ash fractions U2 (45-75 μm), and Kaneb ash subfractions F2 (ferro-magnetic), C2 (carbonaceous), and M2 (mineral). See p. 53 for a description of these

TABLE 2.1 CONDITIONS EMPLOYED FOR VAPOR DEPOSITIONS

Deposition description	Compound	Deposition type	oven 1	oven 2
pyrene/adsorbents	pyrene	subsaturation	100°	105°
1-nitropyrene/adsorbents	1-nitropyrene	subsaturation	145°	150°
pyrene/succinic acid/adsorbents	succinic acid	saturation	180°	185°
	pyrene	subsaturation	100°	105°
n-decane/pyrene/adsorbents	pyrene	subsaturation	100°	105°
	n-decane	saturation	85°	95°

samples. Adsorbates were 1-nitropyrene, pyrene, pyrene in the presence of succinic acid, and pyrene in the presence of *n*-decane. All samples used in these experiments resulted from vapor deposition experiments.

2.4-B Control Exposures

To establish *baseline* values against which results of photochemical experiments involving 1-nitropyrene, pyrene, and pyrene in the presence of coadsorbates could be compared, adsorbents containing these adsorbates were assayed (see pp. 70-71, coverage levels of adsorbate quantified in μg adsorbate/g of adsorbent) immediately after vapor depositions were effected. When not in use, samples were stored in the dark in a desiccator. The long-term non-photochemical stability of 1-nitropyrene was evaluated by quantifying coverage levels of that compound on silica gel at three and 10 weeks after the deposition was performed.

2.4-C Irradiations

The experimental set-up used to carry out these experiments was first described by Yokley [109]. The basic apparatus is schematically represented in **Figure 2.7.** A xenon lamp (Cermax KX 300), operated at a lamp current of 11 A, was positioned at a distance of approximately 75 cm from a quartz cell containing the adsorbate/adsorbent sample. The output of the lamp as a function of wavelength is shown in **Figure 2.8.** In order to eliminate near infrared radiation a water-filled quartz jacket was positioned between the lamp and the quartz sample cell. For photochemical experiments involving succinic acid the lamp output was further filtered (to eliminate radiation in the 200-300 nm region and to eliminate the observed photochemical degradation of succinic acid evident when unfiltered output was used) by placing a Pyrex watch glass in the light path just past the water-filled quartz container.

A more detailed diagram of the quartz sample cell is shown in **Figure 2.9.** Cells were 10-15 cm long, with an inside diameter of 1 cm, and contained a 5 cm segment of a 2 mm o.d. quartz rod mounted in the inside. The cell was attached to a rotary evaporator motor at a tapered ground glass joint for rotation (75 rpm) of the cell (around its longitudinal axis) during the illumination experiments. This insured an adequate mixing of sample and exposure of all surfaces to incident light. This process was aided by the quartz rod mounted inside the cell.

All irradiations proceeded for 24 or 48 hrs. To insure that adsorbates did not *desorb* from adsorbent surfaces because of the action of the rotary evaporator, coverages of pyrene and succinic acid on silica gel were quantified before and after 24 hours of a *dark* experiment (i.e., samples rotated in the absence of light).

A representative UV/visible absorption spectrum of each adsorbate was obtained using a Hewlett Packard (Model # 842) spectrophotometer, which is equipped with a diode array detector. Solutions 10 ppm in pyrene, 1-nitropyrene, and succinic acid were prepared in UV grade methanol (American Burdick and Jackson). A solution 10 ppm in *n*-decane was prepared in UV grade hexane (American Burdick and Jackson). A 0.75 ppm solution of 1-nitropyrene (in methanol) was used to

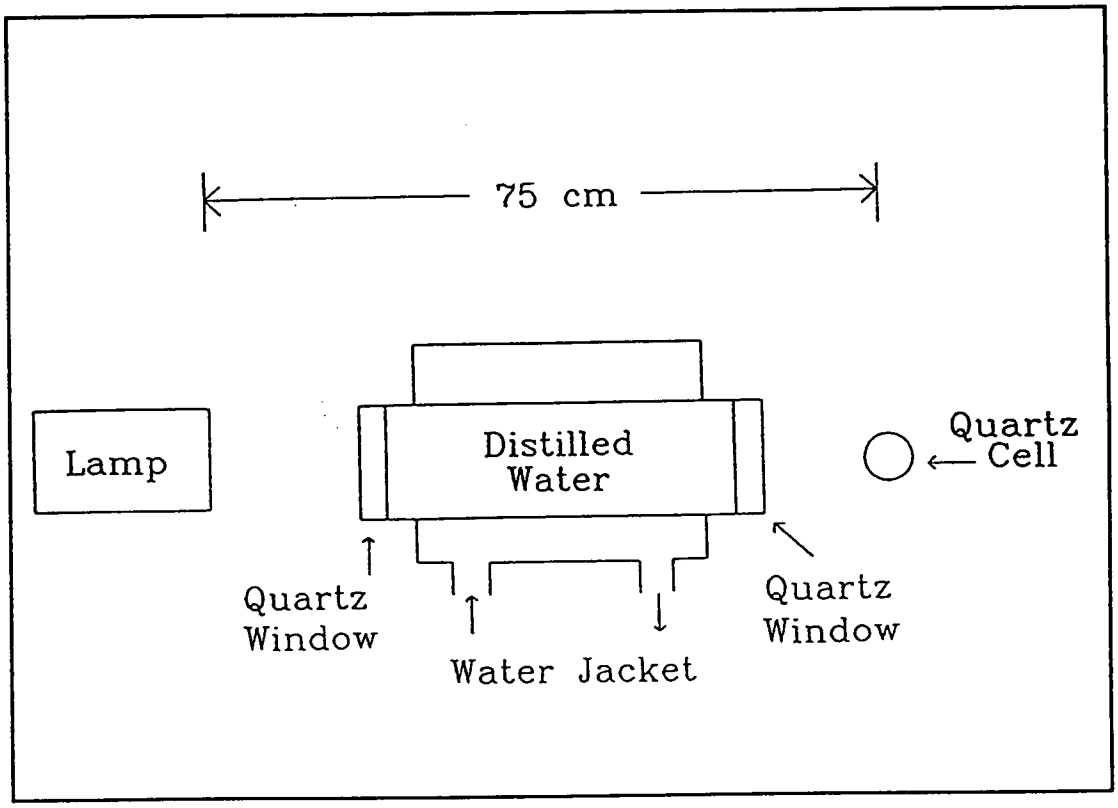

Figure 2.7 Schematic diagram of irradiation apparatus.
Source: Engelbach, R.J. *Photochemical Investigation of Polycyclic Aromatic Hydrocarbons Vapor-Adsorbed on Coal Fly Ash*, Ph.D Dissertation, University of Tennessee, Knoxville, 1986, 24.

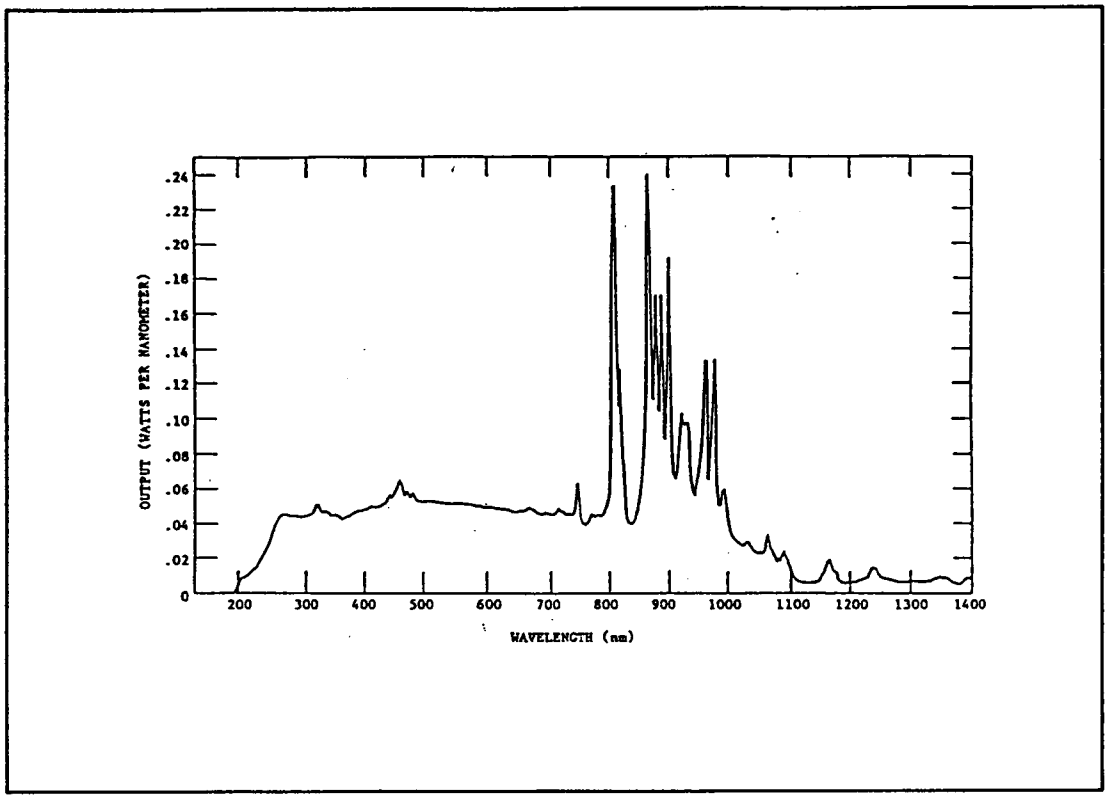

Figure 2.8 Xenon lamp output.

Source: Yokley, R.A. *The Photochemistry of Polycyclic Aromatic Hydrocarbons Adsorbed on the Surface of Coal Fly Ash*, Ph.D. Dissertation, University of Tennessee, Knoxville, 1985, p. 42.

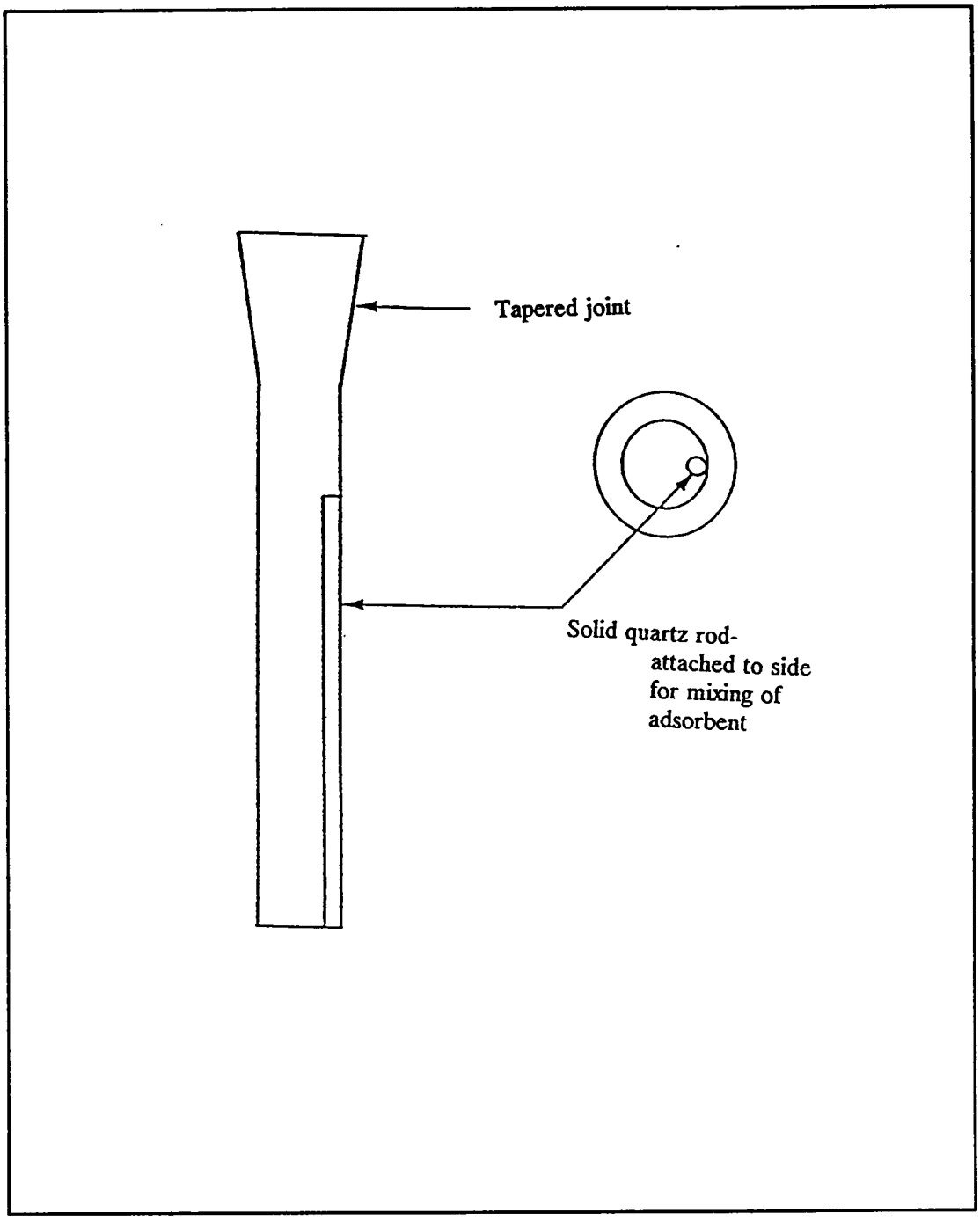

Figure 2.9 Quartz irradiation cell.
Source: Yokley, R.A. *The Photochemistry of Polycyclic Aromatic Hydrocarbons Adsorbed on the Surface of Coal Fly Ash*, Ph.D. Dissertation, University of Tennessee, Knoxville, 1985, p. 44.

evaluate the day-to-day non-photochemical stability of that compound in solution. Samples were assayed using a quartz cuvette of 1 cm path length.

2.5 Extraction and Quantification of Sorbed Organic Compounds

2.5-A Supercritical Fluid Extractions

2.5-A1 Apparatus

Pyrene, 1-nitropyrene, and decane were removed from adsorbent surfaces and the coverage levels of these adsorbates were quantified using the apparatus designed and described by Mauldin [104]. It is schematically depicted in **Figure 2.10**. The system consisted of an Isco LC-2600 syringe pump which pressurized and delivered the extractant fluid via 1/16" o.d. stainless steel tubing through an oven (Blue M Stabil-Therm, model # C-4850-Q) which contained the adsorbate/adsorbent sample in a stainless steel cell. The cell was a 5-10 cm segment of 1/8" o.d. tubing flanked by two 1/8-1/16" stainless cell reducing unions with stainless steel frits of pore diameter = 2.0 μm.

Extractant fluid and adsorbate were delivered via a heated transfer line (1/16" o.d. stainless steel tubing wrapped with a heating tape) to the head of a gas chromatographic column. The interface between the transfer line and the on-column injection port of the gas chromatograph consisted of a 15 cm by 25 μm i.d. segment of polyimide-coated fused silica capillary tubing (Polymicro Technologies). This device, termed the *restrictor* since it *restricts* the escape of extractant, thus maintaining a high system pressure, was housed in a Supelco Supltex M-2A 15 % graphite, 85 % polyimide ferrule (0.4μm o.d.) in a 1/16" Swagelok stainless steel union.

The gas chromatograph was a Hewlett Packard Model # 5890A. The unit housed a 10 m segment of a 0.53 mm i.d. capillary column. The column was loaded with a 2.65 μm diameter film of

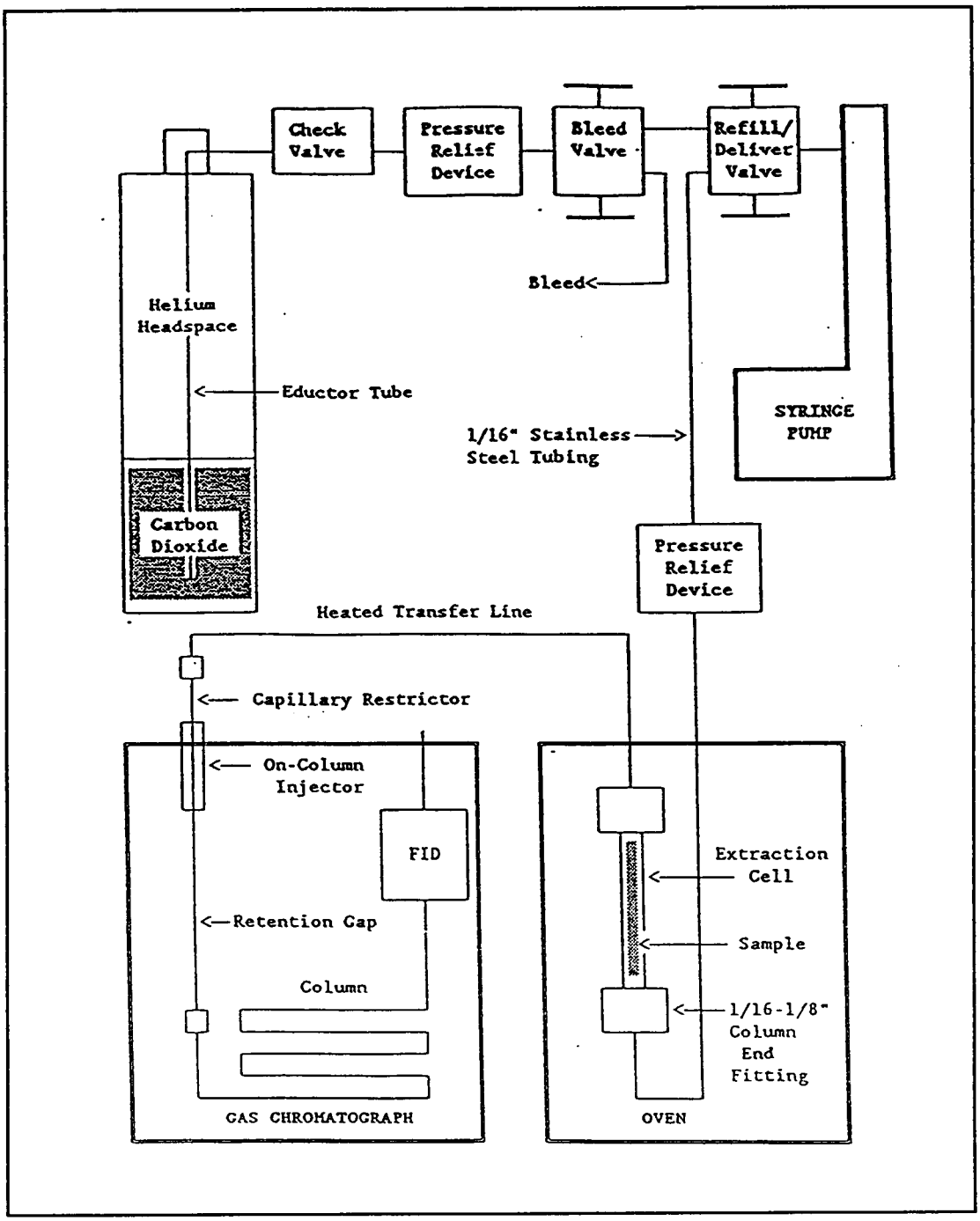

Figure 2.10 Schematic diagram of supercritical fluid extraction apparatus.
Source: Mauldin, R.F. *Photochemical and Supercritical Fluid Extraction Studies of Polycyclic Aromatic Hydrocarbons Adsorbed on Coal Stack Ash Particles*, Ph.D. Dissertation, University of Tennessee, Knoxville, 1990, p. 47.

HP-5 (5 % phenyl methyl silicone, slightly polar) stationary phase. The unit also contained a flame ionization detector with built-in electrometer. The detector/electrometer output was coupled to a Kipp and Zonen BD40 chart recorder. Alternatively, the restrictor may be decoupled from the on-line injection port and SFE eluent may be collected in 5-10 mL of an appropriate solvent (e.g., for 1-nitropyrene and pyrene, methanol; hexane for *n*-decane). The quantity of adsorbate collected may then be quantified by alternative means such as UV/visible absorption spectophotometry or gas chromatography/mass spectrometry.

2.5-A2 Procedure

The basic procedure used in carrying out these extractions/quantifications was as follows: 20 mL of supercritical grade carbon dioxide (critical temperature = 31° C, critical pressure = 73 atm; supplied by Scott Specialty Gases) was loaded into the syringe pump by opening the refill and top bleed valves (see **Figure 2.10**, previous page). The fluid was then pressurized to 400 atm and CO_2 was then cycled through the sample cell. This was achieved by opening the deliver valve while the *bleed* and *refill* valves were closed. The pump then recompressed the fluid to 400 atm. The downstream restrictor allowed fluid to be cycled through the system while maintaining system pressure at 400 atm. The cell contained 5-100 mg of adsorbate/adsorbent. The oven was switched on at the start of the experiment and during the course of the extraction attained a temperature of ≈ 100° C. The heated transfer line was maintained at a temperature of ≈ 150° C. The oven of the gas chromatograph was at a temperature of 25° C for the duration of the extraction.

When the extraction was deemed complete (pump pressure < 100 atm), the extraction cell was vented by loosening the 1/10'-1/18' column end fitting at the entry of the extraction cell. The flame ionization detector was ignited and the gas chromatograph oven temperature was set to 75° C. As soon as the oven temperature equilibrated, a temperature program which featured a 7.5°/min ramp to 225° C (held for 5 min) was initiated. Total run time was 25 min. The electrometer was set at a range of

10^{-11} A and an attenuation of *2* for the bulk of these extractions. The chart recorder was set at an input of 1 mV. Chart speed was 10 mm/min.

Extractions of 1-nitropyrene and pyrene were quantified (μg adsorbate/g adsorbent) by comparing analyte peak areas with those generated by *off-line* injections (1 μL) of standard solutions of 1-nitropyrene, assayed according to the above temperature program. It is shown (see **Chapter 4**, pp. 102-103) that detector response for 1-nitropyrene and pyrene were equivalent so a corresponding calibration plot of pyrene vs. detector response was not generated. Calibration plots for 1-nitropyrene were generated by removing the restrictor from the on-column injection port and injecting methanol (analytical reagent grade; Mallinckrodt) solutions of 1-nitropyrene with a syringe whose needle had been replaced by a 10 cm segment of restrictor tubing. 1-Nitropyrene peak areas were quantified (cut-and-weigh) vs. concentrations of standard solutions.

n-Decane was not retained at the head of the capillary column but was apparently carried downstream to the detector by the stream of expanding CO_2. The extraction/quantification procedure was amended for determination of *n*-decane/adsorbent coverages as follows: The restrictor was removed from the gas chromatograph injection port and placed in a 10 mL volumetric flask containing 6-8 mL of UV grade hexane (American Burdick and Jackson). The volumetric flask was contained in an ice bath for the duration of the extraction. Upon completion of the extraction, the contents of the volumetric flask were diluted to volume and the quantity of extracted decane was determined using gas chromatography/mass spectrometry (GC/MS).

The GC/MS unit consisted of a Hewlett Packard 5890 gas chromatograph and a Hewlett Packard 5970 *mass selective detector* (quadrupole mass filter). This unit featured a splitless injection port (maintained at 250° C) and a capillary column (Restek # 10123, 30m x 0.25μm i.d., RTX1 stationary phase [100% dimethyl polysiloxane, non-polar]; film thickness = 2.5 μm). The mass spectrometer operated in *electron impact* ionization mode and was maintained at 280° C. The temperature program utilized an initial temperature of 25° C (held for 4 min) and a 25°/min ramp to 125°. Total run time was 6 min. Injection volume was 1 μL. *n*-Decane solution concentrations were

quantified by comparing analyte peak areas (detector integration) to those obtained from injections of standard solutions of *n*-decane in hexane.

2.5-B Ultrasonic Extractions

It was determined that succinic acid lacked sufficient volatility to be analyzed by gas chromatography so an alternate extraction/quantification scheme was employed for experiments which featured this compound as an adsorbate. Following depositions and/or photochemical experiments, 0.1-1.0 g of adsorbent samples containing succinic acid were weighed into 50 mL beakers. Samples were diluted to 10 mL with distilled water (total volume added $\approx$ 9 mL) and then placed for 30 min in an ultrasonic cleaner (Branson model #B-22-4).

After the extraction samples were removed and, after allowing time (> 1 hr) for settling of the adsorbent, 5 mL aliquots of each liquid were pipetted into 150 mL beakers. These were diluted to 20 mL with distilled water and then titrated to a phenolphthalein endpoint with 1.0 x 10^{-2} M NaOH. Adsorbate/adsorbent coverages were calculated according to sample size and the volume of titrant required to reach the endpoint. The base was standardized against known quantities of succinic acid in aqueous solutions.

CHAPTER 3

FRACTIONATION AND CHARACTERIZATION OF KANEB COAL STACK ASH

3.1 Introduction

3.1-A Background

In Section 1.4 (p. 16) it is noted that chemical compositions and physical properties of coal fly ash particles vary from one power plant to another or for a given power plant as operating conditions change. Section 1.4 concludes with the observation (p. 23) that coal fly/stack ash particles, in general, consist of a wide variety of chemical components and manifest themselves in a wide variety of sizes and shapes. Sections 1.5 (pp. 24-32) and 1.6 (pp. 32-41) contain discussions showing that individual physical properties and chemical constituents exert different influences on the interactions and transformations of PAH sorbed on these surfaces. Thus, any ash chosen for study should, if possible, be fractionated and characterized according to those physical properties and chemical components believed to be most important in influencing behaviors of sorbed PAH.

As pointed out in **Chapter 2** (p. 48), the first step in the fractionation of Kaneb ash was to separate it according to particle size. The fraction with particle diameter ranging from 45-74 μm was chosen for further study and for further fractionation according to chemical composition. This choice could be considered somewhat controversial in light of the conventional view (see p. 11) that the most important atmospheric particles are those in the 0.1-10 μm size range.

How *relevant* are particles in the 45-74 μm size range? Though too large to be respirable, are they capable of atmospheric lifetimes sufficient to interact with PAH and related compounds, to influence the transformations of these compounds, and to serve as vehicles by which these compounds may be deposited into soil, vegetation, and water supplies? Furthermore, do they possess surface properties and important chemical constituents at levels comparable to those of particles in the 0.1-10 μm size range? Are they, therefore, able to serve as a good *model* for smaller particles?

First of all, it should be pointed out that the actual atmospheric abundance of coarse particles may be greater than that indicated through the use of devices commonly used to collect atmospheric particles and to determine size distributions of those particles. Any such device utilizes some type of sample inlet, fractionation elements designed to separate particles according to size, and some means of detecting particles as a function of particle size [112,113]. Liu and Pui [112] have theoretically evaluated various approaches to ambient particle sampling. Wedding and co-workers [113] have experimentally evaluated the effectiveness of several such devices. Both studies concluded that the effectiveness of typical particle sampling devices decreases as a function of particle size. Wedding and co-workers [113] report that a typical *Hi-Volume* sampler, the EPA-approved device for collecting atmospheric partices, has a collection efficiency of nearly 100 % for particles 5 μm in diameter. Less than 60 % of particles with diameters greater than 15 μm in diameter are collected by such a device. Finlayson-Pitts and Pitts [15] report that a typical Hi-Volume sampler has a collection efficiency of approximately 90 % for particles 1.0 μm in diameter. Wedding and co-workers [113] point out that the increased inertia of coarse particles renders them prone to deposit on sample inlet and/or fractionation element surfaces, and inhibits their efficient transport to downstream detection systems.

It is pointed out in **Chapter 1** (p. 11) that coarse particles (> 2 μm particle diameter) have been shown to be responsible for the transport of a number of pollutants to the surface of the earth. Noll and co-workers [114] used a rotating collection device to sample and measure abundances of atmospheric particles with diameters of 5-100 μm over a 15 month period at one urban and one rural site. The device was equipped with rectangular collectors, or stages, which discriminated against specific

particle sizes as a function of collector width and rotational speed. For both the urban and rural sites, collection was effected at approximately 10 m above ground. It was found that the mass median diameter of sampled particles varied between 15 and 30 μm as a function of time of day, season, climatic conditions, and wind velocity. The overall average diameter of collected particles, for the duration of the experiment, was $\approx$ 20 μm for both the urban and rural sites.

Noll and co-workers also found that the total abundance of particles with diameters greater than 20 μm increased with increasing wind speed while that of particles with diameters less than 11 μm decreased. For five collections where the average wind speed was > 10 miles/hr, the mass median diameter of sampled particles was 29 μm. Turbulent atmospheric conditions, then, enhance the suspension of coarse particles, and may, according to these authors, allow the transport of coarse particles over significant distances. In support of this contention, they observed that the overall abundance of coarse particles at the rural site increased when the wind was blowing from the urban site (source of anthropogenic coarse particles) 23 miles away.

In a later set of studies [26,115], Noll and co-workers measured the numbers and masses of particles (lowest particle size limit detectable = 1 μm) settling from the atmosphere as a function of particle size. They attached a rectangular plastic deposition plate to a wind vane atop a 12 m tall building in a mixed institutional, commercial, and residential area such that the top of the plate faced at an angle (10° relative to horizontal) into the wind. The top of the plate was covered with a thin film of Mylar that was greased to trap deposited particles. Particles settled onto the plate due to gravitational (downward velocity of particles) and inertial (air turbulence) forces. To assess the tendency of particles to remain suspended, the bottom of the plate was also covered with the *activated* Mylar surface. Particles settling on the lower plate were those whose inertial (upward) velocities were greater than their gravitational velocities.

They found that the numerical median diameter (i.e., most abundant particle size by number of particles) was 2 μm for the upper and lower plates. From a mass standpoint, however, more than 99 % of deposition was due to particles with diameters greater than 2 μm. The mass median diameter

for the upper stage was 161 μm, while for the lower stage it was 73 μm. The difference in these numbers indicates a particle size cut-off above which inertial particle velocities are not sufficient to overcome gravitational forces. It is interesting to note that the size median for particles which do tend to be suspended is as high as 73 μm. Wind speed for the collection periods used in these experiments varied between 1 and 10 miles/hr. These results cannot be attributed, therefore, to collection during unusually turbulent atmospheric conditions.

No estimate of the atmospheric lifetimes of particles as a function of particle size are offered by the authors of the studies just cited. Likewise, no values are given relative to how far a particle may be transported as a function of particle size. Nonetheless, these studies do imply that particles in the 45-74 μm size range may be suspended in the atmosphere for significant periods of time and may be transported over appreciable distances.

Other studies indicate that atmospheric lifetimes of coarse particles are sufficient to allow interaction with semivolatile pollutants such as PAH. Holsen *et al.* [116] have monitored the deposition of polychlorinated biphenyls (PCBs) as a function of atmospheric particle size. They used a greased, Mylar-covered plate to sample atmospheric particles at an urban site (sampling height = 15 m) and at a college located in a suburban area (sampling height = 1 μm) over periods of several months. They found significant concentrations of PCBs associated with small particles (50 μg/g for particles less than 1 μm in diameter) and on large particles (30 μg/g for particles larger than 25 μm in diameter). Both PAHs and PCBs are considered as *semivolatile organic compounds*, and these compound classes have similar gas-to-particle distributions in the atmosphere [117]. One can infer from these observations that PAH may also be found at similarly significant levels on large particles such as coal fly ash.

The preceding discussion suggests that coal fly ash particles with diameters between 45-74 μm may exhibit atmospheric lifetimes sufficient to interact with PAH and related compounds and to influence the atmospheric behavior of these compounds. Particles in this size range can also be viewed as environmentally relevant if it can be shown that they are an appropriate model for smaller particles,

which have greater atmospheric lifetimes and which pose a threat because they are respirable. Unfortunately, this task is difficult because of the paucity of comparative information on small and large particles.

For instance, the discussion of particle morphology in **Chapter 1** (pp. 18-20) is based on inspections of coal stack ash particles with diameters between 2 and 20 μm. It is not known if this information is applicable to smaller particles. Smith and co-workers [35] have evaluated and compared formation mechanisms for fine and coarse particles. They concluded that the most plausible route to fine particle formation is by *bursting* of coarse particles, followed by coagulation of small fragments. If formation of fine particles is indeed an extension of the process by which coarse particles are formed, then fine particles may exhibit similar morphologies to those of coarse particles. It would follow, then, that surface irregularities of fine and coarse particles might be similar.

Specific surface areas for fine and coarse particles have been compared (see results presented in **Table 1.7**, p. 27) but no distinction was made between the influence of particle size (smaller particles have inherently larger areas per unit mass) and that of particle morphology on those results. As can be seen, the specific surface areas of particles less than 2.3 μm in diameter were more than four times greater than that of the particles 21-150 μm in diameter. Any PAH/coal fly ash behaviors enhanced (or inhibited) by an increase in specific surface area of the ash may be further enhanced (or inhibited), then, by fine particles.

Carbon has been identified as the most important constituent of coal stack ash in influencing the interaction of coal fly/stack ash with PAH (pp. 26-32) and the photochemical behavior (pp. 38-41) of sorbed PAH. **Table 1.5** (p. 23) compares the total carbon content of three coal stack ashes as a function of particle size. Carbon contents for the 21-150 μm particle size ranges were 5-6 times greater than those of the corresponding fine particles. Small particles do, however, contain carbon. It is safe to assume, then, that the interactions of PAH with small particles and the behaviors of PAH associated with small particles will be influenced by the presence of carbon, albeit possibly to a lesser degree than corresponding interactions and behaviors on large particles.

In summary, available comparative information on coarse vs. fine particles does not rule out the use of coarse coal stack ash particles in the 45-74 μm size range as models for smaller coal fly ash particles. However, any extrapolations of coarse coal stack ash particle behaviors (as a function of physical properties and chemical compositions) to behaviors expected for fine coal fly ash particles should be made with caution and take into account the known differences between these particle types.

There are also compelling experimental reasons for choosing particles with diameters greater than 45 μm. The vapor deposition apparatus and procedure are described in **Chapter 2** (pp. 55-62). An important feature of this system is the glass diffusion cell on which an adsorbent resides during the course of a deposition. Specifically, adsorbent is placed on a glass frit with, for the current work, pore diameters of 25-50 μm. This pore diameter introduces a lower cutoff for particle diameters appropriate for a given diffusion cell. While frits with pore diameters significantly smaller than 25-50 μm are available, experience has shown that problems with backpressure (see p. 59), and, therefore, reduced mass flow of adsorbate vapor, occur with decreasing pore diameter. There are perhaps alternatives to glass frits that are permeable to gases and would satisfactorily *secure* adsorbents (i.e., not allowing their passage to upstream and/or downstream plumbing/system components) without leading to backpressure problems, and without causing loss of mass flow of adsorbate. This author, however, is not aware of any materials which fit these criteria.

The *frit* problem also manifests itself in the primary extraction/quantification procedure used in the current work. The supercritical fluid extraction apparatus (see pp. 68-72) also employs a cell with a frit (stainless steel, pore diameter = 2.0 μm) to secure adsorbate/adsorbent samples. The pore size here, however, is not as restrictive with respect to allowed adsorbent particle sizes as that of the vapor deposition cells (2 μm pore diameter for extraction cell frits vs. 25-50 μm pore diameters for deposition cell frits), and would, therefore, permit the use of smaller adsorbent particles.

One alternative to the limitations imposed by sample cell frits is to employ an alternative method for depositing PAH on coal stack ash surfaces. *Solution* depositions (described on p. 54) are an alternative means of *loading* adsorbates onto adsorbents. No apparent limitation on particle size is

mandated by implementation of this technique. However, such depositions do not mimic actual atmospheric association of PAH with coal fly ash as well as do vapor depositions [111]. Furthermore, exposure of coal stack ash particles to solvent may alter the surface in such a way as to change the nature or the strength of the association between PAH and the coal stack ash [104]. The choice of the 45-74 μm coal stack ash particles for use in this work was, then, an attempt to balance the issue of *environmental relevance* with inherent instrumental constraints.

3.1-B Objectives

The particular coal stack ash (called the *Kaneb ash*) used in this work has been extensively characterized by previous members of this research group. **Table 3.1** lists % carbon and % iron values for Kaneb ash fractions comparable to those used in the current work. Also listed are the % of the total bulk mass comprised by a given fraction or subfraction. For the unfractionated ashes U2 (45-74 μm) and U3 (75-124 μm), the values listed represent their respective contributions to the mass of the unfractionated Kaneb ash. For the ferromagnetic (F3), mineral (M3), and carbonaceous (C3) subfractions, values represent the % by mass of the size fractionated (U3) ash fraction.

The general goal of the work described in this chapter was to characterize the ash fractions used in photochemical studies described in **Chapters 4** (pp. 84-113) and **5** (pp. 114-142). Specific goals were:

1. to assess the mass % of each subfraction obtained as a result of fractionation experiments. This information can then be weighed against the influence of a particular fraction or subfraction on the interactions and behaviors of sorbed PAH and related compounds.
2. to determine % carbon values and % iron values for each fraction and subfraction used in this work. This information indicates the effectiveness of fractionation procedures designed to isolate mineral non-magnetic, mineral magnetic, and carbonaceous components.

TABLE 3.1 PROPERTIES OF KANEB COAL STACK ASH FRACTIONS

Fraction		% of bulk mass	% carbon	% Fe_2O_3
U2		17 %	4.72	- - -
	F2	- -	0.56	- - -
	M2	- -	- - -	- - -
U3		10 %	7.42	- - -
	F3	5 %	0.64	66.11
	C3	18 %	67.30	2.23
	M3	77 %	0.87	8.15

Source: Mauldin, R.F. *Photochemical and Supercritical Fluid Extraction Studies of Polycyclic Aromatic Hydrocarbons Adsorbed on Coal Stack Ash Fractions*, Ph.D. Dissertation, University of Tennessee, Knoxville, 1990, pp. 16, 18, 21.

3.2 Results and Discussion

3.2-A Kaneb coal stack ash fractionation

The procedure used to obtain the ash fraction adsorbents used in this work is summarized in **Figure 2.2**, p. 52. This figure is reproduced in **Figure 3.1** with the yields for of the ferromagnetic (F2), carbonaceous (C2), and mineral (M2) subfractions included. Note that these yields are comparable to those of equivalent subfractions isolated from the 75-124 μm size fraction (U3) by Mauldin (see **Table 3.1**). It is pointed out in **Chapter 1** (pp. 18-22) that the mineral non-magnetic fraction is by far the most abundant component of a typical coal stack ash. As seen in **Figure 3.1**, the mineral non-magnetic fraction M2 was responsible for the bulk of the mass of the Kaneb U2 (45-74 μm) coal stack ash fraction.

The percentage of the carbonaceous subfraction C2, as a fraction of the mass of U2, is lower than that of the C3 subfraction as a fraction of the mass of U3. As pointed out on page 22, and as shown in **Table 1.5** (p. 23), carbon content increases with increasing particle size. The subfraction

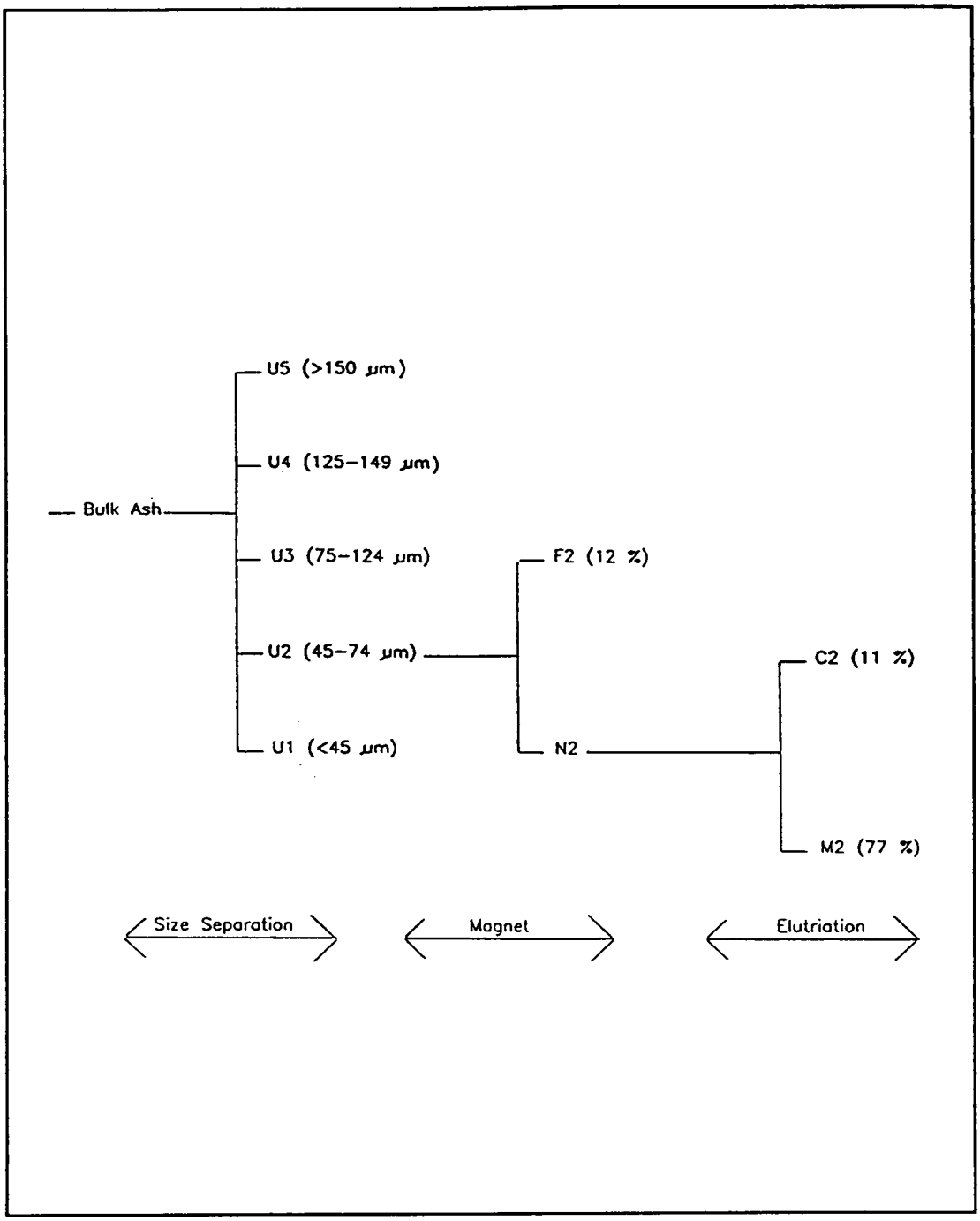

Figure 3.1 Fractionation scheme for Kaneb coal ash: size fraction 2 (45-74 μm) to subfractions. Mass % of each subfraction is listed.

enriched in carbonaceous particles should, therefore, constitute a greater percentage of the overall mass of the U3 (75-124 μm) fraction than of the corresponding subfraction of U2 (45-74 μm).

It is pointed out in **Chapter 1** (p. 20) that levels of magnetic iron oxides increase with decreasing particle size. It is not surprising, then, that the ferromagnetic subfraction F2, used in the current work, constituted a greater percentage of the overall mass (11 %) of U2 (45-74 μm) than the corresponding subfraction F3 (5 %) of U3 (75-124 μm).

3.2-B Kaneb coal stack ash characterization

Table 3.2 lists % carbon and % iron values for the bulk size fraction U2 (45-74 μm) and of the ferromagnetic (F2), mineral (M2), and carbonaceous (C2) subfractions. Compare these results with those listed in **Table 3.1**, p.80. Again, the lower carbon content in the carbonaceous subfraction C2 relative to that of C3 is expected. Similarly, the carbon content of the U2 (45-74 μm) fraction is lower than that of the U3 (75-124 μm) fraction listed in **Table 3.1** (p. 80). Note also that the carbon content of U2, **Table 3.2**, is quite similar to that of U2, **Table 3.1** (p. 80). These fractions are not identical, but were obtained under equivalent fractionation schemes (i.e., a previously unused portion of Kaneb stack ash was used to generate the U2 fraction used for the current work). These observations indicate that the fractionation scheme is quite reproducible.

The mineral non-magnetic (M2) and mineral magnetic (F2) subfractions of **Table 3.2** (as did F3, M3, **Table 3.1**, p. 80) contained less than 1 % carbon. This observation indicates that the fractionation procedure used to isolate the carbonaceous particles from the mineral particles was quite effective.

The % iron values for the carbonaceous and mineral enriched subfractions C2 and M2 indicate that the procedure used to isolate magnetic particles was somewhat less effective than the procedure used to isolate carbonaceous particles. It is pointed out in **Chapter 1** (p. 20) that the magnetic fraction of coal stack ash consists of a ferrite ($FeAl_xO_y$) component and oxides of iron. The latter are often

TABLE 3.2 KANEB COAL STACK ASH FRACTIONS: % CARBON, IRON

Fraction	% Carbon	% Iron (Fe_2O_3)
U2	6.25 %	11.7 %
F2	< 0.5 %	62.8 %
C2	23.22 %	4.7 %
M2	0.94 %	6.9 %

dissolved in the glassy aluminosilicate matrix of the mineral fraction. This would inhibit the separation of magnetic and non-magnetic mineral particles, at least via the simple procedure (passing a bar magnet over the bulk ash; see pp. 48-49) used to effect that separation for the work described herein.

It is also pointed out in **Chapter 1** (pp. 20,22) that the surfaces of carbonaceous particles often contain mineral contaminant inclusions. Iron was listed as one of several possible contaminant species. The relatively high iron contents of C2 and M2 are not, therefore, unexpected. Note that the % iron value for F2 is comparable to that of F3, **Table 3.1** (p. 80). Again, it should be kept in mind that iron content usually increases with decreasing particle size.

3.3 Conclusions

The fractionation procedures used to isolate the carbonaceous, magnetic mineral, and non-magnetic mineral components of Kaneb coal stack ash U2 (45-74 μm) have been shown to be effective (see **Table 3.2**). This was particularly true for the procedure used to isolate carbonaceous particles. The adsorbents so generated were, therefore, considered appropriate for studies of PAH/coal stack ash behavior as function of chemical composition of the ash.

CHAPTER 4

PHOTOCHEMISTRY OF 1-NITROPYRENE SORBED ON COAL STACK ASH

4.1 Introduction

4.1-A Background

The primary goal of the experiments described in this chapter was to simulate the atmospheric exposure of nitro-PAH, sorbed onto coal stack ash at atmospherically relevant coverages, to sunlight. In so doing, the likelihood of atmospheric photodegradation of particle-associated members of this compound class can be evaluated. A secondary goal was to assess the affinity of coal stack ash for nitro-PAH. Both sets of behaviors, sorptivity and photochemistry, were to be evaluated relative to equivalent behaviors of the unsubstituted parent from which the chosen nitro-PAH derived.

This section describes the rationale used in choosing a representative nitro-PAH for these studies. A justification is provided for the choice of the method used to quantify adsorbate/adsorbent coverages. The appropriateness of the irradiation system as a model for atmospheric sunlight is also evaluated. Finally, the approach used to evaluate the affinity of coal stack ash adsorbents for pyrene and 1-nitropyrene is briefly outlined.

A list of several criteria were used in identifying an appropriate nitro-PAH for this work. It was decided that any such compound chosen should:

1. be identified in the literature as being associated with coal fly ash or other atmospheric particles;

2. be sufficiently benign that health risks associated with exposure to the compound were minimal;
3. be sufficiently stable against non-photochemical degradation so that any losses seen during irradiation experiments could be attributed to photochemical transformation;
4. be sufficiently photoreactive that the photochemistry of the compound could be investigated without having to result to inordinately long irradiation times.

Table 4.1 compares atmospheric abundances and mutagenicities of the two nitro-PAH originally targeted for further study. Listed are atmospheric particulate levels of 1-nitropyrene,

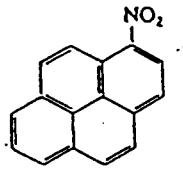

the 1-nitro-substituted analogue of pyrene, and 9-nitroanthracene,

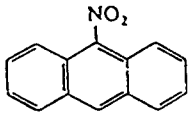

the 9-nitro-substituted analogue of anthracene, found on atmospheric particles derived from specified combustion sources or on particles (designated as *atmospheric*) sampled in environments not associated with a particular combustion source.

Also included are data which provide a comparison of the mutagenic activities of these compounds. Values listed are *revertants/nmole* induced by the compounds in the Ames *Salmonella*/Mammalian-Microsome test. In this assay [6] a bacterial strain is mutated such that it

TABLE 4.1 ATMOSPHERIC ABUNDANCES AND MUTAGENICITIES OF NITRO-PAH[a]

Compound	Particle type	Coverage, μg/g	Revertants/nmole, Ames assay[b]
9-nitroanthracene	diesel exhaust	81-552	0.32[c]
1-nitropyrene	atmospheric	0.06-0.56	467 ± 25
	gasoline exhaust	0.6-4.3	
	diesel exhaust	8.6-150	

[a]Source: Tokiwa, H.; Ohnishi, Y. *CRC Crit. Rev. Toxicol.*, **1986**, *27*, 32.
[b]for *Salmonella* strain TA98.
[c]Source: Pitts, J.N., Jr.; Lokensgard, D.M.; Harger, W.; Fisher, T.S.; Mejia, V.; Schuler, J.J.; Scorziell, G.M.; Katzenstein, Y.A., *Mutat. Res.*, **1982**, *103*, 245.

cannot produce an amino acid (histidine) necessary for its growth. Certain compounds are able to convert the mutated strain back to its natural form, and it is then able to produce histidine and initiate cell growth. The number of colonies (*revertants*) produced per nmole of a given compound is a measure of the *mutagenic activity* of that compound. A link has been established, for some compounds, between the mutagenic activity displayed in the Ames test and the ability to initiate tumors in laboratory animals.

As can be seen in **Table 4.1**, both 1-nitropyrene and 9-nitroanthracene have been identified on atmospheric particles. According to Pitts [95], 1-nitropyrene is one of the most abundant nitro-PAH on atmospheric particulate matter sampled at or near combustion sources or in remote environments. Harris *et al.* [118] report a 0.012 μg/g 1-nitropyrene coverage on coal stack ash that they sampled from a coal fired power plant.

9-Nitroanthracene exhibits little or no mutagenic activity [119] while 1-nitropyrene is moderately mutagenic relative to other mononitro-substituted PAH [89]. For the sake of comparison, 1,8-dinitropyrene, one of the most potent mutagens analyzed to date, produces 257,439 ± 2873 revertants/nmole in the Ames assay [89]. Rosenkranz [92] estimates that 1-nitropyrene accounts for about 20 % of the mutagenicity exhibited by organic extracts of diesel particulate emissions. Salmeen and co-workers [120] assert that even a 1 % contribution (to overall mutagenic activity) is significant,

considering that there are hundreds of compounds present in extracts of diesel particles. Harris *et al.* [118] attributed 0.03-0.16 % of the total mutagenic activity of the organic extract from coal stack ash they sampled to the presence of 1-nitropyrene. 1-Nitropyrene was found to induce tumors in 42 % (320 μmole dose) to 63 % (800 μmole dose) of laboratory animals force fed this compound [121].

Because of its benign nature, 9-nitroanthracene was originally chosen as the best compound with which to initiate these studies. Unfortunately, 9-nitroanthracene is prone to undergo extremely efficient photodegradation to anthraquinone [122],

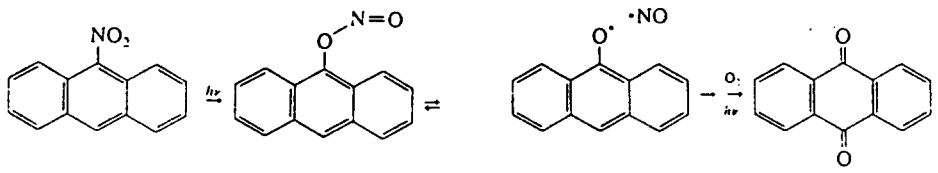

It was also found during preliminary evaluations that this conversion occurred quite rapidly, in the absence of light, for 9-nitroanthracene in methanol or toluene solution and when this compound was sorbed on silica gel. The tendency to degrade was such that the efficacy of analytical calibrations (i.e., quantification of peak areas of gas chromatographic injections of standard solutions; see pp. 71-72) was compromised, and it was feared that significant non-photochemical degradation of sorbed 9-nitroanthracene would occur during short-term sample storage.

It was, therefore, decided to use 1-nitropyrene and exercise considerable care (see p. 54) when handling this compound. Preliminary investigations relative to the stability of this compound (in solution) in the presence and absence of light are described in the next section. Others have found 1-nitropyrene to be quite stable against non-photochemical degradation, but also able to undergo degradation under irradiation within a reasonable time frame. Benson *et al.* [123] coated 1-nitropyrene on glass plates (from acetone solution) and exposed the plates to natural sunlight. They found that 72 % of the original compound remained after 4 weeks of exposure. No degradation was observed for samples stored in the dark for the same period of time. Holloway and co-workers [124] exposed 1-

nitropyrene in DMSO solution and on silica gel (*solution*-deposited from benzene solution) to a medical phototherapy illumination source. The half-life of 1-nitropyrene in solution was 1.2 days and, on silica gel, 6 days.

It was deemed appropriate to conduct photochemical studies of 1-nitropyrene on silica gel and Kaneb ash fractions and subfractions and to compare its behavior relative to that of its parent, pyrene. In the only known direct comparison of the photochemical stabilities of pyrene and 1-nitropyrene, Holloway and co-workers [124] report a half-life in DMSO solution of 1.2 days for 1-nitropyrene and a half-life of more than 4 days for pyrene. Based on these data, and previous experience with pyrene, it was assumed that 1-nitropyrene was sufficiently photoreactive to be a suitable candidate for these studies.

Pyrene, the model compound with which 1-nitropyrene photochemistry was compared, has been frequently identified on atmospheric particulate matter sampled near combustion sources and at remote sites. For instance, Masclet and co-workers [30] determined total (particulate and gaseous) emission levels of pyrene to vary between 2.42 and 771 μg/g at seven fossil fuel power stations. Roussel and co-workers [125] found atmospheric levels of pyrene ranging from 6.1-1352 μg/g on atmospheric particles sampled near aluminum smelters. Bjorseth [22] *et al.* found an average pyrene concentration of 3.5 μg/g on atmospheric particulate matter sampled at a remote site in Alaska.

The gas-to-particle distributions of atmospheric pyrene have been evaluated by several research groups. Cautreels and van Cauwenberghe [126] determined the average gas/particle ratio to be 2.05 for pyrene in a residential area. Broddin *et al.* [48] found that gas/particle ratios for pyrene varied from 0.13 to 3.2 in a residential area. Masclet and co-workers [47] found that gas/particle ratios varied between 2 and 4 at a remote site in France during dry climatic conditions and between 6 and 13 during rainy conditions. (It is pointed out in **Chapter 1**, p. 13, that pollutants associated with particles are more easily scavenged by rain than are gaseous pollutants.) Thus, depending on conditions a significant fraction of atmospheric pyrene may exist in the particulate phase. As pointed out in **Chapter 1** (p. 43),

1-nitropyrene is more polar than pyrene and, therefore, should be more prone than pyrene to be associated with atmospheric particles.

The coal stack ash particles used in this work have properties which affect the ability to quantify coverage levels of a given adsorbate. As pointed out in **Chapter 1** (p. 20), coal stack ash is usually dark in color due to the presence of iron oxides and carbonaceous particles. Garrison *et al.* [127] measured optical absorbances (by diffuse reflectance spectroscopy) of eight representative coal stack ashes in the 260-360 nm region of the electromagnetic spectrum. (As pointed out in **Chapter 1**, p. 33, this is the region in which PAH are likely to absorb.) Observed absorbances ranged from 0.4-1.7 absorbance units. This phenomenon renders the use of *in situ* optical spectrometric techniques ineffective for quantifying adsorbate/adsorbent coverages. The only discernible alternative is to extract adsorbates from adsorbents prior to quantification, and to quantify the adsorbate content of the resulting extract.

As pointed out in Section 1.5 (pp.24-32), PAH may be strongly adsorbed to coal stack/fly ash samples. Therefore, the ability to work with environmentally relevant adsorbate/adsorbent coverages is compromised, not primarily by the detection limit of any method used to quantify those coverages, but rather by the inability to quantitatively extract available adsorbate from adsorbent surfaces. Mauldin and co-workers [131] have compared the extraction efficiencies of pyrene from carbonaceous subfractions (particle size 75-124 μm) of coal stack ash using ultrasonic extraction, micro-soxhlet extraction, and supercritical fluid extraction. He found that these techniques yielded similar recoveries of pyrene. For supercritical fluid extraction with CO_2, 66 % of the pyrene was recovered. Recoveries for the micro-soxhlet and ultrasonic techniques were 60 % and 63 %, respectively. All three techniques permit the use of a variety of post-extraction quantification methods (e.g., absorption or fluorescence spectrometry, gas or liquid chromatography).

Extractions using supercritical fluids have increased in popularity in recent years [128]. Supercritical fluid extraction systems which are interfaced to gas chromatographs (SFE/GC) have proven to be particularly popular. Supercritical fluid extraction systems interfaced to gas chromatographs have been used to extract organic compounds from atmospheric particulate matter [129], from fuel-

contaminated sediment [130] and from coal stack ash [131]. As described in **Chapter 2** (pp. 68-72), such a system was used in the current work. Interfaced supercritical fluid extraction systems allow for the direct deposition, without dilution, of analyte onto the head of a capillary gas chromatographic column. In so doing, they provide a theoretical advantage in detection limit relative to traditional liquid extraction procedures, which employ some finite *dilution* volume. This is the primary reason that supercritical fluid extractions were used in the current work.

Unfortunately, this advantage is offset by the tendency of supercritical fluids to contain (or to extract from system plumbing components) impurities which may impart a substantial background to *blank* signals [132]. The minimum adsorbate coverage level for baseline/photochemical experiments, then, is determined not only by the efficiency with which an adsorbate is extracted from a particular adsorbent, but also by the ability to distinguish a gas chromatographic peak of an adsorbate from background peaks. The most widely used supercritical fluid extractant, and the one used in the current work, is CO_2 [128]. Supercritical CO_2 is a reasonably good solvent for moderately polar species such as PAH, its critical temperature and pressure (31° C, 73 atm) are relatively low, it is of low toxicity, and it is relatively inexpensive [128].

A portion of the spectral output of sunlight is shown in **Figure 1.7**, p. 34. For the spectral region shown (300-700 nm), solar intensity ranges from 10^{15} to 10^{17} photons/cm^{2}s. Hipps [133] has determined that the average power of the type of xenon lamp used in the work described herein was 2×10^{16} photons/cm^{2}s for the wavelength range 200-700 nm. The intensity of the source used in these experiments was comparable, then, to typical solar intensities. The output of the xenon lamp as a function of wavelength is shown in **Figure 2.8**, p. 66. A comparison of the outputs in **Figures 1.7** and **2.8** reveals that the lamp used in irradiation experiments has a higher output of photons in the 200-300 nm range than does natural sunlight. Nonetheless, this source is a more accurate model for the intensity and wavelength distribution of atmospheric sunlight than any other common, high intensity radiation source.

Several techniques for evaluating the affinity of coal stack ash for PAH were described in Chapter 1 (pp. 26-31). Engelbach and co-workers [108] quantified the amount of adsorbate extracted from a given adsorbent relative to the amount predicted to be present on that adsorbent following a vapor deposition experiment. By comparing the percentage recoveries of PAH from coal stack ash fractions, they evaluated the relative affinities of those fractions for PAH. A similar approach was used in the current work to estimate the relative affinities of Kaneb coal stack ash fractions for 1-nitropyrene and pyrene.

4.1-B Objectives

The realization of the experimental goals outlined at the first of this chapter (p. 84) required the completion, first of all, of several background experiments. These were designed to evaluate the extraction/quantification technique used in this work and to evaluate relative photochemical behaviors of 1-nitropyrene and pyrene. Specific experiments carried out toward these ends included:

1. an evaluation of the non-photochemical stability of 1-nitropyrene;
2. a determination of the practical detection limit of the supercritical fluid/gas chromatographic system.

Following the completion of these experiments, those more germane to the specific goals were carried out. These included:

1. depositions of 1-nitropyrene and pyrene onto silica gel and Kaneb ash fractions;
2. a comparison of the affinities of coal stack ash fractions for 1-nitropyrene and pyrene;
3. an evaluation of the non-photochemical stability of sorbed 1-nitropyrene as a function of adsorbent composition;

4. a comparison of the photochemical behavior of 1-nitropyrene and pyrene, both sorbed on coal stack ash fractions.

4.2 Results and Discussion

4.2-A Background experiments: 1-nitropyrene photochemistry

UV/visible absorption spectra of 1-nitropyrene and pyrene are shown in **Figures 4.1** and **Figure 4.2**, respectively. The absorption spectra of these compounds are quite similar. It was decided to evaluate the non-photochemical stability of 1-nitropyrene before proceeding with photochemical experiments. The absorption spectrum of a 0.75 ppm solution of 1-nitropyrene (in methanol) was obtained just after preparation and each successive day for 6 days following preparation. There was no discernible change in the appearance of the spectrum over the course of the experiment. Furthermore, the relative standard deviation (RSD) of the absorbance readings at 234 nm, the wavelength of maximum absorbance, was 6 %.

Solution-deposited samples of 1-nitropyrene on silica gel prepared from 1-nitropyrene solutions stored for 3-17 days were then analyzed via supercritical fluid extraction/gas chromatography (see pp. 68-72). No evidence for non-photochemical decomposition of 1-nitropyrene was provided by these experiments (i.e., no degradation product peaks were observed). It was assumed, then, that non-photochemical degradation of sorbed 1-nitropyrene would not occur to an appreciable extent over periods of several days, and this compound was deemed an appropriate representative nitro-PAH for these studies. Experiments designed to assess the extent of non-photochemical degradation of sorbed 1-nitropyrene are described in Section **4.2-E** (pp. 107-109).

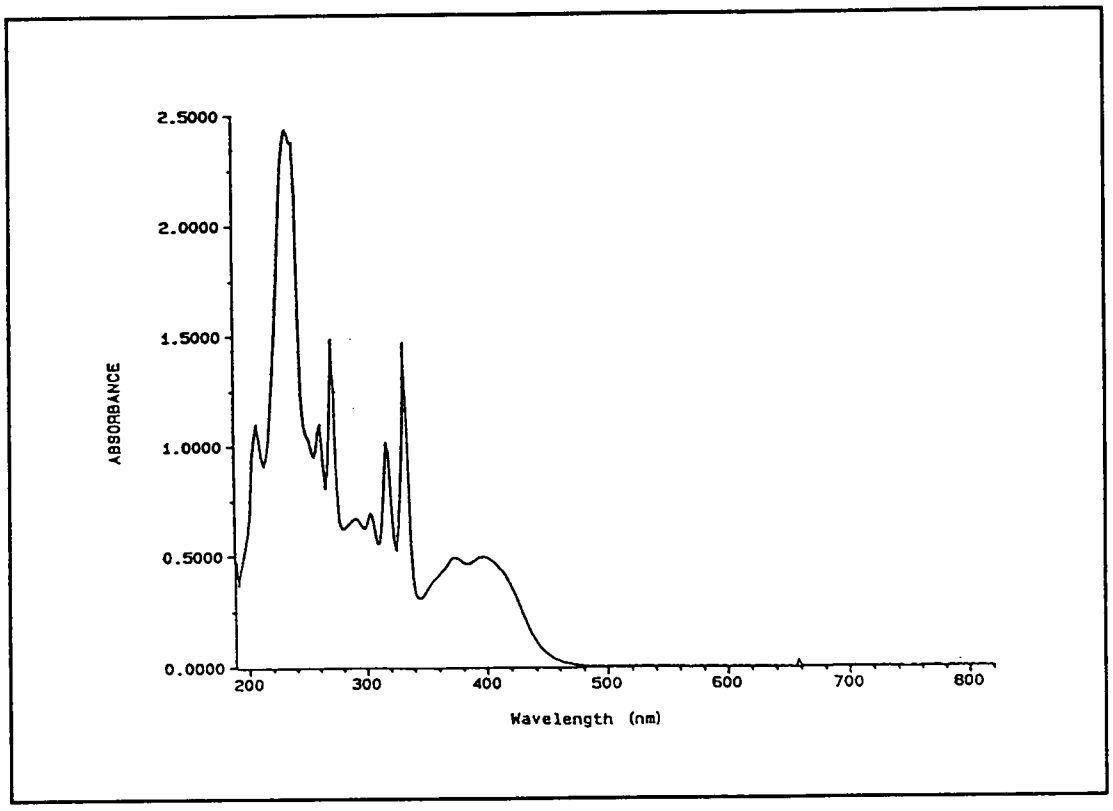

Figure 4.1 UV/visible absorption spectrum: **1-nitropyrene**, 10 ppm in methanol.

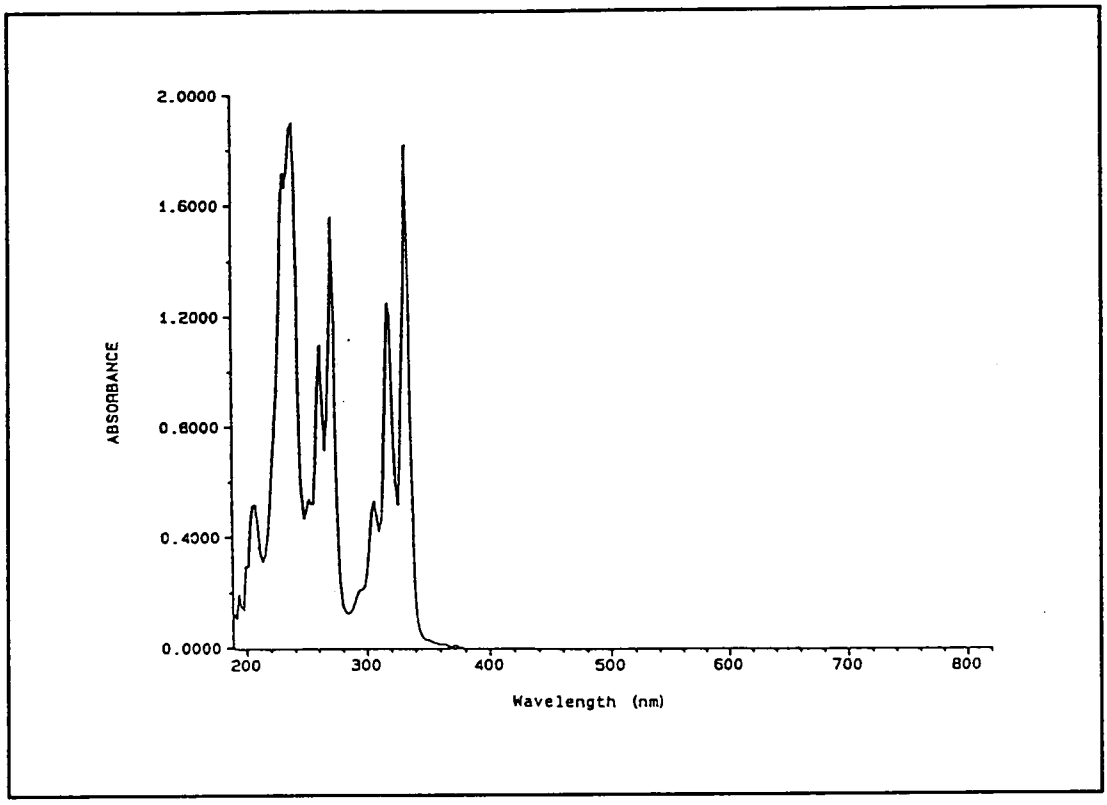

Figure 4.2 UV/visible absorption spectrum: **pyrene,** 10 ppm in methanol.

4.2-B Background experiments: supercritical fluid extractions

Blank (CO_2-only) extractions of empty cells were performed at a variety of flame ionization detector settings to determine those at which the problem with CO_2-derived impurities (see p. 95) was minimized. **Figure 4.3** shows chromatograms from runs at two different detector settings. Each integral increase in range or attenuation reduces the output signal by a factor of 2. The chromatogram obtained at settings of range = 8, attenuation =2 contains several peaks of undetermined origin. To avoid the possibility of additive interferences with analyte peaks, detector settings which yielded minimal background *noise* were used for subsequent experiments.

Solution-deposited samples of 1-nitropyrene on silica gel were then used to estimate the minimum detectable quantity of 1-nitropyrene using the supercritical fluid extraction technique. By comparing the peak areas of 1-nitropyrene from 90 μg/g and 1000 μg/g *solution*-deposited samples with those from *off-line* injections of 1-nitropyrene solutions, it was first determined that the supercritical fluid extraction of 1-nitropyrene from this adsorbent was quantitative. Results are summarized in **Table 4.2.** Values reported for *Determined coverage* (and all values in this text for which means ± confidence intervals are given) are at the 90 % confidence interval.

Figure 4.4 contains chromatograms derived from extractions of *solution*-deposited samples of 1-nitropyrene on silica gel. Analyses were at detector range = 11, attenuation =2. The 1-nitropyrene peak occurs at a retention time of 23 min. It can be seen that, at the chosen detector settings, the minimum detectable quantity of 1-nitropyrene is approximately 1 μg (10 μg/g coverage x 100 mg sample or 100 μg/g coverage x 10 mg sample). For the sake of comparison, a chromatogram obtained by analyzing a sample of silica gel that did not contain 1-nitropyrene is included in **Figure 4.4.** It can also be seen that deposition of 10 μg of 1-nitropyrene (100 μg/g x 100 mg) onto the head of the column yields a chromatographic peak easily discernible from baseline.

As pointed out on p. 89, Mauldin *et al.* [131] reported a 66 % recovery of pyrene from a carbonaceous subfraction of Kaneb coal stack ash (original coverage = 105 μg pyrene/g ash; size fraction = 75-124 μm). In order to allow for similar (or poorer) recoveries of 1-nitropyrene from Kaneb

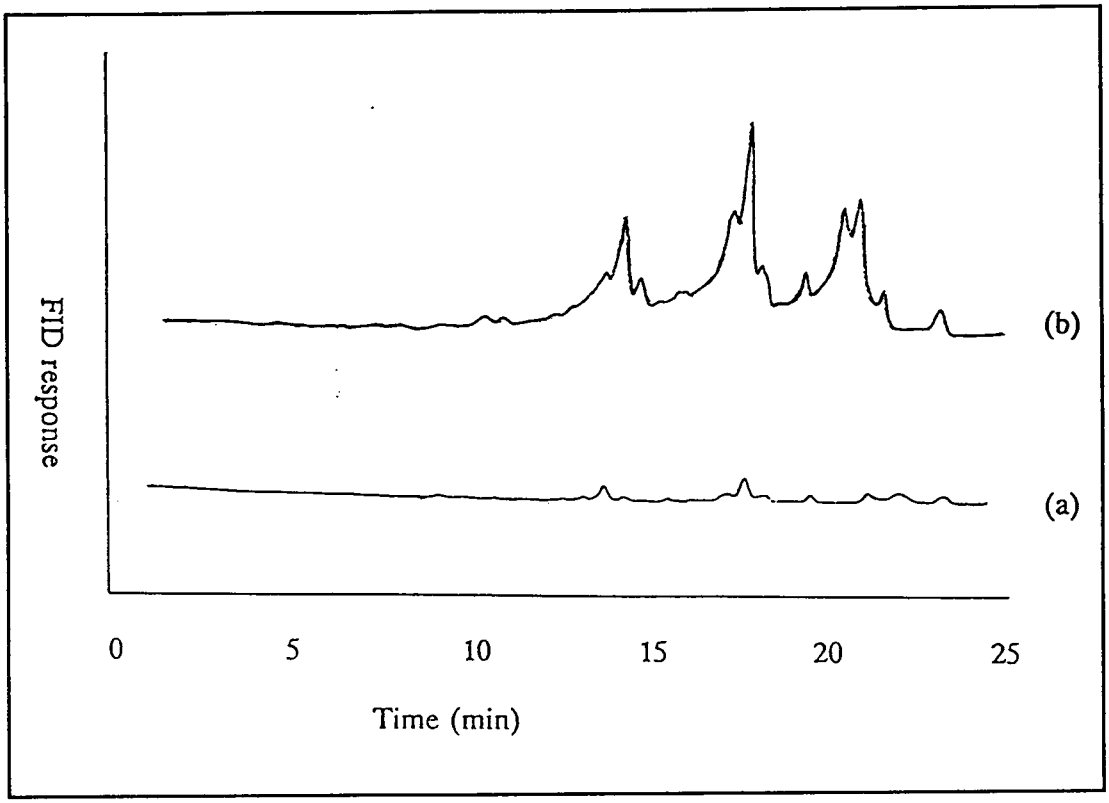

Figure 4.3 SFE/GC chromatograms for *blank* (CO_2-only) runs.
(a) range = 11; attenuation = 2.
(b) range = 8; attenuation = 2.

TABLE 4.2 EXTRACTION OF 1-NITROPYRENE FROM SILICA GEL

Predicted coverage[a]	Determined coverage[b]	% Recovery
90 μg/g	88 ± 3 μg/g	96 %
1000 μg/g	1068 ± 52 μg/g	107 %

[a]known quantity of 1-nitropyrene *solution-deposited* onto a known mass of silica gel.
[b]extracted and quantified by SFE/GC.

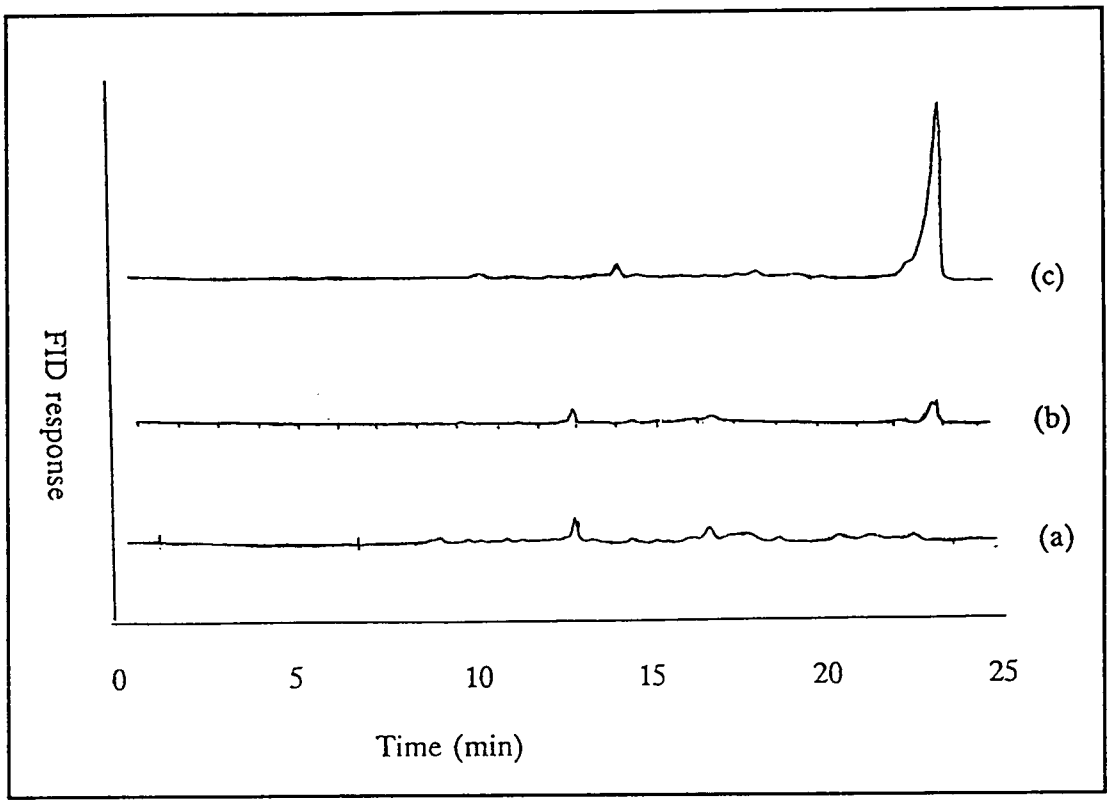

Figure 4.4 SFE/GC chromatograms as a function of 1-nitropyrene coverage level (deposited from solution on silica gel).

(a) blank silica gel; 81.6 mg.
(b) 1-nitropyrene on silica gel; 10 μg/g, 87.4 mg of sample.
(c) 1-nitropyrene on silica gel; 90 μg/g, 83.8 mg of sample.

coal stack ash fractions and, in order to generate detectable 1-nitropyrene peaks, it was decided to attempt to target vapor-deposited coverages of 1-nitropyrene or pyrene on Kaneb stack ash in the 10^2-10^3 μg/g range.

Finally, the precision of the supercritical fluid extraction/gas chromatography system was evaluated by running five replicate extractions/quantifications of a solution-deposited sample of 1-nitropyrene on silica gel (coverage = 90 μg/g). The RSD for these analyses was 3.7 %. This compares favorably with the 4 % RSD reported by Mauldin [104] for supercritical fluid extractions or the average of 4.4 % RSD reported by Dunstan *et al.* [44] and Yokley *et al.* [74] for micro-soxhlet extractions.

4.2-C Vapor depositions of 1-nitropyrene and pyrene

As described in **Chapter 2** (p. 59) the mass flow rate of adsorbate during a deposition can be estimated by passing the flow of adsorbate/carrier through a *calibration coil*, immersed in an ice bath, and quantifying the amount of adsorbate trapped in a specified period of time. The mass flow rate (in μg/hr) is used in conjunction with the period of time encompassed by a deposition and the fraction of adsorbate mass flow retained by the adsorbent (see **Chapter 2**, p. 60) to calculate the predicted adsorbate/adsorbent coverage level. However, a malfunctioning electrometer (flame ionization detector signal processing unit) prevented the monitoring of the FID signal profile during the time period when 1-nitropyrene depositions were carried out. A rigorous determination of the predicted 1-nitropyrene/adsorbent coverage levels was not, therefore, possible.

It was decided to circumvent this problem by determining the mass flow rate of 1-nitropyrene by the procedure outlined on p. 59. To summarize briefly, the quantity of 1-nitropyrene extracted from silica gel exposed to 1-nitropyrene/carrier flow for a specified period of time (1-4 hr) was used to determine the mass flow for that time period. This approach is a more direct determination of the mass flow of adsorbate that is retained by an adsorbent per unit time than the *off-line* collection/determination approach used previously. It eliminates the need to incorporate the fraction

of mass flow of adsorbate retained by the adsorbent (obtained from the flame ionization detector profile). The predicted adsorbate/adsorbent coverage level is, then, simply the product of the measured mass flow rate and deposition time, divided by the mass of the adsorbent.

There are, however, several potential problems in using this approach. First of all, the recovery of 1-nitropyrene from silica gel must be quantitative if the *available* mass flow rate is to be determined accurately. According to results presented in **Table 4.2**, p. 97, recovery is quantitative. The use of this approach also mandates the assumption that the fraction of 1-nitropyrene retained does not vary as a function of the composition of the adsorbent. Previous work with pyrene sorbed on silica gel and on Kaneb coal stack ash adsorbents [134] indicates that this is not necessarily true. Some of the work is summarized in **Table 4.3**.

The depositions in which these data were generated were all stopped before the point where adsorbent was *saturated* with pyrene (i.e., the point where a maximum quantity of adsorbate has been retained; see p. 60 and **Figure 2.6**, p. 61). Values in the *Pyrene retained/total mass flow rate of pyrene* column of **Table 4.3** would be considerably lower than those listed if depositions were allowed to proceed to *saturation*.

According to the results in **Table 4.3**, the fraction of pyrene retained by an adsorbent does vary as a function of the composition of the adsorbent. It is expected that corresponding values for 1-nitropyrene on these adsorbents would follow a similar trend. Nonetheless, it was decided that predicted 1-nitropyrene/adsorbate coverages could be approximated according to the method outlined above without unduly compromising the accuracy of those determinations, provided those depositions were at *sub-saturation* levels.

Deposition at *sub-saturation* coverages also minimizes the possibility that 1-nitropyrene might be *layered* onto the surfaces of adsorbents. Such a situation might lead to an inhibition of photolysis of 1-nitropyrene, not only through some substrate-dependent phenomena, but also via a *shielding* (from incident radiation) of inner *layers* of 1-nitropyrene by outer *layers*.

TABLE 4.3 RETENTION OF MASS FLOW OF PYRENE BY SILICA GEL AND KANEB COAL STACK ASH FRACTIONS

Adsorbent	Pyrene retained/total mass flow of pyrene[a]
silica gel	90 %
F3 (ferromagnetic, 75-124 μm)	67 %[b]
C3 (carbonaceous, 75-124 μm)	81 %[b]
M3 (mineral, 75-124 μm)	77 %[b]

[a]determined from flame ionization detector signal profile during the course of a vapor deposition experiment.
[b]Source: Mauldin, R.F., unpublished results.

One may estimate the *saturation* coverages of a given adsorbate on a given adsorbent if one knows the molecular area of the adsorbate and the surface area of the adsorbent. Schure [135] lists a molecular area of pyrene = 90 $Å^2$ (or 90 x 10^{-20} m^2). One may assume that the molecular area of 1-nitropyrene is similar (it would be slightly larger than that of pyrene). Sanders [105] has determined the specific surface areas of fractions of Kaneb coal stack ash and of the silica gel used in this work. Taking the values for those ash fractions most comparable to the fractions used in this work, the estimated *saturation* coverages of 1-nitropyrene may be calculated. These are listed in **Table 4.4.** To the extent that the area of a 1-nitropyrene molecule is greater than that for pyrene, these estimates are slightly higher than the actual values. For a given mass flow rate of 1-nitropyrene, the time required to achieve *saturation* of a particular adsorbent can be estimated and the deposition can be stopped short of that time. With the specified assumptions, the time required to achieve *saturation* for the adsorbents used in these studies is also listed in **Table 4.4.**

A knowledge of adsorbate/adsorbent coverage levels is important primarily for sorptivity experiments, for which the amount extracted is compared to the predicted value. For photochemical experiments, the important value is the coverage level after an illumination relative to the coverage level

TABLE 4.4 ESTIMATED SATURATION COVERAGES OF ADSORBENTS FOR 1-NITROPYRENE

Adsorbent	Measured Specific surface area[a], m^2/g	Calculated Saturation coverage, $\mu g/g$	Calculated Saturation time[b]
Silica gel	400	170,000	666 hr
U2	6.5	2750	11 hr
F2	0.75	375	1.5 hr
C2	20	10,312	41 hr
M2	1.7	708	2.8 hr

[a]Source: Sanders, J.K. *Chromatographic and Spectroscopic Studies of the Interaction of Pyrene with Coal Stack Ash*, Ph.D. Dissertation, University of Tennessee, Knoxville, 1991; pp. 130-134.
[b]for 250 $\mu g/hr$ mass flow of 1-nitropyrene, 1.0 g of adsorbent.

before illumination. So long as the extraction efficiency remains constant, and so long as sub-monolayer coverage of the adsorbent by the adsorbate is known to be achieved, the accuracy of the predicted coverage is of little importance.

A problem with the on-column injection port of the gas chromatograph (see **Figure 2.10**, p. 69) mandated that quantification of chromatographic peak areas of pyrene (e.g., for mass flow rate determinations and all subsequent extractions involving pyrene) be carried out against previously effected off-line injections of 1-nitropyrene solutions. It was assumed that the response of the flame ionization detector for pyrene was equivalent to that for 1-nitropyrene. To test the validity of that assumption, peak areas for extractions of *solution-deposited* samples of 1-nitropyrene and pyrene were compared. Results are summarized in **Table 4.5**. The calculated pyrene/silica gel coverage level was within 10 % of that of a 1-nitropyrene/silica gel sample with an identical coverage level.

Tables 4.6 and **4.7** summarize the experimental conditions employed and the predicted coverages obtained for 1-nitropyrene and pyrene depositions, respectively. Specified are the adsorbent sample size and deposition time for each. 1-Nitropyrene depositions were stopped well short of the time

TABLE 4.5 COMPARISON OF FID RESPONSE FOR 1-NITROPYRENE AND PYRENE

Compound	Predicted coverage[a]	Calculated coverage[b]	% Difference
1-nitropyrene	1000 μg/g	1068 ± 52 μg/g	+ 7 %
pyrene	1000 μg/g	1172 ± 44 μg/g	+ 17 %

[a]known quantity of adsorbate *solution-deposited* onto a known mass of silica gel.
[b]extracted and quantified via SFE/GC vs. *off-line* injections of 1-nitropyrene solutions.

TABLE 4.6 DEPOSITION PARAMETERS AND PREDICTED COVERAGE LEVELS FOR 1-NITROPYRENE

Adsorbent	Sample size, g	Deposition time[a], hr	Predicted coverage[b], μg/g
Silica gel	2.0013	16.0	1100
U2	1.9620	4.0	280
U2 # 2	2.0007	8.0	550
F2	2.9276	2.5	120
F2 # 2	3.0085	3.0	140
C2	2.5320	20.0	1100
C2 # 2	2.0094	36.0	2500
M2	1.5320	3.0	270
M2 # 2	2.0022	4.0	410

[a]at oven 1 = 140° C, oven 2 = 145° C; measured mass flow rate of 1-nitropyrene = 140 μg/hr.
[b]predicted coverage = ([mass flow rate]*[deposition time])/sample size; in μg 1-nitropyrene/g adsorbent.

TABLE 4.7 DEPOSITION PARAMETERS AND PREDICTED COVERAGE LEVELS FOR PYRENE

Adsorbent	Sample size, g	Deposition time[a], hr	Predicted coverage[b], μg/g
Silica gel	2.0028	16.2	2200
U2	1.0026	8.0	2200
F2	1.0018	1.0	270
C2	1.5000	36.0	6500
M2	1.4992	2.5	450

[a]at oven 1 = 100° C, oven 2 = 105° C; measured mass flow rate of pyrene = 270 μg/hr.
[b]predicted coverage = ([mass flow rate]*[deposition time])/sample size; in μg pyrene/g adsorbent.

at which *saturation* of an adsorbent might occur (see **Table 4.4**, p. 102). Pyrene depositions were, likewise, stopped short of *saturation* (according to FID signal profile; see **Figure 2.6**, p. 61). Predicted coverage levels for both adsorbates were determined as outlined on p. 106. The actual coverage for a given adsorbate may be 70-90 % of that listed. According to the data of **Table 4.3** (p. 101), error in the predicted coverage is likely greatest for the ferro-magnetic fraction (F2).

Two sets of 1-nitropyrene depositions (**Table 4.6**, previous page) were carried out so that sorptivity and photochemical behavior for that adsorbate could be evaluated over a limited range of coverages. The average measured mass flow rate of 1-nitropyrene for those depositions was 140 μg/hr. The average measured mass flow rate of pyrene for the depositions listed in **Table 4.7** was 270 μg/hr. Coverage levels listed for 1-nitropyrene and pyrene are greater than those expected for atmospheric particles containing those adsorbates (see **Table 4.1**, p. 86, for 1-nitropyrene values; see pp. 88 for pyrene values).

4.2-D Sorptivity of 1-nitropyrene and pyrene

The quantity of 1-nitropyrene that could be extracted, as a function of adsorbent sample size, from each of the 1-nitropyrene/adsorbent samples listed in **Table 4.6** (p. 103) was determined by SFE/GC (pp. 68-72). Results are summarized in **Table 4.8.** Recovery of 1-nitropyrene from silica gel was nearly quantitative (as it was for *solution*-deposited 1-nitropyrene/silica gel; see **Table 4.2**, p. 97). The carbonaceous subfraction (C2) of Kaneb coal stack ash shows a strong affinity for 1-nitropyrene. Note that a detectable quantity of 1-nitropyrene could not be extracted from a carbonaceous sample containing 1100 μg/g 1-nitropyrene. Recovery from a carbonaceous sample that contained a coverage more than two times greater was only 3 %.

A greater percentage of the original coverage of 1-nitropyrene was extractable from ferromagnetic (F2, F2 # 2) and mineral (M2, M2 # 2) enriched subfractions. For these adsorbents the recovery did not vary significantly over a limited range of 1-nitropyrene/adsorbent coverages. Note that recovery of 1-nitropyrene from U2 and U2 # 2, the unfractionated samples of Kaneb coal stack ash (particle diameter = 45-74 μm), was less than that of the ferromagnetic and mineral samples. This is somewhat surprising since, as shown in **Figure 3.1** (p. 81), the F2 and M2 subfractions accounted for 89 % of the mass of U2. Results in **Table 4.8** suggest that a significant portion of the 1-nitropyrene sorbed on U2 is associated with the carbonaceous component of U2.

Results for extractions/quantifications of pyrene/adsorbent samples are listed in **Table 4.9.** Recovery is nearly quantitative from silica gel. Among coal stack ash fractions separated according to chemical composition, the strongest affinity for pyrene was exhibited by the carbonaceous subfraction, followed by the mineral fraction. The weakest adsorbent was the ferromagnetic subfraction.

These results parallel those of Dunstan *et al.* (reference 44; see p. 31), who noted a similar trend for pyrene on equivalent subfractions of Kaneb coal stack ash (particle diameter = 75-124 μm). As was the case for 1-nitropyrene, the ability to extract pyrene from the unfractionated ash (U2) was apparently inhibited by association of pyrene with the carbonaceous component of that ash. The effect does not seem to be as pronounced as for 1-nitropyrene on U2.

TABLE 4.8 1-NITROPYRENE EXTRACTION RECOVERIES[a]

Adsorbent	Predicted coverage[b]	Measured coverage[c]	% Recovery
silica gel	1100	981 ± 51	89 %
U2	280	52 ± 10	19 %
U2 # 2	550	98 ± 10	18 %
F2	120	52 ± 6	43 %
F2 # 2	140	64 ± 6	46 %
C2	1100	ND[d]	0 %
C2 # 2	2500	67 ± 6	3 %
M2	270	85 ± 6	31 %
M2 # 2	410	111 ± 6	27 %

[a]all coverages in μg 1-nitropyrene/g adsorbent.
[b]based on mass flow rate of 1-nitropyrene, deposition time, and adsorbent sample size.
[c]determined by SFE/GC.
[d]none detected.

TABLE 4.9 PYRENE EXTRACTION RECOVERIES[a]

Adsorbent	Predicted coverage[b]	Measured coverage[c]	% Recovery
silica gel	2200	1980 ± 100	90 %
U2	2200	928 ± 28	42 %
F2	270	153 ± 9	57 %
C2	6500	2643 ± 124	41 %
M2	450	228 ± 22	51 %

[a]all coverages in μg pyrene/g adsorbent.
[b]based on mass flow rate of pyrene, deposition time, and adsorbent sample size.
[b]determined by SFE/GC.

The sorptivities of 1-nitropyrene and pyrene are compared in **Table 4.10.** Values listed for 1-nitropyrene are, where appropriate, the means of recoveries from duplicate samples. With the exception of silica gel, recoveries are greater for pyrene than 1-nitropyrene, regardless of the composition of the ash fraction. This may be partly due to that fact that supercritical CO_2 is a better solvent for non-polar pyrene than for its polar derivative, 1-nitropyrene [128].

There does seem to be a disproportionate association of 1-nitropyrene with the carbonaceous component of coal stack ash that cannot be attributed solely to a *solvent* effect. If one multiplies the % by mass (of U2; see **Figure 3.1**, p. 81) of the subfractions F2 (12 %), C2 (11 %), and M2 (77 %) by the % recovery of adsorbate from each subfraction, one obtains a value that should equal the % recovery from U2, assuming that each subfraction independently influences the recovery of U2 in a manner proportional to its mass %. For pyrene, the recovery from U2 should be 51 %. The actual recovery, 42 %, was 82 % of that value. For 1-nitropyrene, the expected recovery from U2 is 27 %. The actual recovery, 18 %, was only 67 % of that value. Also note that the recovery of 1-nitropyrene from C2 is only 7 % of the recovery of pyrene attainable from C2 (3 % for 1-nitropyrene vs. 41 % for pyrene). If it is true, as pointed out on p. 31, that the interaction of PAH with carbonaceous particles is due to dispersion forces between the PAH and surface carbon that is graphitic (i.e., aromatic), then such interactions (i.e., induced dipole between *pi* electron clouds of PAH and surface carbon) might be enhanced by a substituent such as the $-NO_2$ group, which *withdraws* electron density from the aromatic ring system of PAH.

4.2-E Non-photochemical degradation of 1-nitropyrene

The initial coverages of 1-nitropyrene on silica gel and on Kaneb coal stack ash fractions were determined (by SFE/GC; see pp. 68-72) less than 1 week following the vapor deposition experiment, at 3 weeks after the deposition, and at 10 weeks after the deposition. (As pointed out in **Chapter 2**, p. 63, samples were stored in the dark in a desiccator.) Results are summarized in **Table 4.11.** Note that

TABLE 4.10 COMPARISON: 1-NITROPYRENE AND PYRENE EXTRACTION RECOVERIES

Adsorbent	% Recovery, 1-nitropyrene	% Recovery, pyrene
silica gel	89 ± 5 %	90 ± 4 %
U2	18 ± 2 %	42 ± 1 %
F2	44 ± 3 %	57 ± 3 %
C2	3 ± 1 %	41 ± 2 %
M2	29 ± 1 %	51 ± 5 %

TABLE 4.11 1-NITROPYRENE: NON-PHOTOCHEMICAL EXPERIMENTS[a]

Adsorbent	Initial coverage	After 3 wks	% Loss	After 10 wks	% Loss
silica gel	981 ± 51	965 ± 94	2 %	984 ± 70	0 %
U2	98 ± 10	99 ± 11	0 %	93 ± 7	6 %
F2	64 ± 6	64 ± 9	0 %	62 ± 9	3 %
C2	67 ± 19	68 ± 9	0 %	70 ± 9	0 %
M2	85 ± 6	84 ± 3	1 %	80 ± 9	6 %

[a]all data = extracted μg 1-nitropyrene/g adsorbent.

there is virtually no detectable loss of 1-nitropyrene after 3 weeks of storage. Similarly, Korfmacher *et al.* [71] found that pyrene was stable on the 45-74 μm fraction of a bulk coal stack ash for up to 3 weeks. Some loss of 1-nitropyrene is noted after 10 weeks of storage, particularly for the unfractionated Kaneb coal stack ash U2 (45-74 μm) and the magnetic (F2) and mineral (M2) enriched subfractions.

The results in **Table 4.11** (previous page) do not imply that non-photochemical degradation (e.g., by reaction with atmospheric species) of 1-nitropyrene is not possible. Instead, these results (obtained for storage under controlled conditions) serve as a baseline against which the photochemical experiments carried out using samples prepared and stored in identical ways may be compared.

The total period of time encompassed by the vapor deposition experiment, the determination of baseline coverages, and quantification of coverages following irradiations did not exceed 3 weeks for any adsorbent. It was reasonable to assume, then, that any degradation seen during photochemical experiments could be attributed to photolysis, and not to any kind of *dark* loss.

4.2-F Photochemical degradation of 1-nitropyrene and pyrene

The nitropyrene-containing adsorbents listed in **Table 4.6** (p. 103) were subjected to 24 hr illuminations under UV/visible light (pp. 64-68). Excepted was the carbonaceous fraction C2, which did not contain a detectable initial coverage level of 1-nitropyrene (see **Table 4.8**, p. 106, for a summary of extraction recovery experiments for 1-nitropyrene). Separate portions of the C2 # 2 and of the silica gel sample were subjected to parallel 24 hr exposures. The coverage levels of 1-nitropyrene remaining after illumination experiments were determined via SFE/GC (pp. 68-72). These were compared to coverage levels determined initially (i.e., less than 1 week after vapor deposition). Results are summarized in **Table 4.12.**

Significant photodegradation was evident for 1-nitropyrene on silica gel. Among coal stack ash fractions, the extent of photodegradation was greatest for the mineral enriched fractions (M2 and M2 # 2). Somewhat less photodegradation was evident on the ferromagnetic enriched subfractions (F2 and

TABLE 4.12 1-NITROPYRENE: PHOTOCHEMICAL EXPERIMENTS[a]

Adsorbent	Initial coverage	After 24 hr exposure	% Loss
silica gel	981 ± 51	577 ± 19	41 %
run # 2		657 ± 79	33 %
U2	98 ± 10	98 ± 13	0 %
U2 # 2	52 ± 10	53 ± 11	0 %
F2	64 ± 6	56 ± 9	12 %
F2 # 2	58 ± 4	52 ± 3	10 %
C2	67 ± 19	71 ± 9	0 %
run # 2		73 ± 6	0 %
M2	85 ± 6	68 ± 22	20 %
M2 # 2	111 ± 6	88 ± 16	21 %

[a]all data = extracted μg 1-nitropyrene/g adsorbent.

F2 # 2). The reproducibility of the irradiation technique, as evidenced by the two silica gel runs, was adequate. Furthermore, over the narrow range of initial coverages of F2 and M2 samples, the extent of degradation did not vary significantly. The extent of degradation was slightly higher for slightly higher coverages. There was no apparent photodegradation of 1-nitropyrene on the carbonaceous fraction C2, nor on the unfractionated Kaneb coal stack ash (U2 and U2 # 2; particle diameter = 45-74 μm).

Results for photochemical experiments carried out on pyrene-containing adsorbents are summarized in **Table 4.13**. These may be compared to results in **Table 1.14**, p. 35 (pyrene on silica gel; 24 hr exposure) and to those in **Table 1.18**, p. 40 (pyrene on unfractionated Kaneb ash, < 45 μm particle diameter, and on 75-124 μm fractions enriched in ferromagnetic, carbon, and mineral content; 24 hr exposures). Results in **Table 4.13** are quite similar to those obtained previously for photochemical experiments with pyrene on equivalent adsorbents. The reproducibility of experimental conditions is, therefore, validated by the current experiments. As for previous experiments, the extent of photodegradation of pyrene (and of 1-nitropyrene) is greatest on mineral enriched fractions. Less

TABLE 4.13 PYRENE: PHOTOCHEMICAL EXPERIMENTS[a]

Adsorbent	Initial coverage	After 24 hr exposure	% Loss
silica gel	1980 ± 100	644 ± 65	68 %
U2	928 ± 28	839 ± 70	10 %
F2	153 ± 9	139 ± 8	9 %
C2	2693 ± 124	2608 ± 97	3 %
M2	228 ± 22	181 ± 14	21 %

[a]all data = extracted μg pyrene/g adsorbent.

photodegradation is evident on ferromagnetic enriched fractions. The least amount of photodegradation appeared to occurr on carbonaceous enriched fractions.

1-Nitropyrene and pyrene photochemical results are compared in **Table 4.14.** Values listed for 1-nitropyrene are the means of dupilicate runs listed in **Table 4.12** (previous page). It is not immediately apparent why there was less photodegradation of 1-nitropyrene on silica gel than of pyrene on silica gel. Sorbed 1-nitropyrene may be, in general, less prone to photolysis than pyrene. However, Holloway and co-workers (see reference 124 and p. 88) noted that, in solution, 1-nitropyrene was more prone to photodegradation than pyrene. Losses of 1-nitropyrene from ferromagnetic fractions (F2) and mineral fractions (M2) were approximately equal to losses of pyrene on F2 and M2. A comparison of sorptivity results (**Table 4.9**, p. 106) does not imply a stronger association of 1-nitropyrene with silica gel than of pyrene with silica gel.

What is apparent from **Table 4.14** is that 1-nitropyrene undergoes no detectable photolysis when associated with carbonaceous particles or with the unfractionated coal stack ash (U2). The phenomenon is even more pronounced than for pyrene on carbonaceous particles and on U2, for which only slight degradation was evident. The imprecision in the % photochemical loss data for pyrene on C2 and U2 inhibits a definitive assertion that 1-nitropyrene has a stronger tendency than pyrene to be associated

TABLE 4.14 COMPARISON OF PHOTOCHEMICAL RESULTS FOR 1-NITROPYRENE AND PYRENE[a]

Adsorbent	% Loss, 1-nitropyrene	% Loss, pyrene
silica gel	37 ± 6 %	68 ± 7 %
U2	0 %	10 ± 8 %
F2	11 ± 6 %	9 ± 8 %
C2	0 %	3 ± 6 %
M2	20 ± 15 %	21 ± 12 %

[a]all exposures = 24 hr.

with the carbonaceous component of coal stack ash. As did those in **Table 4.10** (p. 110), these results do, however, imply that this is true. Multiplying, as for the sorptivity data (p. 107), the % by mass (of U2) of each fraction by the % loss on that fraction yields the expected loss by photodegradation on U2, assuming a proportional (by mass) influence of each fraction on the photochemistry of U2. For pyrene, that value is 17 %, while for 1-nitropyrene, the expected loss from U2 is 15 %. Actual values, as reported in **Table 4.14**, were 10 % for pyrene and 0 % for 1-nitropyrene.

The differences in the extent of photolysis of 1-nitropyrene and pyrene on carbonaceous particles and on the unfractionated ash may be due in some way to a stronger association of 1-nitropyrene with the carbonaceous component of coal stack ash. It seems unlikely that these differences, if real, are attributable to a greater tendency of 1-nitropyrene to penetrate porous adsorbent surfaces and thereby be *shielded* from incident light. Molecular areas of 1-nitropyrene and pyrene should be similar and, likewise, their relative abilities to penetrate surface pores should be approximately equivalent. In fact, 1-nitropyrene, which should possess a slightly greater molecular area than pyrene, should be even less likely to penetrate into surface pores than pyrene.

4.3 Conclusions

Results in this chapter clearly demonstrate a strong association of 1-nitropyrene with the carbonaceous component of coal stack ash. Even with limitations in the ability to predict initial adsorbent coverages (p. 100), the results in **Table 4.10** (p. 108) strongly support this contention. Results in **Table 4.14** (p. 112), specifically the similarity of photochemical losses of 1-nitropyrene on carbonaceous and unfractionated coal stack ashes, also imply a strong association between 1-nitropyrene and carbonaceous particles. A comparison of 1-nitropyrene sorptivity and photochemical results with pyrene results (**Tables 4.10** and **4.14**) suggests that the $-NO_2$ group plays a significant role in the interaction of nitro-PAH with coal stack ash.

There was no apparent photodegradation of 1-nitropyrene when sorbed to a carbonaceous enriched (23.27 % carbon; see **Table 3.2**, p. 83) fraction of coal stack ash or to an unfractionated ash (6.25 % carbon). It has been pointed out (p. 48) that the coal stack ash used in these studies had an atypically high percentage of carbon. Results in **Tables 1.5** (p. 23), **1.8** (p. 27), and **1.10** (p. 29) suggest that the carbon content of coal fly ash may be a factor of 10 or more less than the carbon content of the coal stack ash used herein. It has also been pointed out (p. 22) that *fine* particles ($< 2.5\ \mu m$ particle diameter), in general, contain less carbon than *coarse* particles (e.g., 45-74 μm particles).

Based on these observations, it would seem likely that the suppression of photolysis of 1-nitropyrene would be less pronounced on small, respirable particles more likely to be in the atmosphere. However, the 1-nitropyrene coverage levels used herein (e.g., $\approx 500\ \mu g/g$ for the unfractionated ash) were as much as 10^3 to 10^4 times higher than those expected for atmospheric particles (see **Table 4.1**, p. 86). In other words, there is likely to be significantly less 1-nitropyrene available for interaction with the carbon associated with atmospheric coal fly ash particles, and that which is available should still be preferentially associated with the carbonaceous component of those particles. It can be concluded, therefore, that photolysis does not appear to represent a significant avenue for degradation of nitro-PAH that is associated with coal fly ash particles in the environment.

CHAPTER 5

PHOTOCHEMISTRY OF ADSORBED PYRENE IN THE PRESENCE OF COADSORBATES

5.1 Introduction

5.1-A Background

The primary goals of experiments described in this chapter were to evaluate the effect of coadsorbates on the photochemistry of sorbed pyrene, and the effect of coadsorbates on the ability to extract sorbed pyrene from coal stack ash. Material in this section describes the rationale used in choosing coadsorbates for these experiments. Also described are experimental constraints imposed by the use of two adsorbates and the approaches used to evaluate and deal with those constraints.

It was decided that any adsorbate chosen for study should have the following characteristics:

1. a tendency, as noted in the literature, to be associated with atmospheric particles such as coal fly ash;
2. low toxicity;
3. sufficient volatility such that the ability to deposit onto coal stack ash substrates could be demonstrated;
4. stable against photochemical as well as non-photochemical degradation.

The last characteristic is important because the tendency of a coadsorbate to degrade, in the absence or presence of light, would complicate the evaluation of whether or not the coadsorbate affects

the sorptivity or photochemical behavior of sorbed PAH. In other words, if coadsorbate and degradation product were present, it would be very difficult to ascertain conclusively whether any changes in the photochemical behavior of sorbed PAH were due to the presence of the coadsorbate or the presence of degradation product(s).

Table 1.19, p. 45, lists the molecular formulas and abundances of several carboxylic acids and *n*-alkanes that have been found on atmospheric particles. Two of those listed were initially targeted as potential coadsorbates: succinic acid and tricosane. The goal of this work, as stated on p. 49, was to evaluate the photochemical behavior of pyrene under two types of conditions: (1) when deposited onto coal stack fractions that already contained a coadsorbate, and (2) when deposited onto *clean* coal stack ash fractions, then subsequently *covered* with a coadsorbate. Any coadsorbate used for the first of these studies should be less volatile than pyrene (so that it is less likely to be desorbed at oven conditions necessary to carry out pyrene depositions). Any coadsorbate chosen for the second of these studies should be more volatile than pyrene (so that depositions can be effected at oven temperatures unlikely to cause desorption of pyrene).

Table 5.1 lists the melting points and boiling points for pyrene, succinic acid, tricosane, and other organic compounds eventually evaluated as potential coadsorbates. It was found that succinic acid would sublime at an oven 1 temperature (see **Figure 2.3**, p. 56) of 180° C. In an attempt to find a coadsorbate which could be effectively *layered* on pyrene (i.e., one more volatile than pyrene), the other compounds listed in **Table 5.1** were evaluated. It was found that tricosane did not sublime at temperatures up to its melting point. Likewise, adipic acid ($C_6H_{10}O_4$), listed as the third most abundant of thirteen carboxylic acids found on atmospheric particles sampled by Grosjean *et al.* [102], and stearic acid (see **Table 1.19**, p. 45, for typical atmospheric abundance), were determined to be unsuitable coadsorbates because they did not sublime at temperatures below their respective melting points.

It was then decided to identify an alkane which was a liquid at room temperature, and which had a boiling point low enough to assure a significant vapor pressure at a reasonable oven 1 temperature (practical oven limit ≈ 200° C). *n*-Decane, found by Garcia *et al.* [98] in coal power station emissions

TABLE 5.1 MELTING AND BOILING POINTS OF PYRENE AND POTENTIAL COADSORBATES

Compound	Melting point, ° C	Boiling Point, ° C
Pyrene	156	393
Succinic acid	188	235 d[a]
Tricosane	47.6	380.2
Adipic acid	153	265 (100 torr)
Stearic acid	71.5	360 d[a]
n-Decane	-29.7	174.1

[a]decomposes.
Source: CRC Press, Inc. *CRC Handbook of Chemistry and Physics*, 58th edition, Weast, R.C. (Ed.), 1977-78; pp. C/270-C/532.

(gaseous and particulate) at an average level of 0.23 μg/g, was found to fit this criterion. Succinic acid and *n*-decane, then, were identified as potentially suitable coadsorbates. Finally, alkyl carboxylic acids and *n*-alkanes do not possess functional groups which render them likely to absorb a significant amount of radiation in the visible and near ultraviolet regions of the electromagnetic spectrum [66].

5.1-B Objectives

The realization of the experimental goals listed on p. 114 mandated the completion of several background experiments. These included:

1. evaluation of the tendency of sorbed succinic acid to resist desorption at oven temperatures compatible with deposition of pyrene;
2. evaluation of the tendency of sorbed pyrene to resist desorption at oven temperatures compatible with *n*-decane depositions;

3. evaluation of the photochemical and non-photochemical stability of succinic acid and *n*-decane.

It was assumed that the tendency of an adsorbate to be desorbed from an adsorbent surface (whether by volatilization or displacement by a second coadsorbate) or to be subject to non-photochemical or photochemical degradation would be most pronounced for adsorbate on silica gel. This adsorbent, at least for PAH as adsorbate, allows for much higher extraction efficiencies than coal stack ash adsorbents (see **Table 4.10**, p. 108). These studies were, therefore, carried out with adsorbate on silica gel, and not on coal stack ash fractions.

Following the completion of these experiments, those addressing the primary goals of the work were carried out. These included:

1. depositions of succinic acid, and then pyrene, onto the surfaces of coal stack ash and model adsorbents;
2. depositions of pyrene, and then *n*-decane, onto the surfaces of coal stack ash and model adsorbents;
3. a study of the sorptivity and photochemical behavior of sorbed pyrene in the presence of succinic acid relative to those behaviors exhibited in the absence of succinic acid;
4. equivalent studies for pyrene coadsorbed with *n*-decane.

5.2 Results and Discussion

5.2-A Retention of Sorbed Succinic Acid

To determine the ability of the technique used to extract succinic acid from adsorbent surfaces (ultrasonic extraction in water, see p. 72) to quantitatively remove that adsorbate from silica gel, a *solution*-deposited sample of succinic acid on silica gel (10,000 μg/g) was extracted and quantified.

Three such determinations indicated a 97 ± 5 % recovery. The mass flow rate of succinic acid, then, was determined (as for 1-nitropyrene, pyrene, see p. 59) by quantifying the amount of adsorbate extracted from a silica gel sample exposed for a specified time to adsorbate/carrier flow.

A vapor deposited sample of succinic acid on silica gel (predicted coverage = 6.7×10^4 $\mu g/g$) was then used to determine the optimum temperatures at which to carry out pyrene depositions (i.e., those at which succinic acid desorption was minimized). Portions of this sample (in oven 2, see **Figure 2.3**, p.56) were exposed to carrier-only flow at oven temperatures estimated to be compatible with pyrene depositions (starting with an oven 1 temperature ≈ 20° C below melting point of pyrene; oven 2 temperature = oven 1 temperature + 5° C) and at successively lower oven temperatures. Following 24 hour exposures, the percentage loss of succinic acid was determined. These results are summarized in **Table 5.2.**

A roughly linear decrease in succinic acid loss with decreasing oven temperatures was observed, though the decline seemed to diminish at the 100°/105° mark. Note that there was virtually no detectable succinic acid loss for flow of carrier at room temperature. Since each reduction in oven 1 temperature causes a corresponding reduction in the achievable mass flow rate of pyrene, there is an inherent trade-off in adjusting the oven 1 temperature. In other words, each reduction in temperature increases the time required for depositions of pyrene at a given coverage, and offsets, to some degree, any advantage gained with respect to the ability to retain succinic acid. It was therefore decided to carry out subsequent pyrene depositions at 100°/105°.

Such an experiment does leave unanswered the question of whether or not adsorbed succinic acid may be displaced by pyrene during the course of a pyrene deposition. Significant losses of this nature would lead to a situation that differed little from deposition of pyrene onto *clean* adsorbents. The quantity of succinic acid extractable from a portion of the vapor-deposited sample of succinic acid on silica gel (predicted coverage = 6.8×10^4 $\mu g/g$) that had been exposed to 8 hr (the time required to yield the desired pyrene on silica gel coverage) of pyrene/N_2 flow was determined. This quantity was compared to the amount extractable from an equivalent sample exposed to 8 hr of carrier-only flow.

TABLE 5.2 RETENTION OF SORBED SUCCINIC ACID AS A FUNCTION OF OVEN TEMPERATURES[a]

Temperature of Oven 1/Oven 2, °C	Succinic acid/silica gel coverage after 24 hr[b]	% Loss
130°/135°	3.7×10^4 μg/g	43 %
120°/125°	4.5×10^4 μg/g	31 %
110°/115°	5.3×10^4 μg/g	19 %
100°/105°	5.7×10^4 μg/g	13 %
90°/95°	5.8×10^4 μg/g	10 %
room temp	6.6×10^4 μg/g	1 %

[a]test sample = vapor-deposited succinic acid/silica gel; predicted coverage = 6.7×10^4 μg/g.
[b]determined by ultrasonic extraction in water and titration with OH^-.

For both experiments, oven 1 was at 100° C and oven 2 was at 105° C. These results are summarized in **Table 5.3**. Though some loss of succinic acid was observed (relative to baseline values) for both exposures, there was no discernible difference between the sample subjected to carrier-only flow and that subjected to carrier + pyrene flow. It was assumed, then, that pyrene did not significantly displace sorbed succinic acid during deposition of the former upon adsorbent samples that contained the latter.

5.2-B Retention of Sorbed Pyrene

It was necessary to evaluate the retention of adsorbed pyrene under conditions used to carry out depositions of *n*-decane. A portion of a vapor-deposited sample of pyrene on silica gel (predicted coverage was 2200 μg/g) was subjected to a 10 minute exposure of *n*-decane/carrier; the measured mass flow rate of *n*-decane = 2.0×10^4 μg/hr. (Ten minutes was the time required for *saturation* coverage of *n*-decane on silica gel.) The quantity of pyrene extracted was compared to the quantity extracted

TABLE 5.3 RETENTION OF SORBED SUCCINIC ACID DURING DEPOSITIONS OF PYRENE[a]

Conditions	Succinic acid/silica gel coverage level[b]	% Loss
initial coverage	6.4×10^4 μg/g	- - -
after 8 hr of N_2-only flow[c]	6.0×10^4 μg/g	6 %
after 8 hr N_2 + pyrene flow[c,d]	6.0×10^4 μg/g	6 %

[a]test sample = vapor-deposited succinic acid/silica gel; predicted coverage = 6.7×10^4 μg/g.
[b]determined by ultrasonic extraction in water and titration with OH^-.
[c]succinic acid/silica gel samples in oven 2; temperature = 105° C.
[d]measured mass flow rate of pyrene = 270 μg/hr.after 10 min of carrier-only flow.

For both experiments, oven 1 was at 85° C and oven 2 was at 95° C. These results are summarized in **Table 5.4.**

Some loss of pyrene from silica gel can, according to these results, be attributed to displacement by *n*-decane. Such a phenomenon complicates the ability to compare the sorptivity of pyrene in the absence of coadsorbate to that when coadsorbate is present. In other words, the tendency to extract a smaller quantity of pyrene in the presence of *n*-decane may be due not only to the fact that pyrene is *covered* with *n*-decane, but also because some pyrene has been displaced during deposition of *n*-decane. No loss of pyrene occurred when pyrene/silica gel was installed in the illumination set-up (i.e., under vacuum; see p. 64) in the absence of light.

5.2-C Non-photochemical and photochemical stability of succinic acid

As is pointed out on pp. 114-115, it was necessary to choose experimental conditions such that succinic acid did not photolyze, and did not undergo non-photochemical degradation, when co-sorbed with pyrene on model and coal stack ash adsorbents. **Figure 5.1** shows a representative absorption spectrum of succinic acid. The vertical (absorbance) scale is identical to that of the pyrene spectrum

TABLE 5.4 RETENTION OF PYRENE UNDER CONDITIONS USED FOR *n*-DECANE EXPERIMENTS[a]

Conditions	Pyrene/silica gel coverage level[b]	% Loss
initial coverage	1980 ± 100 μg/g	- - -
after 10 min of N_2-only flow[c]	2047 ± 84 μg/g	0 %
after 10 min of N_2 + *n*-decane flow[c,d]	1626 ± 54 μg/g	25 %
24 hr *dark* exposure[e]	2008 ± 205 μg/g	0 %

[a]test sample = vapor-deposited pyrene/silica gel; predicted coverage = 2200 μg/g.
[b]coverage levels determined by SFE/GC.
[c]pyrene/silica gel samples in oven 2; temperature = 95° C.
[d]measured mass flow rate of *n*-decane = 2.0×10^4 μg/g.
[e]pyrene/silica gel in irradiation set-up but with lamp off. in **Figure 4.2** (p. 94).

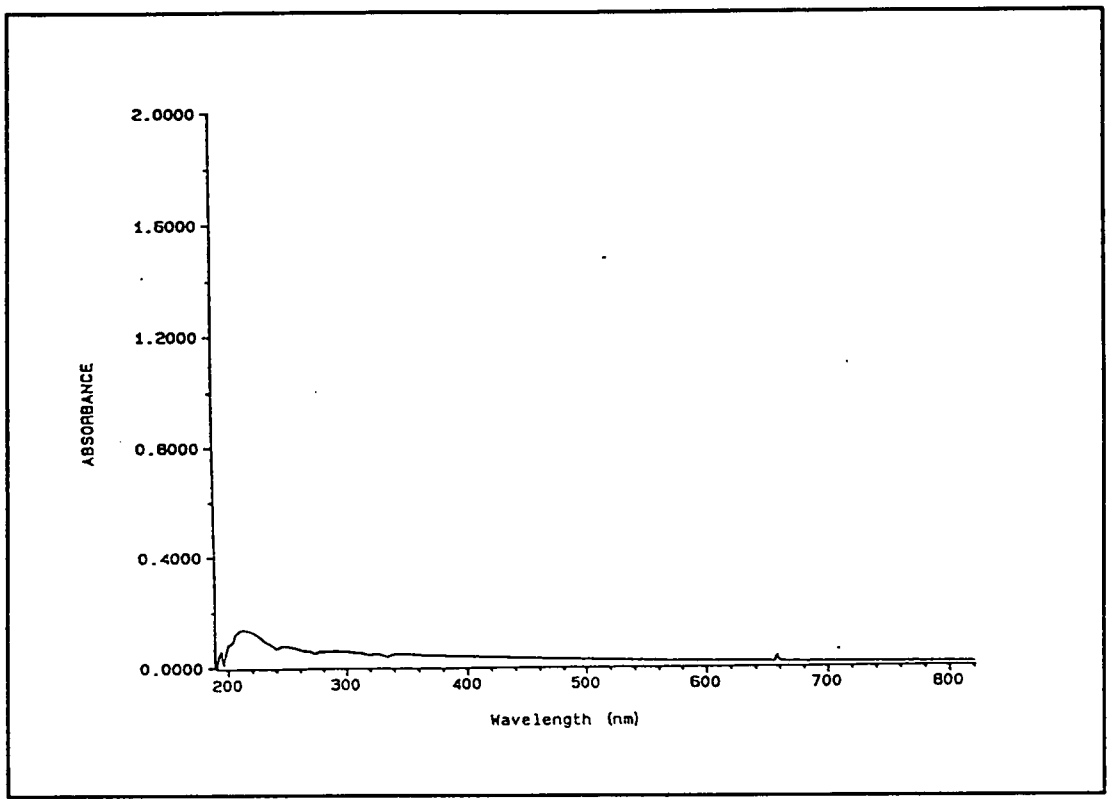

Figure 5.1 UV/visible absorption spectrum: **succinic acid**, 10 ppm in methanol.

A comparison of **Figures 4.2** (p. 94) and **5.1** (previous page) reveals that succinic acid should absorb far fewer photons from the photolysis source than does pyrene.

To assess the stability of succinic acid to non-photochemical degradation, a *solution*-deposited sample of succinic acid on silica gel (predicted coverge = 6.7×10^4 $\mu g/g$) was subjected to supercritical fluid extraction and the coverage level quantified (see p. 71) just after the vapor deposition experiment in which the sample was generated, and at 2, 3, and 4 weeks after the deposition. Results are summarized in **Table 5.5**. They confirm the stability of this compound when stored in the dark.

Experiments carried out to evaluate the stability of succinic acid to photochemical degradation are summarized in **Table 5.6**. A 24 % loss of succinic acid was observed for the 24 hr illumination. This experiment was repeated and a separate portion of the succinic acid/silica gel sample was placed in an irradiation cell, installed in the illumination set-up, and rotated in the dark for 24 hr (see **Figure 2.7**, p. 65, and **Figure 2.9**, p. 67). The purpose of this experiment was to investigate the possibility that the observed loss of succinic acid during illumination was due to vacuum-induced volatilization. Again, there was significant loss under illumination, but no loss in the absence of light. A thermometer was then inserted into a portion of the succinic acid/silica gel sample housed in a quartz irradiation cell (**Figure 2.9**, p. 67), and the cell was positioned in the light path of the illumination source. The temperature of the adsorbent bed rose only 3° C during the course of a 24 hr exposure, implying that the observed loss of succinic acid was not due to thermal degradation.

A closer inspection of **Figure 5.1** (previous page) reveals that, though succinic acid does not absorb appreciably in the 300-800 nm region of the electromagnetic spectrum, it does absorb weakly in the 200-300 nm range. A filter sufficient to remove these wavelengths from the incident light was sought. **Figure 5.2** shows the absorption spectrum of Pyrex. Compare this with the absorption spectrum of quartz (from which materials in light path are fabricated; see **Figure 2.7**, p. 61, and **Figure 2.9**, p. 67) in **Figure 5.3**. As can be seen, Pyrex selectively removes radiation in the 200-300 nm region. A Pyrex watch glass was positioned in the light path just past the water-filled quartz jacket (see **Figure 2.7**, p.

TABLE 5.5 STABILITY OF SUCCINIC ACID TO NON-PHOTOCHEMICAL DEGRADATION [a]

Weeks since deposition	Succinic acid/silica gel coverage level[b]	% Loss
0	6.5×10^4 μg/g	- - -
2	6.4×10^4 μg/g	2 %
3	6.9×10^4 μg/g	0 %
4	6.2×10^4 μg/g	5 %

[a]test sample = vapor-deposited succinic acid/silica gel; predicted coverage = 6.7×10^4 μg/g.
[b]determined by ultrasonic extraction in water and titration with OH^-.

TABLE 5.6 STABILITY OF SUCCINIC ACID TO PHOTOCHEMICAL DEGRADATION[a]

Conditions	Succinic acid/silica gel coverage level[b]	% Loss
initial coverage	6.4×10^4 μg/g	- - -
after 24 hr illumination	4.8×10^4 μg/g	24 %
initial coverage	6.9×10^4 μg/g	- - -
after 24 hr illumination	5.6×10^4 μg/g	19 %
after 24 hr in dark	6.9×10^4 μg/g	0 %
initial coverage	6.2×10^4 μg/g	- - -
after 24 hr illumination[c]	6.3×10^4 μg/g	0 %
after 48 hr illumination[c]	6.1×10^4 μg/g	2 %

[a]test sample = vapor-deposited succinic acid/silica gel; predicted coverage = 6.7×10^4 μg/g.
[b]determined by ultrasonic extraction in water and titration with OH^-.
[c]with Pyrex watch glass in light path.

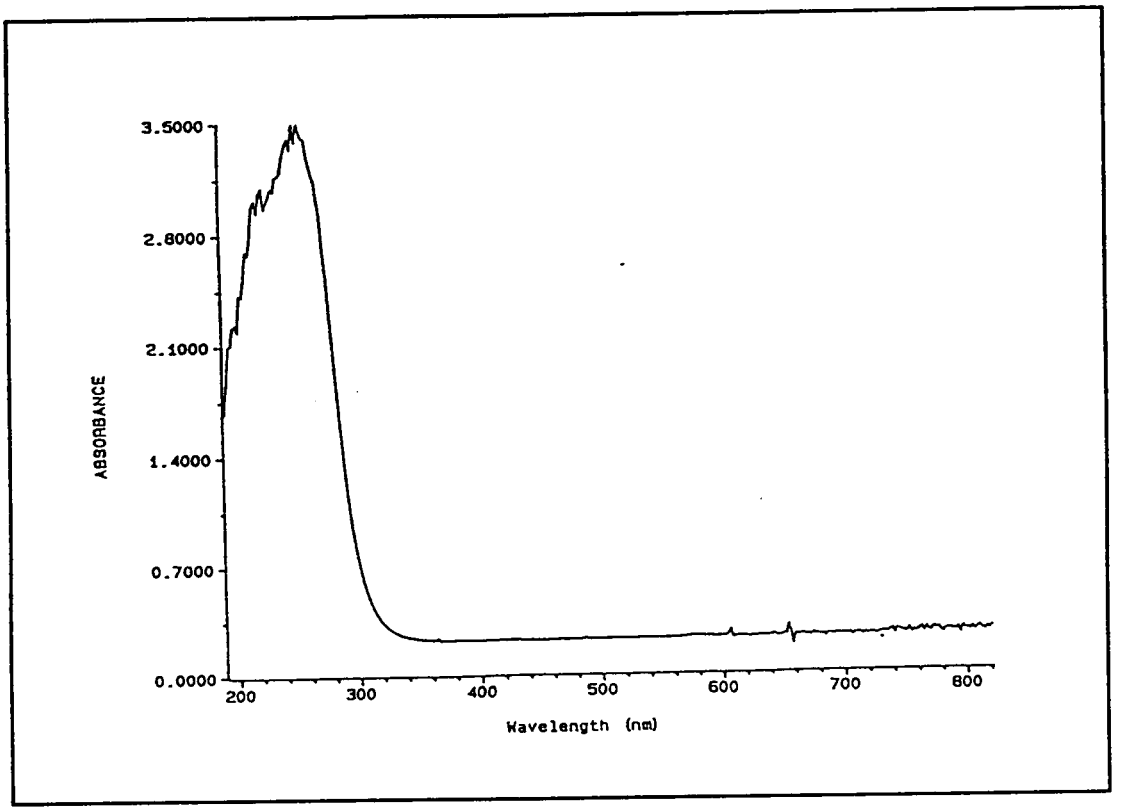

Figure 5.2 UV/visible absorption spectrum: **Pyrex** test tube.

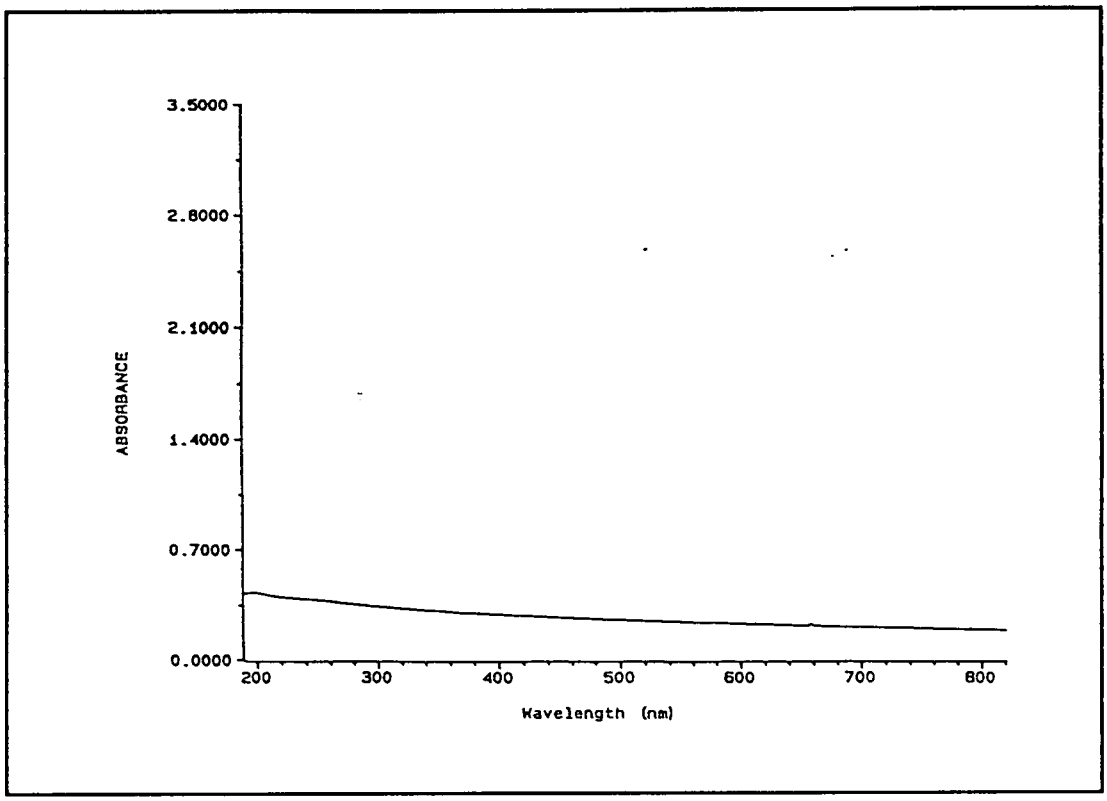

Figure 5.3 UV/visible absorption spectrum: **quartz** cuvette.

68), and the 24 hr exposure of the succinic acid/silica gel sample repeated. As can be seen in **Table 5.6**, the use of the Pyrex filter inhibited the photochemical loss of succinic acid.

Unfortunately, an inspection of **Figure 4.2** (p. 94) reveals that removal of incident light in the 200-300 nm range by a Pyrex filter removes a significant fraction of the photons likely to be absorbed by pyrene. In fact, a 24 hr illumination of a vapor-deposited pyrene/silica gel sample with the filter in place resulted in only a 17 % loss of pyrene. The same sample experienced a 68 % loss for a 24 hr illumination when no filter was in place (**Table 4.13**, p. 111). A 48 hr illumination resulted in a 39 % loss of pyrene. Thus, in order to increase the likelihood that some photolysis would occur for pyrene and for pyrene + succinic acid on coal stack ash adsorbents, all irradiations with succinic acid as coadsorbate (as well as comparative illuminations of pyrene) proceeded for 48 hr with the Pyrex filter in place.

In order to insure that there would be no appreciable photodegradation of succinic acid at this longer exposure time, the succinic acid/silica gel sample used for these experiments was exposed to a 48 hr illumination under filtered light. As can be seen from the final entry in **Table 5.6** (p.124), there was no significant loss of succinic acid due to photolysis at the longer exposure time.

5.2-D Non-photochemical and photochemical stability of *n*-decane

In order to assess the stability of *n*-decane to non-photochemical degradation, a vapor-deposited sample of *n*-decane/silica gel (predicted coverage = 1.2 x 10^4 μg/g) was analyzed (extraction by supercritical fluid CO_2, *off-line* collection of eluent in 10 ml of hexane, and analysis by GC/MS; see pp. 71-72) just after the vapor deposition experiment in which it was generated, at 1 week after deposition, and at 2 and 4 weeks after the deposition. Results are summarized in **Table 5.7**. No significant loss of *n*-decane was observed for the four week period.

A representative absorption spectrum of *n*-decane is shown in **Figure 5.4**. There was no detectable absorbance relative to that generated by a solvent-only *blank*. **Table 5.8** contains results for

TABLE 5.7 STABILITY OF *n*-DECANE TO NON-PHOTOCHEMICAL DEGRADATION[a]

Weeks since deposition	*n*-Decane/silica gel coverage level[b]	% Loss
zero	1.2×10^4 μg/g	- - -
two	1.4×10^4 μg/g	0 %
four	1.0×10^4 μg/g	8 %

[a]test sample = vapor-deposited *n*-decane/silica gel; predicted coverage = 1.4×10^4 μg/g.
[b]determined by SFE, collection in hexane, GC/MS analysis.an exposure of the *n*-decane/silica gel sample

TABLE 5.8 STABILITY OF *n*-DECANE TO PHOTOCHEMICAL DEGRADATION[a]

Conditions	*n*-Decane/silica gel coverage level[b]	% Loss
initial coverage	1.2×10^4 μg/g	- - -
after 24 hr illumination	1.3×10^4 μg/g	0 %

[a]test sample = vapor-deposited *n*-decane/silica gel; predicted coverage = 1.4×10^4 μg/g.
[b]determined by SFE, collection in hexane, GC/MS analysis.

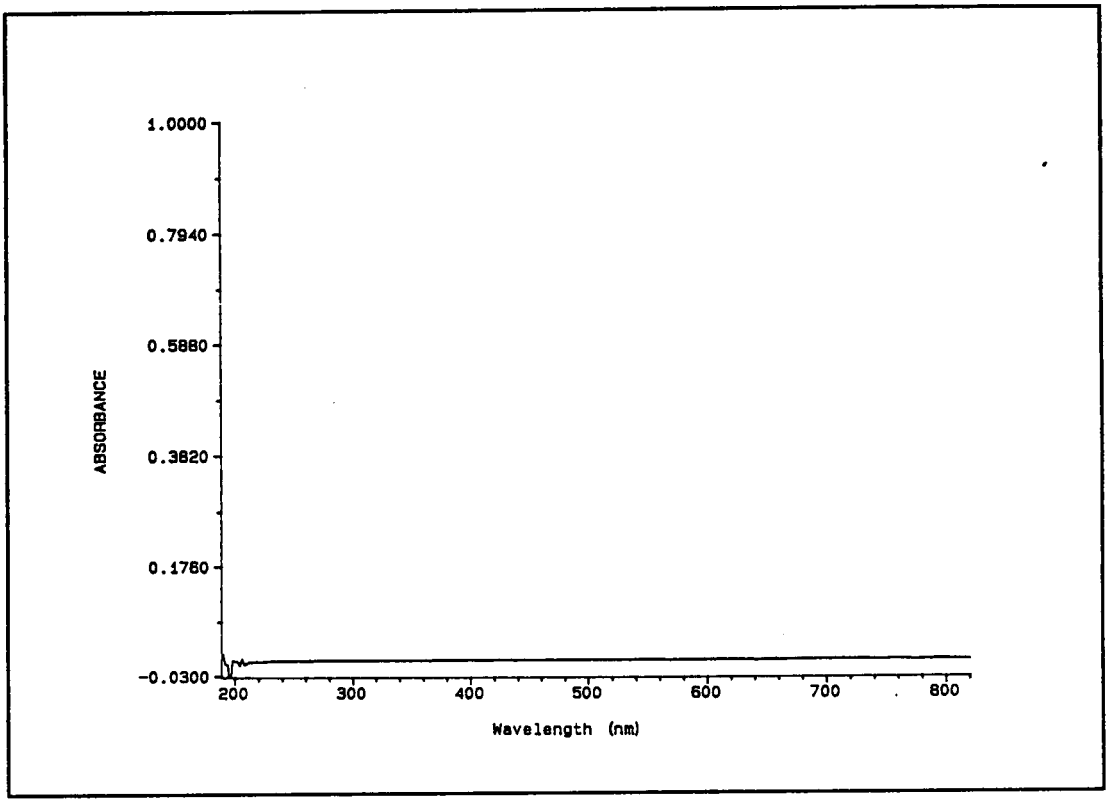

Figure 5.4 UV/visible absorption spectrum: ***n*-decane, 10 ppm in hexane.**

to 24 hr of incident light (pp. 64). There was no loss of *n*-decane for the 24 hr illumination, confirming that *n*-decane was not susceptible to loss by photolysis, nor to loss by a vacuum-induced volatilization (i.e., when *n*-decane-containing adsorbents were secured in the irradiation apparatus; see p, 64). Furthermore, results show that recovery of *n*-decane from silica gel is quantitative, insuring the validity of mass flow rate determinations (as outlined on p. 59).

5.2-E Vapor depositions of pyrene and coadsorbates

The conditions used to generate adsorbent samples containing succinic acid and the predicted succinic acid/adsorbent coverage levels of those samples are summarized in **Table 5.9**. The average mass flow rate of succinic acid for the depositions (determined as described on p. 59) was 3.4×10^4 μg/hr. All depositions were stopped near the point of adsorbent *saturation* (i.e., the point at which an adsorbent has retained a maximum amount of adsorbate; see p. 60).

Pyrene was deposited onto adsorbents containing succinic acid according to the conditions outlined in **Table 5.10**. Also listed are predicted coverage levels of pyrene on each adsorbent. The FID profile (see **Figure 2.6**, p. 61) was monitored during the course of these depositions and they were stopped when the adsorbate mass flow through the system was at a mimimum. Deposition experiments were planned so that pyrene/adsorbent coverage levels would be comparable to those for pyrene on adsorbents that contained no coadsorbate (see **Table 4.7**, p. 104). Pyrene and succinic acid coverage levels for adsorbents on which they were coadsorbates are listed in **Table 5.11**. Note that *saturation* levels of succinic acid on the unfractionated ash (U2) and on the carbonaceous fraction (C2) are significantly less than *sub-saturation* levels of pyrene on those same adsorbents, implying a greater affinity of carbonaceous particles and the unfractionated ash for pyrene than for succinic acid.

n-Decane was vapor-deposited onto silica gel and coal stack ash adsorbents containing pyrene. The conditions used in carrying out these depositions and the *n*-decane/adsorbent coverage levels so generated are summarized in **Table 5.12**. (The conditions used in generating pyrene-containing

TABLE 5.9 DEPOSITION PARAMETERS AND PREDICTED COVERAGE LEVELS FOR SUCCINIC ACID

Adsorbent	Sample size, g	Deposition time[a], hr	% Adsorption[b]	Predicted coverage[c], μg/g
silica gel	3.0000	4.0	0.74	34,000
U2	0.5001	0.033	0.61	1400
F2	1.0004	0.033	0.53	590
C2	1.5000	0.17	0.62	2400
M2	1.5003	0.033	0.61	460

[a]at oven 1 = 180° C, oven 2 = 185° C; measured mass flow rate of succinic acid = 3.4×10^4 μg/hr.
[b](mass flow of succinic acid retained by adsorbent)/total mass flow of succinic acid).
[c]predicted coverage = ([mass low rate]*[deposition time]*[% adsorption])/[sample size].

TABLE 5.10 DEPOSITION PARAMETERS AND PREDICTED COVERAGE LEVELS FOR PYRENE WITH SUCCINIC ACID AS COADSORBATE

Adsorbent	Sample size, μg/g	Deposition time[a], hr	Predicted coverage[b], μg/g
silica gel	1.0055	8.5	2300
U2	0.4508	4.25	2500
F2	0.9968	1.0	270
C2	1.2379	34.5	7525
M2	1.4916	2.5	450

[a]at oven 1 = 100° C, oven 2 = 105° C; measured mass flow rate of pyrene = 270 μg/hr.
[b]predicted coverage = ([mass flow rate]*[deposition time])/[sample size].

TABLE 5.11 SUMMARY OF COVERAGE LEVELS FOR PYRENE AND SUCCINIC ACID AS COADSORBATES

Adsorbent	Pyrene: predicted coverage, μg/g	Succinic acid: predicted coverage, μg/g
silica gel	2300	34,000
U2	2500	1400
F2	270	590
C2	7525	2400
M2	450	460

TABLE 5.12 DEPOSITION PARAMETERS AND PREDICTED COVERAGE LEVELS FOR *n*-DECANE

Adsorbent	Sample size, g	Deposition time[a], hr	% Adsorption[b]	Predicted coverage[c], μg/g
silica gel	0.2028	0.17	0.83	14,000
U2	0.2101	0.034	0.71	2300
F2	0.3094	0.017	0.64	700
C2	0.4011	0.068	0.68	2300
M2	0.3090	0.017	0.66	730

[a]at oven 1 = 85° C, oven 2 = 95° C; measured mass flow rate of *n*-decane = 2.0×10^4 μg/hr.
[b](mass flow of *n*-decane retained by adsorbent)/(total mass flow of *n*-decane).
[c]predicted coverage = ([mass flow rate]*[deposition time]*[% adsorption])/[sample size).

adsorbents are listed in **Table 4.7**, p. 104.) The average measured mass flow rate of *n*-decane (determined as described on p. 59) was 2.0 x 10^4 μg/hr. Depositions were stopped, as were those involving succinic acid, just prior to the point of saturation. Pyrene and *n*-decane coverage levels for adsorbents on which these compounds were coadsorbates are listed in **Table 5.13.** As for pyrene/succinic acid depositions (**Table 5.11**, previous page), *saturation* coverages of *n*-decane on the unfractionated ash (U2) and on the carbonaceous fraction (C2) are considerably less than *sub-saturation* coverages of pyrene on those adsorbents.

5.2-F Sorptivity of pyrene in the presence of coadsorbates

The ability to extract pyrene from the surfaces of adsorbents which contained no coadsorbates is described in Section **4.2-D** (pp. 105-107). Those experiments are summarized in **Table 4.9** (p. 106). The quantities of pyrene that could be extracted, as a function of adsorbent sample size, from silica gel and from coal stack ash adsorbents containing coadsorbates (see **Table 5.11**, previous page, and **Table 5.13**) were determined by supercritical fluid extraction/gas chromatography (pp. 68-72). Results for recovery of pyrene in the presence of succinic acid are summarized in **Table 5.14.** Results for recovery of pyrene in the presence of *n*-decane are summarized in **Table 5.15.** For both sets of data, recoveries of pyrene follow the same general trend as for recoveries of pyrene from adsorbents containing no coadsorbates. Recovery of pyrene is greatest from silica gel. Among coal stack ash fractions separated according to chemical composition, pyrene is most strongly retained by the carbonaceous fraction (C2), less strongly retained by the mineral fraction (M2) and the ferromagnetic fraction (F2).

A comparison of results in **Table 4.9** (p. 106; recovery of pyrene in the absence of coadsorbates) with those in **Tables 5.14** and **5.15** is provided in **Table 5.16.** Recovery of pyrene from silica gel was virtually quantitative, both in the absence and presence of succinic acid. The recovery was slightly greater when succinic acid was present. The ability to recover pyrene from coal stack ash fractions was not influenced dramatically by the presence of succinic acid.

TABLE 5.13 SUMMARY OF COVERAGE LEVELS FOR PYRENE AND *n*-DECANE AS COADSORBATES

Adsorbent	Pyrene: predicted coverage, μg/g	*n*-Decane: predicted coverage, μg/g
silica gel	2200	14,000
U2	2200	2300
F2	270	700
C2	6500	2300
M2	450	730

TABLE 5.14 EXTRACTION RECOVERY OF PYRENE IN THE PRESENCE OF SUCCINIC ACID[a]

Adsorbent	Predicted coverage[b]	Measured coverage[c]	% Recovery
silica gel	2282	2419 ± 107	106 %
U2	2545	980 ± 100	39 %
F2	271	149 ± 5	55 %
C2	7525	2776 ± 121	37 %
M2	453	247 ± 8	55 %

[a]all coverages in μg pyrene/g adsorbent.
[b]based on mass flow rate of pyrene, deposition time, and adsorbent sample size.
[c]determined by SFE/GC.

TABLE 5.15 EXTRACTION RECOVERY OF PYRENE IN THE PRESENCE OF *n*-DECANE[a]

Adsorbent	Predicted coverage[b]	Measured coverage[c]	% Recovery
silica gel	2184	1642 ± 56	75 %
U2	2154	937 ± 57	44 %
F2	270	115 ± 3	43 %
C2	6480	2709 ± 110	42 %
M2	450	180 ± 3	40 %

[a]all coverages in μg pyrene/g adsorbent.
[b]based on mass flow rate of pyrene, deposition time, and adsorbent sample size.
[c]determined by SFE/GC.

TABLE 5.16 PYRENE EXTRACTION RECOVERY IN THE ABSENCE AND PRESENCE OF COADSORBATES

Adsorbent	% Recovery no coadsorbate	% Recovery with succinic acid	% Recovery with *n*-decane
silica gel	90 ± 4 %	106 ± 4 %	75 ± 2 %
U2	42 ± 1 %	39 ± 4 %	44 ± 2 %
F2	57 ± 3 %	55 ± 2 %	43 ± 1 %
C2	41 ± 2 %	37 ± 2 %	42 ± 2 %
M2	51 ± 5 %	55 ± 2 %	40 ± 1 %

Only 75 % of the predicted initial coverage of pyrene was recovered from silica gel when *n*-decane was present. However, results in **Table 5.4** (p. 121) suggest that pyrene is displaced by *n*-decane during the course of deposition of the latter onto adsorbents containing the former, and this factor presumably accounts for the apparently lower extraction recoveries for pyrene in the presence of *n*-decane. Likewise, it is impossible to attribute the apparent relative inability to remove pyrene from the ferromagnetic (F2) and mineral (M2) fractions containing *n*-decane to an inability to extract pyrene because of the presence of *n*-decane; pyrene was not detected after a second extraction of the silica gel, ferromagnetic, and mineral fractions which contained pyrene and *n*-decane as coadsorbates.

There was no significant difference in the apparent ability to extract pyrene from carbonaceous (C2) and unfractionated (U2) fractions when *n*-decane was present than when succinic acid or when no coadsorbate was present. This implies that pyrene associated with carbonaceous particles (and by inference, with the unfractionated stack ash) is less likely to be displaced by *n*-decane than when associated with particles containing little or no carbon.

5.2-G Photochemistry of pyrene in the presence of coadsorbates

The pyrene-containing adsorbents listed in **Table 4.7** (p. 104) were irradiated for 48 hr with the filtered output (see p. 64) of the UV/visible source. Results are summarized in **Table 5.17.** As expected, less photodegradation of pyrene was evident on all adsorbents than for samples exposed to unfiltered radiation (**Table 4.13**, p. 111). Adsorbent samples containing both pyrene and succinic acid were likewise subjected to 48 hr irradiations. Results are summarized in **Table 5.18.**

Photochemical experiments involving pyrene in the absence and presence of succinic acid are compared in **Table 5.19.** The extent of photodegradation of pyrene was greater, regardless of the composition of the adsorbent, when succinic acid was present. For F2 and C2, however, the extent of photodecomposition of pyrene was so small, irrespective of the presence of succinic acid, that the differences in apparent photochemistry of pyrene are not statistically significant. Results presented in

TABLE 5.17 PYRENE: PHOTOCHEMICAL EXPERIMENTS WITH FILTERED LAMP OUTPUT[a]

Adsorbent	Initial coverage	After 48 hr exposure	% Loss
silica gel	1980 ± 100	1154 ± 60	42 %
U2	928 ± 28	906 ± 89	2 %
F2	153 ± 9	146 ± 8	5 %
C2	2736 ± 66	2702 ± 122	1 %
M2	228 ± 22	208 ± 22	9 %

[a]all data = extracted μg pyrene/g adsorbent; no coadsorbate present.

TABLE 5.18 PYRENE: PHOTOCHEMICAL EXPERIMENTS WITH SUCCINIC ACID AS COADSORBATE[a]

Adsorbent	Initial coverage	After 48 hr exposure[b]	% Loss
silica gel	2419 ± 107	738 ± 52	70 %
U2	980 ± 100	934 ± 39	11 %
F2	149 ± 5	141 ± 2	6 %
C2	2776 ± 121	2681 ± 44	3 %
M2	247 ± 8	211 ± 40	15 %

[a]all data = extracted μg pyrene/g adsorbent.
[b]filtered lamp output.

TABLE 5.19 PYRENE: COMPARISON OF PHOTOCHEMICAL LOSS IN THE ABSENCE AND PRESENCE OF SUCCINIC ACID[a]

Adsorbent	% Loss, no coadsorbate	% Loss, with succinic acid
silica gel	42 ± 6 %	70 ± 5 %
U2	2 ± 8 %	11 ± 25 %
F2	5 ± 9 %	6 ± 4 %
C2	1 ± 2 %	3 ± 4 %
M2	9 ± 14 %	15 ± 16 %

[a]48 hr exposure to filtered lamp output.

the previous section (pp. 133-136) suggest that the presence of succinic acid does not *weaken* the association of pyrene with model or coal stack ash adsorbents. The apparent enhancement of pyrene photolysis when succinic acid is present, then, may be due to an inability of pyrene to penetrate surface pores of adsorbents (because they are occupied by succinic acid), and be *shielded* from incident radiation. In view of the relatively large uncertainties in the data, further speculation is not warranted.

Adsorbents containing pyrene and *n*-decane were subjected to 24 hr irradiations with unfiltered lamp output. Results are summarized in **Table 5.20**. Results for equivalent experiments involving pyrene in the absence of coadsorbate are summarized in **Table 4.13** (p. 111). Photochemical experiments involving pyrene in the absence and presence of *n*-decane are compared in **Table 5.21**. The extent of photodegradation of pyrene in the presence of *n*-decane was, in all cases, equal to (for the ferromagnetic fraction, F2) or less than the extent of photodegradation when *n*-decane was not present. The effect of *n*-decane was greatest for those adsorbents on which pyrene exhibits relatively high photoreactivity (silica gel and M2) when no coadsorbate was present. The effect is virtually impossible to detect for pyrene sorbed on U2, F2, and C2, because (even in the absence of *n*-decane) virtually no photodecomposition of pyrene takes place.

TABLE 5.20 PYRENE: PHOTOCHEMICAL EXPERIMENTS WITH *n*-DECANE AS COADSORBATE[a]

Adsorbent	Initial coverage	After 24 hr exposure	% Loss
silica gel	1642 ± 52	1038 ± 63	37 %
U2	937 ± 57	870 ± 38	7 %
F2	115 ± 3	95 ± 6	9 %
C2	2709 ± 110	2673 ± 55	1 %
M2	180 ± 3	168 ± 9	7 %

[a]all data = extracted μg pyrene/g adsorbent.

TABLE 5.21 PYRENE: COMPARISON OF PHOTOCHEMICAL LOSS IN THE ABSENCE AND PRESENCE OF *n*-DECANE[a]

Adsorbent	% Loss, no coadsorbate	% Loss, with *n*-decane
silica gel	68 ± 7 %	37 ± 5 %
U2	10 ± 8 %	7 ± 7 %
F2	9 ± 8 %	9 ± 3 %
C2	3 ± 6 %	1 ± 3 %
M2	21 ± 12 %	7 ± 5 %

[a]24 hr exposure.

These results tend to parallel those of Koester and Hites (see reference 103 and p. 44), who observed a reduction in the extent of photodegradation of polychlorinated dibenzo-p-dioxins and polychlorinated dibenzofurans when those compounds were sorbed on silica gel and *covered* with organic compounds extracted from incinerator fly ash. Their hypothesis, that compounds sorbed onto adsorbents first are *shielded* from incident radiation by compounds *layered* over them, is a reasonable rationalization for the behaviors observed here, i.e., the inhibition of the photolysis of pyrene when *n*-decane is present. Since *n*-decane does not absorb a significant amount of UV/visible light (see **Figure 5.4**, p.129), this *shielding* may conceivably be achieved by a scattering or reflection of incident radiation.

The change in the extent of photodegradation of pyrene brought about by the presence of succinic acid and *n*-decane may be expressed as a % difference in loss of pyrene in the presence of coadsorbate relative to loss when no coadsorbate is present. Such calculations were made based on the results of **Tables 5.19** (p. 138) and **5.21** (previous page). The results of these calculations are summarized in **Table 5.22**. Great significance should not be ascribed to the numerical values tabulated, in view of the relatively large relative uncertainties in some of the data (especially for U2, F2, and C2, where the extent of pyrene phototransformation was very small in all cases).

A general trend, however, is evident in results presented in **Table 5.22**. The photolysis of pyrene on all adsorbents was enhanced when succinic acid was present (all values in *succinic acid* column are positive). Conversely, the photolysis of pyrene on all adsorbents was unchanged (F2) or inhibited when *n*-decane was present (all values in *n-decane* column are ≤ 0).

5.3 Conclusions

Experiments described in this chapter indicate that the presence of a coadsorbate affects the photochemical behavior of pyrene sorbed on coal stack ash. Results in **Tables 5.19** (p. 138), **5.21** (p. 139), and **5.22** demonstrate that when pyrene is deposited onto an adsorbent which contains a

TABLE 5.22 PYRENE: COMPARISON OF PHOTOCHEMISTRY WITH SUCCINIC ACID AND *n*-DECANE AS COADSORBATES[a]

	Succinic acid	*n*-Decane
Adsorbent	% change in apparent pyrene photolysis, with/without coadsorbate	% change in apparent pyrene photolysis, with/without coadsorbate
silica gel	67 %	-46 %
U2	450 %	-30 %
F2	20 %	0 %
C2	200 %	-200 %
M2	67 %	-67 %

[a]all data = ([% loss pyrene with coadsorbate] - [% loss pyrene with no coadsorbate]) / [% loss with no coadsorbate].

coadsorbate (succinic acid), the photolysis of pyrene is enhanced. When pyrene-containing adsorbents are *loaded* with a coadsorbate (*n*-decane), the photolysis of pyrene, for most adsorbents, is inhibited. There is no evidence, based on the experiments utilized herein (see results in **Tables 5.15** and **5.16**, p. 135, to suggest that the presence of a coadsorbate significantly alters the strength of the association between pyrene and coal stack ash adsorbents.

It is difficult to predict, based on results presented herein, the effect of coadsorbates on the photochemical behavior of pyrene sorbed on atmospheric coal fly ash. The coal stack ash particles used in this work have chemical and physical properties which may differ from those of atmospheric particles (p. 76-78). Probably more important, coverage levels of adsorbates used herein are several orders of magnitude greater than those typical of atmospheric particles. (Compare coverages in **Tables 5.11**, p. 132, and **5.13**, p. 134, with those listed in **Table 1.19**, p. 45, and given on p. 88.)

Furthermore, experiments described herein represent a simplified approximation of the situation expected for atmospheric particles, which are likely to contain a large number of PAH, and a large

number and variety of coadsorbates. It is reasonable to assume, however, that the photochemical behavior of PAH sorbed on coal fly ash may be significantly altered by the presence of coadsorbates. Coadsorbates may penetrate the surface of coal fly ash particles, and increase the likelihood that sorbed PAH will be exposed to incident light. Alternatively, coadsorbates may shield sorbed PAH molecules from incident light by absorbing that light, or by scattering or reflecting of incident light.

CHAPTER 6

SUMMARY

6.1 Conclusions

The studies described in this dissertation have shown that the photochemical behavior of PAH and related compounds, sorbed on coal stack ash, is influenced by both the chemical properties of the compounds and the chemical composition and physical properties of the particles with which they are associated. In **Chapter 4** (pp. 84-113), the photochemical behavior of pyrene and 1-nitropyrene was evaluated on a model adsorbent, on unfractionated coal stack ash, and on fractions thereof enriched in ferromagnetic, carbonaceous, and mineral content. It was found that 1-nitropyrene exhibited a greater tendency than pyrene to be associated with coal stack ash when sorbed on carbonaceous particles, and also to be more resistant than pyrene to photolysis. 1-Nitropyrene and pyrene have similar physical properties (e.g., molecular areas), but they differ from each other chemically because of the presence of the $-NO_2$ group. Differences in the photochemical behavior and sorptivity of 1-nitropyrene and pyrene as a function of the composition of the adsorbent were attributed to differences in the chemical properties of the compounds and of the particles.

In **Chapter 5** (pp. 114-142), the photochemical behavior of pyrene, sorbed on a model adsorbent, on coal stack ash, and on ash fractions enriched in ferromagnetic, carbonaceous, and mineral content in the presence of a coadsorbate, was compared to the photochemical behavior of sorbed pyrene in the absence of a coadsorbate. There was no evidence to suggest that the strength of the association between pyrene and coal stack ash was significantly altered by the presence of a coadsorbate. It was found, however, that the photolysis of pyrene was enhanced when pyrene was deposited onto adsorbents

(especially silica gel and mineral coal stack ash particles) containing a coadsorbate (succinic acid). The photolysis of pyrene was inhibited when pyrene was deposited onto adsorbents prior to deposition of a coadsorbate (*n*-decane). These phenomena were most pronounced on adsorbents on which significant photodecomposition of pyrene occurs in the absence of coadsorbate. It is suggested that coadsorbates inhibit or enhance the photolysis of sorbed PAH by altering the extent to which PAH are shielded from incident light.

6.2 Suggestions for Future Work

There are a number of worthwhile directions in which this work might proceed, and a few of those are highlighted here. It is unlikely that other nitro-PAH would exhibit photochemical behaviors significantly different than those characteristic of 1-nitropyrene. There are, however, other substituted PAH of environmental importance which could be justifiable candidates for photochemical studies. These include, among others, oxygenated PAH and aza- and thio-heterocyclic PAH [6]. Of particular interest might be those which possess a ring substituent that is *electron donating* (e.g., -OH). This would contrast with studies involving PAH with an *electron withdrawing* substituent such as $-NO_2$. It is feasible that such compounds might interact differently with coal stack ash than compounds studied to date and might exhibit novel photochemical behaviors.

There are many organic compounds that could be used as coadsorbates in an extension of the work described herein. The available number and variety, however, are limited by the ability to generate and sustain an appreciable vapor-phase concentration of any compound chosen. Furthermore, experiments described herein are representative of the two extremes of situations likely to be encountered for atmospheric PAH and coadsorbates on coal fly ash (i.e., deposition of PAH onto adsorbents containing a coadsorbate, and deposition of a coadsorbate onto adsorbents containing PAH). It might be interesting, however, to investigate whether the simultaneous presence of several

coadsorbates might influence the photochemistry of sorbed PAH to a greater degree than the presence of a single coadsorbate.

A final area of research that might yield interesting results is a study of the reactions of sorbed PAH and related compounds with atmospheric species. It was pointed out in **Chapter 1** (p. 42) that the most widely accepted mechanism for the formation of atmospheric nitro-PAH is the reaction of gas-phase parent with OH/NO_x, followed by condensation (onto atmospheric particles) of the less volatile product. No one has evaluated this reaction scheme to see if it might also lead to nitration of sorbed PAH, or to further nitration of sorbed nitro-PAH. If it were found that nitro-PAH and dinitro-PAH could be formed in this manner, the environmental implications would be significant for several reasons. First, association with coal fly ash prolongs the atmospheric lifetime of PAH (see p.13). This property provides an extended time frame in which reactions between sorbed PAH and nitro-PAH and OH/NO_x could occur, if such reactions were possible. Association of PAH and nitro-PAH facilitates the transport of these compounds (and any reaction products formed en route) to remote environments; and (3) nitration of PAH and nitro-PAH invariably leads to compounds which are potentially more dangerous than those from which they derive (p. 42).

An attempt was made by the present author to initiate such a study. An apparatus which was to house adsorbents containing PAH and nitro-PAH in the path of a dilute mixture of OH and NO_x in an inert gas was constructed. An attempt was made to generate OH radicals by passing H_2 in N_2 through a microwave discharge device, and mixing H atoms so generated with an excess of NO_2 in N_2 to yield a mixture of OH, NO, and NO_2. The study was, however, abandoned, due to an inability to convincingly demonstrate the production of OH.

The suggested research areas briefly outlined here are, it is believed, logical extensions of the work described in this text. There are undoubtedly many other avenues that might be explored toward a better understanding of the interactions and behaviors of PAH and related compounds with and on coal fly ash.

LIST OF REFERENCES

LIST OF REFERENCES

1. Lodge, J.P., Jr. *The Smoake of London*, Maxwell Reprint Company: Elmsford, NY, 1969.
2. Finlayson-Pitts, B.J.; Pitts, J.N., Jr. *Atmospheric Chemistry: Fundamentals and Experimental Techniques*, Wiley: New York, 1986; Chapter 1.
3. Schwartz, S.E. *Science*, **1989**, *243*, 753-763.
4. McElroy, M.B.; Salawitch, R.J. *Science*, **1989**, *243*, 763-770.
5. Schneider, S.H. *Science*, **1989**, *243*, 771-781.
6. Finlayson-Pitts, B.J.; Pitts, J.N., Jr. *Atmospheric Chemistry: Fundamentals and Experimental Techniques*, Wiley: New York, 1986; Chapter 13.
7. Baek, S.O.; Field, R.H.; Goldstone, M.E.; Kirk, P.W.; Lester, J.N.; Perry, R. *Water Air Soil Pollut.*, **1991**, *60*, 279-300.
8. Ames, B.N.; McCann, J.; Yamasaki, E. *Mutat. Res.*, **1975**, *31*, 347-364.
9. Nielsen, T.; Ramdahl, T.; Bjorseth, A. *Environ. Health Perspect.*, **1983**, *47*, 103-114.
10. Pitts, J.N., Jr. *Environ. Health Perspect.*, **1983**, *47*, 115-140.
11. Valerio, F.; Bottino, P.; Ugolini, D.; Cimberle, M.R.; Tozzi, G.A.; Frigerio, A. *Sci. Tot. Environ.*, **1984**, *40*, 169-188.
12. Wild, S.R.; Jones, K.C.; Johnston, A.E. *Atmos. Environ.*, **1992**, *7*, 1299-1307.
13. Basu, D.K.; Saxena, J. *Environ. Sci. Technol.*, **1978**, *12*, 795-798.
14. National Research Council. Subcommittee on Airborne Particles. *Airborne Particles*, University Park Press: Baltimore, 1979; Chapter 1.
15. Finlayson-Pitts, B.J.; Pitts, J.N. Jr. *Atmospheric Chemistry: Fundamentals and Experimental Techniques*, Wiley: New York, 1986; Chapter 12.
16. Chrisp, C.E.; Fisher, G.L.; Lammert, J.E. *Science*, **1978**, *199*, 73-75.
17. Lofroth, G. *Chemosphere*, **1978**, *7*, 791-798.

18. Fisher, G.L.; Chrisp, C.E.; Raabe, O.G. *Science*, **1979**, *204*, 879-881.

19. Natusch, D.F.S. *Environ. Health Perspect.*, **1978**, *22*, 79-90.

20. Fisher, G.L. *Environ. Health Perspect.*, **1983**, *47*, 189-199.

21. Committee on Health and Environmental Effects of Increased Coal Utilization, *Environ. Health Perspect.*, **1980**, *36*, 135-154.

22. Bjorseth, A.; Lunde, G.; Lindskog, A. *Atmos. Environ.*, **1979**, *13*, 45-53.

23. Daisey, J.M.; McCaffrey, R.J.; Gallagher, R.A. *Atmos. Environ.*, **1981**, *13*, 1353-1363.

24. Leithe, W. *The Analysis of Pollutants*, Ann Arbor Science Publishers: Ann Arbor MI, 1970; p. 3.

25. Schroeder, W.H.; Lane, D.A. *Environ. Sci. Technol.*, **1988**, *22*, 240-246.

26. Holsen, T.M.; Noll, K.E. *Environ. Sci. Technol.*, **1992**, *26*, 1807-1815.

27. Lee, M.L. ; Novotny, M.; Bartle, K.D. *Anal. Chem.*, **1976**, *48*, 1556-1572.

28. Lao, R.C.; Thomas, R.S.; Oja, H.; DuBois, L. *Anal. Chem.*, **1973**, *45*, 908-915.

29. Bjorseth, A.; Ramdahl, T. In *Handbook of Polycyclic Aromatic Hydrocarbons, Vol. 2: Emission Sources and Recent Progress in Analytical Chemistry*, Bjorseth, A., Ramdahl, T., Eds.; Marcel Dekker: New York, 1985; Chapter 1.

30. Masclet, P.; Bresson, M.A.; Mouvier, G. *Fuel*, **1987**, *66*, 556-562.

31. Ting, F.T.C. In *Coal Structure*, Meyers, R.A., Ed.; Academic Press: New York, 1982; Chapter 2.

32. Schobert, H.H. *J. Chem. Ed.*, **1989**, *66* 242-244.

33. Renton, J.J. In *Coal Structure*, Meyers, R.A., Ed.; Academic Press: New York, 1982; Chapter 7.

34. Flagan, R.C.; Friedlander, S.K. In *Recent Developments in Aerosol Science*, Shaw, D.T., Ed.; John Wiley and Sons: New York, 1978; Chapter 2.

35. Smith, R.D.; Campbell, J.A.; Nielson, K.K. *Atmos. Environ.*, **1979**, *13*, 607-617.

36. Hulett, L.D., Jr.; Weinberger, A.J.; Northcutt, K.J.; Ferguson, M. *Science*, **1980**, *210*, 1356-1358.

37. Hulett, L.D., Jr.; Weinberger, A.J. *Environ. Sci. Technol.*, **1980**, *14*, 965-970.

38. Lauf, R.J.; Harris, L.A.; Rawlston, S.S. *Environ. Sci. Technol.*, **1982**, *16*, 218-220.

39. Norton, G.A.; Markuszewski, R.; Shanks, H.R. *Environ. Sci. Technol.*, **1988**, *20*, 409-413.

40. Griest, W.H.; Harris, L.A. *Fuel*, **1985**, *64*, 821-826.

41. Soltys, P.A.; Mauney, T.; Natusch, D.F.S.; Schure, M.R. *Environ. Sci. Technol.*, **1986**, *20*, 175-180.

42. Fisher, G.L.; Prentice, B.A.; Silberman, D.; Ondov, J.M.; Biermann, A.H,; Ragaini, R.C.; McFarland, A.R. *Environ. Sci. Technol.*, **1978**, *12*, 447-451.

43. Keyser, T.R.; Natusch, D.F.S.; Evans, C.A., Jr.; Linton, R.W. *Environ. Sci. Technol.*, **1978**, *12*, 768-773.

44. Dunstan, T.D.J.; Mauldin, R.F.; Zhong, J.; Hipps, A.D.; Wehry, E.L.; Mamantov, G. *Environ. Sci. Technol.*, **1989**, *23*, 303-308.

45. Hansen, L.D.; Silberman, D.; Fisher, G.L. *Environ. Sci. Technol.*, **1981**, *15*, 1057-1082.

46. Eiceman, G.A.; Vandiver, V.J. *Atmos. Environ.*, **1983**, *17*, 461-465.

47. Masclet, P.; Pistikopoulos, P; Beyne, S.; Mouvier, G. *Atmos. Environ.*, **1988**, *22*, 639-650.

48. Broddin, G.; Cautreels, W.; van Cauwenberghe, K. *Atmos. Environ.*, **1980**, *14*, 895-910.

49. van Vaeck, L.; van Cauwenberghe, K. *Atmos. Environ.*, **1978**, *12*, 2229-2239.

50. Brunauer, S.; Emmett, P.H.; Teller, E. *Science*, **1938**, *60*, 309-319.

51. Mahajan, O.P. In *Coal Structure*, Meyers, R.A., Ed.; Academic Press: New York, 1982; Chapter 3.

52. Griest, W.H.; Tomkins, B.A. *Environ. Sci. Technol.*, **1986**, *20*, 291-295.

53. Morrison, T.M.; Boyd, R.N. *Organic Chemistry, 4th Edition*; Allyn and Bacon, Inc.: Boston, 1983; 1232.

54. Fitch, W.L.; Smith, D.H. *Environ. Sci. Technol.*, **1979**, *13*, 341.

55. Atkinson, R.; Aschmann, S.M.; Winer, A.M.; Pitts, J.N., Jr. *Int. J. Chem. Kinet.*, **1982**, *14*, 507-516.

56. Biermann, H.W.; MacLeod, H.; Atkinson, R.; Winer, A.M.; Pitts J.N., Jr. *Environ. Sci Technol.*, **1985**, *19*, 244-248.

57. Arey, J.; Zielinska, B.; Atkinson, R.; Winer, A.M.; Ramdahl, T.; Pitts, J.N., Jr. *Atmos. Environ.*, **1986**, *20*, 2339-2345.

58. Atkinson, R.; Arey, J.; Zielinska, B.; Aschmann, S.M. *Int. J. Chem. Kinet.*, **1990**, *22*, 999-1014.

59. Kamens, R.M.; Guo, Z.G.; Fulcher, J.N.; Bell, D.A. *Environ. Sci. Technol.*, **1988**, *22*, 103-108.

60. Grosjean, D.; Fung, K.; Harrison, J. *Environ. Sci. Technol.*, **1983**, *17*, 673-679.

61. Pitts, J.N., Jr.; Paur, H.R.; Zielinska, B.; Arey, J.; Winer, A.M.; Ramdahl, T.; Mejia, V. *Chemosphere*, **1986**, *15*, 675-685.

62. Kamens, R.M.; Guo, J.; Guo, Z.; McDow, S.R. *Atmos. Environ.*, **1990**, *24A*, 1161-1173.

63. Butler, J.D.; Crossley, P. *Atmos. Environ.*, **1981**, *15*, 91-94.

64. Pitts, J.N., Jr.; Zielinska, B.; Sweetman, J.A., Atkinson, R.; Winer, A.M. *Atmos. Environ.*, **1985**, *19*, 911-915.

65. Pitts, J.N., Jr.; Sweetman, J.A.; Zielinska, B.; Atkinson, R.; Winer, A.M.; Harger, W.P. *Environ. Sci Technol.*, **1985**, *19*, 1115-1121.

66. Ingle, J.D., Jr.; Crouch, S.R. *Spectrochemical Analysis*, Prentice Hall: Englewood Cliffs, NJ, 1988; 336.

67. Dublin, D.; Mill, T. *Environ. Sci. Technol.*, **1982**, *16*, 815-819.

68. Finlayson-Pitts, B.J.; Pitts J.N., Jr. *Atmospheric Chemistry: Fundamentals and Experimental Techniques*, Wiley: New York, 1986; Chapter 3.

69. Finlayson-Pitts, B.J.; Pitts, J.N., Jr. *Atmospheric Chemistry: Fundamentals and Experimental Techniques*, Wiley: New York, 1986; Chapter 2.

70. Korfmacher, W.A.; Natusch, D.F.S.; Taylor, D.R.; Mamantov, G.; Wehry, E.L. *Science*, **1980**, *207*, 763-765.

71. Korfmacher, W.A.; Wehry, E.L.; Mamantov, G.; Natusch, D.F.S. *Environ. Sci. Technol.*, **1980**, *14*, 1094-1099.

72. Behymer, T.D.; Hites, R.A. *Environ. Sci. Technol.*, **1985**, *19*, 1004-1006.

73. Behymer, T.D.; Hites, R.A. *Environ. Sci. Technol.*, **1988**, *22*, 1311-1319.

74. Yokley, R.A.; Garrison, A.A.; Wehry, E.L.; Mamantov, G. *Environ. Sci. Technol.*, **1986**, *20*, 86-90.

75. Fox, M.A.; Olive, S. *Science*, **1979**, *205*, 582-583.

76. Wehry, E.L. In *Practical Fluorescence*, Guilbault, G., Ed.; Marcel Dekker: New York, 1973; p. 120.

77. Wehry, E.L. In *Analytical Photochemistry and Photochemical Analysis*, Fitzgerald, J.M., Ed.; Marcel Dekker: New York, 1971; p. 173.

78. Miller, V.R.; Wehry, E.L.; Mamantov, G. *Environ. Toxicol. Chem.*, **1990**, *9*, 975-980.

79. Wang, C.Y.; Lee, M.S.; King, C.M.; Warner, P.O. *Chemosphere*, **1980**, *9*, 83-87.

80. Talcott, R.E.; Harger, W. *Mutat. Res.*, **1981**, *91*, 433-436.

81. Cheng-i, W.; Raabe, O.G.; Rosenblatt, L.S. *Environ. Mutagen.*, **1982**, *4*, 249-258.

82. Schuetzle, D.; Riley, T.L.; Prater, T.J. *Anal. Chem.*, **1982**, *54*, 265-271.

83. Paputa-Peck, M.C.; Marano, R.S.; Schuetzle, D.; Riley, T.L.; Hampton, C.H.; Prater, T.J.; Skewes, L.M.; Jensen, T.E.; Ruhle, P.H.; Bosch, L.C.; Duncan, W.P. *Anal. Chem.*, **1983**, *55*, 1946-1954.

84. Henderson, T.R.; Sun, J.D.; Royer, R.E.; Clark, C.R.; Li, A.P.; Harvey, T.M.; Hunt, D.H.; Fulford, J.E.; Lovette, A.M.; Davidson, W.R. *Environ. Sci. Technol.*, **1983**, *17*, 443-449.

85. Ramdahl, T.; Becher, G.; Bjorseth, A. *Environ. Sci. Technol.*, **1982**, *16*, 801-865.

86. Arey, J.; Zielinska, B.; Atkinson, R.; Winer, A.M. *Atmos. Environ.*, **1987**, *21*, 1437-1444.

87. Zielinska, B.; Arey, J.; Atkinson, R.; Winer, A.M. *Atmos. Environ.*, **1989**, *27*, 223-229.

88. Nielsen, T.; Seitz, B.; Ramdahl, T. *Atmos. Environ.*, **1984**, *18*, 2159-2165.

89. Tokiwa, H.; Ohnishi, Y. *CRC Crit. Rev. Toxicol.*, **1986**, *17*, 23-60.

90. Mermelstein, R.; Kiriazides. D.K.; Butler, M.; McCoy, E.C.; Rosenkranz, H.S. *Mutat. Res.*, **1981**, *89*, 187-196.

91. Siak, J.; Chan, T.L.; Gibson, T.L.; Wolff, G.Y. *Atmos. Environ.*, **1985**, *19*, 369-376.

92. Rosenkranz, H.S. *Mutat. Res.*, **1982**, *101*, 1-10.

93. Kagan, J.; Wang. T.P.; Benight, A.S.; Tuveson, R.W.; Wang, G.; Fu, P.P. *Chemosphere*, **1990**, *20*, 453-466.

94. Pitts, J.N., Jr.; Sweetman, J.A.; Zielinska, B.; Winer, A.M.; Atkinson, R. *Atmos. Environ.*, **1985**, *19*, 1601-1612.

95. Pitts, J.N., Jr. *Atmos. Environ.*, **1987**, *21*, 2531-2547.

96. Grosjean, D.; Harrison, J.; Fung, K. *Atmos. Environ.*, **1983**, *17*, 1609-1612.

97. Atkinson, R.; Aschmann, S.M.; Arey, J.; Zielinska, B. *Atmos. Environ.*, **1989**, *23*, 2679-2690.

98. Garcia, J.P.; Beyne-Masclet, S.; Mouvier, G.; Masclet, P. *Atmos. Environ.*, **1992**, *26A*, 1589-1597.

99. Barkenbus, B.D.; MacDougall, C.S.; Griest, W.H.; Caton, J.E. *Atmos. Environ.*, **1983**, *17*, 1537-1543.

100. Seinfeld, J.H. *Science*, **1989**, *243*, 745-752.

101. Kawamura, K.; Kaplan, K. *Environ. Sci. Technol.*, **1987**, *21*, 105-110.

102. Grosjean, D.; van Cauwenberghe, K.; Schmid, J.P.; Kelley, P.E.; Pitts, J.N., Jr. *Environ. Sci Technol.*, **1978**, *12*, 313-317.

103. Koester, C.J.; Hites, R.A. *Environ. Sci Technol.*, **1992**, *26*, 502-507.

104. Mauldin, R.F. *Photochemical and Supercritical Fluid Extraction Studies of Polycyclic Aromatic Hydrocarbons Adsorbed on Coal Stack Ash Fractions*, Ph.D. Dissertation, University of Tennessee, Knoxville, 1990.

105. Sanders, J.K. *Chromatographic and Spectroscopic Studies of the Interaction of Pyrene with Coal Stack Ash*, Ph.D. Dissertation, University of Tennessee, Knoxville, 1991.

106. Nardkarni, R.A. *Anal. Chem.*, **1984**, *56*, 2233-2237.

107. Korfmacher, W.A. *The Decomposition of Organic Matter Adsorbed on Coal Fly Ash*, Ph.D. Dissertation, University of Illinois, Urbana-Champaign, 1978.

108. Engelbach, R.J.; Garrison, A.A.; Wehry, E.L.; Mamantov, G. *Anal. Chem.*, **1987**, *59*, 2541-2543.

109. Yokley, R.A. *The Photochemistry of PAH Adsorbed on the Surface of Coal Fly Ash*, Ph.D. Dissertation, University of Tennessee, Knoxville, 1985.

110. Engelbach, R.J. *Photochemical Investigations of Polycyclic Aromatic Hydrocarbons Vapor-Deposited on Coal Fly Ash*, Ph.D. Dissertation, University of Tennessee, Knoxville, 1986.

111. Miguel, A.H.; Korfmacher, W.A.; Wehry, E.L.; Mamantov, G.; Natusch, D.F.S. *Environ. Sci. Technol.*, **1979**, *13*, 1229-1232.

112. Liu, B.Y.; Pui, D.Y.H.; *Atmos. Environ.*, **1981**, *15*, 589-600.

113. Wedding, J.B.; McFarland, A.R.; Cermak, J.E. *Environ. Sci. Technol.*, **1977**, *11*, 387-390.

114. Noll, K.E.; Pontius, A.; Frey, R.; Gould, M. *Atmos. Environ.*, **1985**, *11*, 1931-1943.

115. Noll, K.E.; Fang, K.Y.P.; Watkins, L.A. *Atmos. Environ.*, **1988**, *22*, 1461-1468.

116. Holsen, T.M.; Noll, K.E.; Liu, S.P.; Lee, W.J. *Environ. Sci. Technol.*, **1991**, *25*, 1075-1081.

117. Bidleman, T.; Foreman, T. In *Sources and Fates of Aquatic Pollutants, Advances in Chemistry Series*, Hites, R.A.; Eisenreich, S.J. (Eds.) American Chemical Society: Washington, D.C., 1987, Chapter 2.

118. Harris, W.R.; Chess, E.K.; Okamoto, D.; Remsen, J.F.; Later, D.W. *Environ. Mutagen.*, **1984**, *6*, 131-144.

119. Pitts, J.N., Jr.; Lokensgard, D.M.; Harger, W.; Fisher, T.S.; Mejia, V.; Schuler, J.J.; Scorziell, G.M.; Katzenstein, Y.A. *Mutat. Res.*, **1982**, *103*, 241-249.

120. Salmeen, I.; Durigin, A.M.; Prater, T.J.; Riley, T.; Schuetzle, D. *Mutat. Res.*, **1982**, *104*, 17-23.

121. El-Bayoumy, K.; Rivenson, A.; Johnson, B.; Dibello, J.; Little, P.; Hecht, S.S. *Cancer Res.*, **1988**, *48*, 4256-4260.

122. Chapman, O.L.; Heckert, D.C.; Reagoner, J.W.; Thackaberry, S.P. *J. Am. Chem. Soc.*, **1966**, *88*, 5550-5554.

123. Benson, J.M.; Brooks, A.L.; Cheng, Y.S.; Henderson, T.R.; White, J.E. *Atmos. Environ.*, **1985**, *19*, 1169-1174.

124. Holloway, M.P.; Blaglow, M.C.; McCoy, E.C.; Ardens, M.; Rosenkranz, H.S.; Howard, P.C. *Mutat. Res.*, **1987**, *187*, 199-207.

125. Roussel,R.; Allarie, M.; Friar, S.R. *J. Air Waste Manage. Assoc.*, **1992**, *42, 1609-1613.*

126. Cautreels, W.; van Cauwenberghe, K. *Atmos. Environ.*, **1978**, *12*, 1133-1141.

127. Garrison, A.A.; Yokley, R.A.; Engelbach, R.J.; Wehry, E.L.; Mamantov, G. ACS Symposium Series No. 319 *Fossil Fuels Utilization: Environmental Concerns*: Markuszewski, R.; Blaustein, B.D. (Eds.) 1986, p. 325-331.

128. Hawthorne, S.B. *Anal. Chem.*, **1990**, *62*, 633A-642A.

129. Wright, B.W.; Frye, S.R.; McMinn, D.G.; Smith,R.D. *Anal.Chem.*, **1987**, *59*, 640-644.

130. Hawthorne, S.B.; Miller, D.L.; Langenfeld, J.J. *J. Chromatogr. Sci.*, **1990**, *28*, 2-8.

131. Mauldin, R.F.; Vienneau, J.M.; Wehry, E.L.; Mamantov, G. *Talanta*, **1990**, *37*, 1031-1036.

132. Wallace, J.C.; Krieger, M.S.; Hites, R.A. *Anal. Chem.*, **1992**, *64*, 2655-2656.

133. Hipps, A.D. *Photochemical Investigations of Surface Adsorbed Polycyclic Aromatic Hydrocarbons*, M.S. Thesis, University of Tennessee, Knoxville, 1989.

134. Mauldin, R.F., unpublished results.

135. Schure, M.R. *The Effect of Temperature upon the Transformation of Polycyclic Organic Matter*, Ph.D. Dissertation, Colorado State University, Fort Collins, 1981.

VITA

Paul Scott Holder was born on November 25, 1958 in Bridgeport, Alabama. He is the son of James Elam and Virginia Nell Henson Holder, currently of Millidgeville, Georgia. The author has an older sister, Deborah Cotney, who resides with her family in Memphis, Tennessee, and an older brother, Clay, who lives with his family in Livingston, Alabama. Another older brother, James *Skippy* Holder, Jr., died in 1973.

The author spent his formative years in Bridgeport, Alabama; Kimball, Tennessee; Adairville, Kentucky; and South Pittsburg, Tennessee, where he graduated from high school in 1976. The author received a Bachelor of Arts degree in Chemistry from David Lipscomb College in Nashville, Tennessee in 1980. After a brief stint in graduate school at the University of Florida in Gainesville, he was employed as a chemist in that community for six years.

In the fall of 1987, Mr. Holder entered graduate school at the University of Tennessee at Knoxville. On June 15, 1991, he married the former Shannon Leigh Ogle, daughter of Larry and Glenna Ogle of Louisville, Kentucky. Following graduation, the author will be employed by Southern Testing and Research Laboratories in Wilson, North Carolina.